INSTITUTE
FOR
AEROSPACE STUDIES

UNIVERSITY OF TORONTO

ROTATIONAL TEMPERATURE AND DENSITY MEASUREMENTS IN UNDEREXPANDED JETS AND SHOCK WAVES USING AN ELECTRON BEAM PROBE

by

Paul V. Marrone

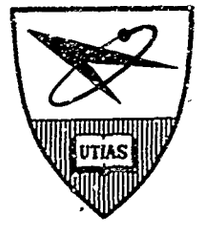

APRIL, 1966

UTIAS REPORT NO. 113

ROTATIONAL TEMPERATURE AND DENSITY MEASUREMENTS IN UNDEREXPANDED JETS AND SHOCK WAVES USING AN ELECTRON BEAM PROBE

by

Paul V. Marrone

Manuscript received January 1966

APRIL 1966 UTIAS REPORT NO. 113

ACKNOWLEDGEMENTS

Special thanks are due to Dr. J. H. de Leeuw for his interest, supervision and counsel during the course of this study.

Thanks for the opportunity to conduct this investigation are extended to the director and faculty of U.T.I.A.S.

My thanks are also extended to others who have contributed, directly or indirectly, to this work. The discussions with Dr J. B. French are appreciated. The author wishes to extend a particular thanks to his colleague, Mr. D. E. Rothe, for his many contributions during the course of this work.

I am indebted to Cornell Aeronautical Laboratory (Buffalo) for financial support, and to Mr. A. Hertzberg of Cornell for his continued interest throughout the investigation. The numerous discussions with Dr. W. Wurster of Cornell concerning the spectrometric aspects of the measurements were extremely helpful.

This work was supported by the Defence Research Board of Canada, and the U.S. Air Force Office of Scientific Research under grants AFOSR 366-64, and 276-64.

SUMMARY

An electron beam probe was used to obtain measurements of rotational temperature and gas density in supersonic nitrogen jets expanding from room temperature. The parameter $P_o d$ (where P_o is the stagnation pressure in torr, and d is the orifice exit diameter in mm) was varied from 15 to 480 torr-mm. This corresponds to a sonic Reynolds number range of 290 to 9,320. Density measurements were made using a photomultiplier with an interference filter centered at 3900 A^o and having a half-width of 100 A^o. The experimental density data follow the axial isentropic density distribution in regions of rotational nonequilibrium. Rotational temperature measurements were obtained from rotational spectra of the N_2^+ first negative 0-0 band at 3914 A^o using a high dispersion spectrograph. The experimentally determined rotational temperature values follow the axial isentropic temperature distribution in a free jet down to approximately 85 °K for $P_o d$ = 15 torr-mm, and 50 °K for $P_o d$ = 480 torr-mm, with a scatter of about $\pm$ 3%. Below these temperatures, the T_R data depart from the isentropic curve and freeze at a constant temperature, which is dependent on the value of $P_o d$.

A shock holder was inserted in the jet and a number of shock waves in the range M = 4 to M = 15 were investigated. Density profiles through the shock waves were obtained. Rotational spectra indicate a large departure from a Boltzmann distribution in the rotational levels in the center of a shock front. This effect is small at M = 4, but very pronounced at M = 15. An apparent non-Boltzmann rotational distribution in the jet expansion flow was also observed.

TABLE OF CONTENTS

I. INTRODUCTORY DISCUSSION

The unconfined expansion from a sonic orifice into a low pressure chamber (referred to as an underexpanded or free jet) has proven to be a very popular and useful source of a high velocity, low density gas flow.

As outlined in the recent review paper by French (Ref. 1), this basic expansion flow is especially useful for facilities having a limited pumping capacity, since the overexpansion in the jet brings the flow to exceedingly high local Mach numbers. The availability of theoretical treatments based on isentropic assumptions enables flow properties to be computed which are applicable over a wide range of conditions of experimental interest.

A number of authors in recent years have investigated theoretically the flow field of an underexpanded jet. Owen and Thornhill (Ref. 2) were the first to consider the problem and used a method of characteristics solution for a gas expanding into a vacuum. When the jet expands into a region of finite pressure, however, a complicated flow pattern, such as diagrammed in Fig. 1 develops. A method of characteristics solution will be valid up to the first Mach disc, since the flow within the barrel shock is uninfluenced by pressure changes along the jet boundary. Investigations at NASA by Love and Associates (Ref. 3) and Vick et al (Ref. 4) have dealt with both theoretical and experimental studies of free jets, where the position of the barrel shock, jet boundary and Mach disc was computed for a variety of conditions.

Extended method-of-characteristics calculations by Woolf for high stagnation to ambient pressure ratios are presented in Ref. 5. The centerline Mach number distributions obtained from these calculations are shown in Fig. 2 for two values of specific heat ratios (γ). Recent theoretical and experimental free jet studies are summarized in the excellent reference paper by Ashkenas and Sherman (Ref. 6), who have shown good agreement between experiment and theory.

Relaxation processes in expanding gas flows, particularly flows occurring in rocket and shock tunnel nozzles, have been studied both theoretically and experimentally for some time. Chemically reacting expansions, for example, have been investigated by Hall, et al (Ref. 7), while the problem of relaxation of the vibrational degrees of freedom of diatomic molecules has been studied theoretically by Stollery and Smith (Ref. 8), and Bray (Ref. 9). The calculations of Treanor (Ref. 10) have shown the possibility of a departure from a Boltzmann population distribution in the vibrational levels of a diatomic molecule during a rapid expansion. Recent experimental investigations such as those of Hurle, Russo and Hall (Ref. 11), and Nagamatsu and Sheer (Ref. 12), for example, have developed techniques to study relaxing expanding gas flows.

All of the above-mentioned studies have been at elevated stagnation temperatures, greater than 2000°K, where there is sufficient excitation of the internal vibrational degrees of freedom. The results of all indicate a departure from equilibrium as a vibrating diatomic gas undergoes a sufficiently rapid expansion. Due to the finite reaction rates involved (i.e. the rather large number of collisions needed, 1000-10,000 to maintain equilibrium among the vibrational and translational degrees of freedom), the slower vibrational modes are unable to follow translation, and depart from equilibrium in the expansion. If the population in the vibrational levels remains Boltzmann, then the results show that the vibrational temperature, T_V, peels away from the

translational temperature, T_T. Finally, sufficiently far downstream, collisions become so rare that the vibrational temperature change is very small, and it is said to be nearly frozen at a value higher than the local translational temperature.

Since most free jets under study are at room temperature stagnation conditions, there is no vibrational excitation of importance in the case of nitrogen. Also, owing to the extreme rates of expansion, the vibrational modes are frozen immediately at their room temperature (ground level) population. However, in the expansion extremely low temperatures are reached, as can be seen from Fig. 3, where the temperature distribution is plotted corresponding to the Mach number distribution of Fig. 2, and at sufficiently low density one may expect the rotational degree of freedom to go out of equilibrium with the translational degrees of freedom. Although the number of collisions needed to equilibrate rotation with translation are small (approx. 5 to 10), the low densities encountered in such flows may lead to conditions where the number of collisions are not sufficient to maintain even this fast internal degree of freedom in equilibrium with translation. A recent theoretical approach to this problem is that of Knuth (Ref. 13), in which the axial distance from the orifice where rotational freezing may occur is predicted, based on a room temperature ($300^{\circ}K$) collision number.

In this type of calculation, the rotational temperature is assumed to be in equilibrium with the translational temperature until a sufficiently low temperature and density (a function of stagnation conditions) are reached in the expanding jet. At this point, the rotational temperature is assumed to depart immediately and remain frozen at a constant value, while the translational temperature continues to decrease in the expansion. This approach is, at best, only approximate for two reasons: the rotational collision number at the low temperatures ($\sim 20^{\circ}K$) encountered in free jets is unknown, and secondly, the rotational degree of freedom does not suddenly freeze at a constant temperature T_R, but may depart gradually from the translational degree of freedom. However, an analysis of this type given by Knuth (Ref. 13) does serve to delineate operating regimes of stagnation pressure (P_o) and orifice exit diameter (d) under which rotational nonequilibrium may occur in an underexpanded jet.

Experimental determination of rotational nonequilibrium in an underexpanded jet has proven to be quite elusive. Impact probe measurements such as those reported by Ashkenas and Sherman (Ref. 6), for example, will not define this departure from equilibrium for most jets under study. The impact probe responds essentially to the quantity (ρu^2), where ρ is the density and u is the velocity in the jet. The flow velocity in an underexpanded jet approaches the limiting velocity in an expansion, $\left(\frac{\gamma + 1}{\gamma - 1}\right)^{\frac{1}{2}} a^*$, (where a^* is the sonic velocity at $M = 1$). The density then, falls off approximately as $(x/d)^{-2}$, since the jet can be approximated as a radial expansion from a source near the orifice (Ref. 6). In addition, for the usual experimental conditions, the rotational energy may be excited in the shock wave ahead of the impact probe, further adding to the complications. As pointed out by Knuth (Ref. 13), the difference in impact pressure at a given x/d is only about 20% for the cases of immediate rotational freezing upstream of the orifice, and the freezing of rotational degrees of freedom at a high Mach number downstream of the orifice.

There is, however, a technique which may be used to investigate the rotational temperature distribution in an underexpanded jet, to determine

the departure, if any, of the rotational degree of freedom from equilibrium. This is the electron beam fluorescence technique described originally by Muntz (Ref. 14). Its usefulness has been further demonstrated by Muntz and Marsden (Ref. 15), Marsden (Ref. 16), Muntz, Abel and Maguire (Ref. 17), and Sebacher (Ref. 18). Recently, this technique has been used by a number of investigators to measure rotational temperatures in expanding flows. Sebacher and Duckett (Ref. 19) and Petrie (Ref. 20), for example, have obtained measurements in high temperature expansions with an arc-tunnel nozzle. In addition, Robben and Talbot (Ref. 21) have investigated underexpanded nitrogen jets expanding from room temperature.

The predominant contribution to the fluorescence observed in nitrogen at low densities arises from the first negative system which represents radiation from excited molecular nitrogen ions. Muntz presented a theoretical analysis of the rotational intensities in the bands of this system, and found experimentally that the rotational temperature, T_R, (and in more detail the relative population distribution in the various rotational energy levels) of the nitrogen molecule before electron excitation could be obtained by using this theory. It is this electron beam fluorescence technique that has been used in the present investigation to study departures from rotational equilibrium in an underexpanded jet.

Since a free jet represents a convenient source of high Mach number flow, it may be used in the study of the structure of strong shock waves by inserting a shock holder in the high velocity flow ahead of the first Mach disc. The electron beam technique in this system will yield data on the rotational distribution within a shock wave. In addition, by measuring the intensity of the total fluorescence due to the beam, the density distribution in a shock wave, and thus a measure of the shock thickness, can be obtained. Earlier studies of shock waves have utilized low density wind tunnels, such as that used by Sherman (Ref. 22) in his heated wire experiment, and shock tubes. Shock thickness measurements have been obtained by a variety of techniques in shock tubes, for example, the optical refractivity method employed at Princeton by Linzer and Hornig (Ref. 23). The attenuation of an electron beam was used by Ballard and Venable (Ref. 24), Russell (Ref. 25), Schultz-Grunow and Frohn (Ref. 26), while the comprehensive measurements of shock thickness of Camac (Ref. 27) utilized the electrons scattered from the primary beam. Camac's technique yields directly a density trace through the shock wave. All of the above mentioned methods depend on the ratio of the density behind the shock to the density ahead of the shock to determine if rotational equilibration has taken place within the shock front. However, by observing the rotational spectra arising from beam fluorescence, it can be determined whether or not there is a departure from rotational equilibrium within the shock front itself. It may be expected, for example, that non-Boltzmann rotational populations may occur in the centre of shock waves. The electron beam technique will indicate whether or not this is in fact so.

The present investigation, utilized the electron beam fluorescence to study the state of the rotational degrees of freedom in underexpanded jets and shock waves. Section II of this report discusses the theory of rotational temperature measurements with the electron beam and the experimental apparatus is described in Section III. The final results and discussions are presented in Sections IV and V.

II. ROTATIONAL TEMPERATURE MEASUREMENTS USING AN ELECTRON BEAM

A beam of energetic electrons when passing through a low density gas excites a fluorescence that can be used to obtain information concerning the gas molecules prior to their excitation. The two properties of interest in the present investigation are the rotational temperature, T_R, of the nitrogen molecule before excitation, and the density of the gas. If the electron beam is well collimated, the fluorescence is maintained in a cylindrical region around the beam. With a carefully designed optical system, it is possible to select a small elemental volume or "point" anywhere along the beam length to obtain emission data. As pointed out by Muntz, et al (Ref. 17), for this technique to be useful, at least one relatively strong emission line must be observed when the gas is bombarded by energetic electrons. For nitrogen at low pressure (i.e. less than 1 mm Hg.), the predominant radiation is emitted from transitions of the N_2^+ molecular ion (the 1st negative system) with the 0-0 vibrational transition being the strongest emitter (see Ref. 15). As the pressure is increased, the main contribution to the fluorescence arises from the N_2 second positive system. This effect was exhibited in the results of Davidson and O'Neil (Ref. 28), where the spectral intensity of the beam fluorescence was observed at pressures ranging from 5 mm Hg. up to approximately one atmosphere.

In addition, the excited state lifetime should be less than 10^{-7} seconds, to eliminate the possibility of the fluorescence being carried downstream in a high velocity gas flow. For the nitrogen first negative system, and in particular the 0-0 transition, the lifetime is approximately 8×10^{-8} seconds, Nicholls (Ref. 29). Thus, at a flow velocity of 20,000 feet per second, an emitting particle would be carried downstream approximately 0.4 mm. For a beam width of one mm, this drift would make good resolution of the beam centerline very difficult. However, the limiting velocity obtained in a free jet expansion from room temperature is approximately 2,500 feet per second for a $\gamma = 1.4$ gas. The drift in this case is about 0.05 mm, and it is possible to obtain better spatial resolution by observing the center portion of the beam.

Since the beam fluorescence arises from a direct excitation - spontaneous emission sequence, there is an upper bound in gas density which indicates the onset of collisional quenching (i.e. the emission increases with density less than with a linear dependence). As noted by Gadamer (Ref.30), at approximately 5 mm Hg. pressure for room temperature air, the quenching de-excitation is very severe. The region of acceptable linearity extends only up to a few hundred microns pressure at room temperature.

A detailed analysis of the beam-excited emission in nitrogen has been presented by Muntz (Ref. 14) and will only be outlined here. The excitation - emission path is indicated schematically as follows:

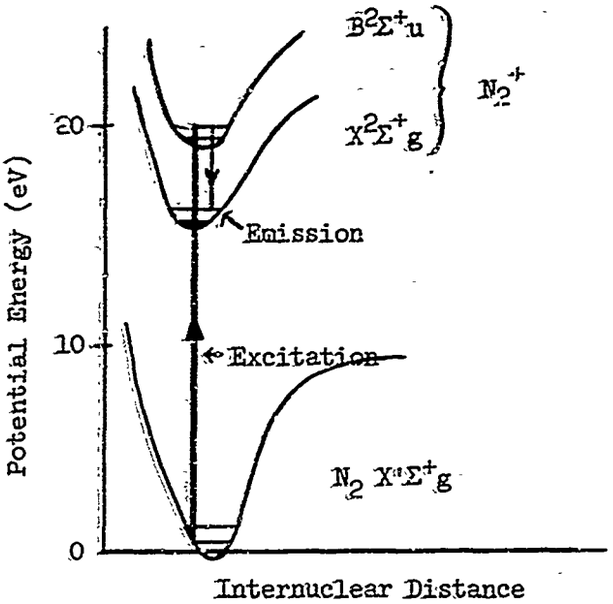

The detailed potential energy curves can be obtained from Gilmore (Ref. 31). The energetic electrons excite and ionize the ground state nitrogen molecule ($N_2 X^1\Sigma$), up to the doublet excited state of the molecular ion ($N_2^+ B^2\Sigma$). The subsequent emission to the ground state ion ($N_2^+ X^2\Sigma$) then comprises the first negative system. It is the 0-0 vibration - rotation band that is used in the present investigation, having a bandhead at 3914A°.

For a gas in thermal equilibrium, the population (N_J) in any J^{th} rotational level is proportional to (following Herzberg, Ref. 32)

$$N_J \propto (2J + 1)\, e^{-J(J+1)\frac{Bhc}{kT}}, \qquad (1)$$

where B is the molecular rotational constant, h is Planck's constant, k is Boltzmann's constant and c is the velocity of light. The combination Bhc/k has dimensions of °K and is called the characteristic rotational temperature of the molecule, θ_R. For the nitrogen molecule, $\theta_R \approx 2.89$ °K. Since the factor (2 J+1) increases linearly with J, the number of molecules in the different rotational levels goes through a maximum as J is increased. This maximum occurs at

$$J_{max} = \sqrt{\frac{T}{2\theta_R}} - \frac{1}{2} \qquad (2)$$

Thus, as the temperature decreases, the population maximum moves toward the lower rotation levels.

The variation of the intensity of the lines in a vibration-rotation band as a function of J is given essentially by the thermal distribution of the rotational levels. In emission, the intensity depends on the mean value of (2 J+1) for the upper and lower states, as indicated.

$$I_{em.} = \frac{Cv^4}{q_r}(J'+J''+1)e^{-J'(J'+1)\frac{\theta'_R}{T}}, \qquad (3)$$

where C is a constant, q_r is the rotational state sum, and J' denotes the upper state, J'' denotes the lower state. Therefore, the intensity distribution resembles closely the population distribution of the rotational levels, a maximum of intensity occurring at $J_{max.}$, with $J_{max.}$ decreasing as the temperature decreases, shown schematically

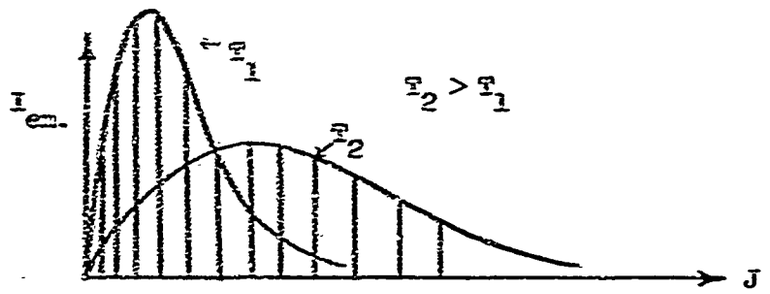

As pointed out by Muntz (Ref. 14), for the 1st negative system of nitrogen, the electron spin coupling in the N_2^+ $B^2\Sigma$ state is very weak, and all transitions between electronic states are governed by Hund's case (b). If the doublets (i.e. for the N_2^+ $B^2\Sigma$ state) are unresolved, the transitions become equivalent to $^1\Sigma \rightarrow {}^1\Sigma$ transitions with rotational levels designated by K, the rotational quantum number apart from spin, $J = K \pm \frac{1}{2}$ (see Ref. 32). The selection rule applying to Hund's case (b) for a $^1\Sigma \rightarrow {}^1\Sigma$ transition is $\Delta K = \pm 1$. This selection rule results in the formation of the two familiar P and R branches in the rotation emission spectrum.

For the R branch, the wave length of emitted light decreases with increasing K' (i.e. the lines are spaced toward the violet end of the spectrum) and spacing between lines increases with K'. The P branch lines are spaced toward the red until this branch doubles back on itself forming a band head. For the C-0 vibration-rotation band studied here, the band origin (K' = 0) is at 3909 A° (Ref. 33), and the band head due to the P branch folding back lies at 3914 A°. The part of the R branch used in the investigation consists of about 21 lines - the reason being that the rotational band head of the 1-1 vibration transition occurs at about 3884 A°, thus the total unobstructed wave length interval involved in the R branch has a span of about 25 A°. This is shown schematically in the sketch below.

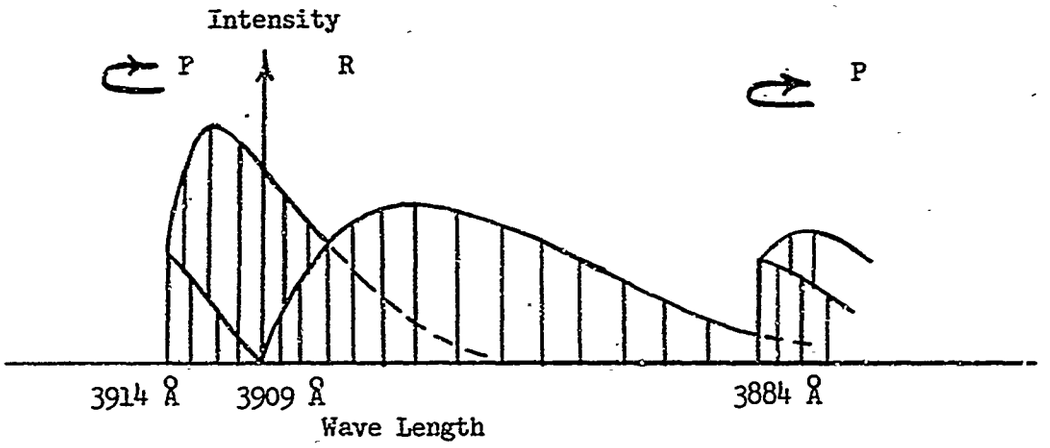

If the assumption is made that the ground state nitrogen molecule before excitation by beam-electrons has a thermal equilibrium distribution of rotational energy (see Eq. 1) at a rotational temperature T_R, and that the electronic transitions are governed by optical selection rules, it is possible to predict the line intensities in the 1st negative system. Muntz's (Ref.14) relation for this, valid for temperatures below about 800°K, (to preclude any appreciable population in all but the lowest vibrational level) is given as

$$(I_{K',K''})_{v';v''} = (K'+K''+1)\, X_4\, [G] \left(\frac{\nu}{\nu_o}\right)^4 e^{-K'(K'+1)\theta_{R_1}/T_R} \qquad (4)$$

Here, X_4 is a constant, one prime indicates the upper electronic state ($N_2^+ B^2\Sigma$), two primes indicate the lower electronic state ($N_2^+ X^2\Sigma$), and the subscript one indicates the ground state molecule (N_2 $X'\Sigma$). The factor [G], which includes the Hönl-London rotational transition probabilities is

$$[G] = \frac{(K'+1)e^{-2(K'+1)\frac{\theta_{R_1}}{T_R}} + K'e^{2K'\frac{\theta_{R_1}}{T_R}}}{2K'+1} . \qquad (5)$$

It is seen that the factor [G] is itself a function of T_R.

From the measured rotational line intensities, the slope technique (Ref. 32) can be used to obtain the value of T_R. This is seen by rewriting Eq. (4) as

$$\log \frac{(I_{K',K''})_{v',v''}}{(K'+K''+1)[G]\left(\frac{\nu}{\nu_o}\right)^4} = -\frac{\theta_{R_1}}{T_R} K'(K'+1) + \text{const.} \qquad (6)$$

Plotting the left side versus K'(K'+1) will yield a straight line, with slope $-\theta_{R_1}/T_R$, from which $T_R = \theta_{R_1}/\text{slope}$. This technique is often used to obtain

temperatures in high temperature, self-radiating gas flows (Ref. 32), and in the electron beam experiments, the energetic electrons are used to stimulate emission in a non-radiating gas. It should be noted that the procedure is iterative, in that a guessed value of T_R has to be used to compute [G] , before a T_R value can be obtained from Eq. 6. This value is then used to compute [G] again, etc. For temperatures not far different from room temperature (i.e. $T_R > 150^oK$) one iteration usually suffices, since [G] is not a strong function of T_R in this range, and only a small error will arise if only the first guess on [G] is used. However, at the low temperatures reached in free jets, [G] becomes a strong function of T_R (i.e. as T_R approaches θ_R in the exponentials), and a complete iteration is necessary. Values of log [G] $(\nu/\nu_o)^4$ are given by Muntz (Ref. 14) for $T_R > 75\ ^oK$, and this compilation has been extended for the present study to $T_R = 8\ ^oK$. These values are given in Table I (where the factor $(\nu/\nu_o)^4$ is ≈ 1, due to the small wave length range involved).

The reduction of the spectral data obtained in the experimental program went as follows:

> the heights (intensity of the rotational lines) were measured with a scale, then
> [log (height)-log (K'+K''+1) - log (G)]
> was plotted versus K'(K'+1). The slope of the resulting straight line enabled the rotational temperature to be computed.

At low temperatures, care would be taken to be sure that the T_R guesses (to compute [G]) would be above and below the actual T_R, and a linear extrapolation between the two was used to obtain the final value of T_R (i.e. guesses of $T_R = 10\ ^oK$ and $T_R = 15\ ^oK$, were used to obtain the actual T_R value of $13\ ^oK$, for example).

As can be seen from Eqs. 1 and 2, the population of the higher rotational levels falls off rapidly as the temperature is decreased. The position of maximum intensity, for example, shifts from $K' \approx 7$ at $300\ ^oK$, to about $K' \approx 2$ at $20\ ^oK$. Thus, the number of intense lines obtained in a spectra decreases with temperature, from 21 lines at 300^oK, to approximately 7 lines at $20\ ^oK$, for example.

The technique described above has been used to obtain rotational temperatures in free jets and shock waves. The various comments concerning position of the maximum intensity line and number of lines obtained in a spectrum, etc., can be more fully appreciated when examining the spectral data presented in Section IV.

III. EXPERIMENTAL APPARATUS

3.1 Low Density Wind Tunnel

All experiments were performed in the UTIAS low density wind tunnel, a facility that has been in operation for a number of years. The original design and operation study of this facility was reported by Enkenhus (Ref. 34) in 1957, and since then, the capability of the facility has been increased with additional instrumentation. An example of this is the electron gun chamber mounted on the top of the test section on a traversing assembly. This allows a beam of energetic electrons to be directed vertically downward in the test section, with this beam capable of traversing in a square of approximately six inches a side (i.e. six inches downstream and three inches radially outward from the tunnel centerline).

The tunnel itself is a continuous running facility having a primary pumping system of nine large booster type oil diffusion pumps. Each of these boosters has a pumping capacity of approximately 1,000 liters per second at tunnel test section pressures from 1 to 60 microns Hg. The booster pumps are connected to a second stage of pumping consisting of two large positive displacement mechanical pumps of 485 cubic feet per minute capacity. The test section is a cylinder 44 inches in diameter, with its axis at right angles to the rest of the tunnel. A schematic of the tunnel can be seen in Fig. 4. A remotely controlled traversing assembly inside of the test section was used in the present experiments to support and align the shock holder in the shock wave studies. The operating conditions for the free jet experiments to be discussed later covered the following ranges:

stagnation pressures (Po) from .5 to 250 mm Hg
and test section or ambient pressures from about 10 to 30 microns Hg.

3.2 Electron Gun Chamber

The traversing electron gun assembly (Ref. 35) mounted atop the tunnel test section is the primary diagnostic tool in the present experiment. For a schematic representation of the gun chamber and vacuum system, see Fig. 5.

A Phillips TV-tube is mounted in the inner of the two concentric tubes shown in the figure. An oil vapor diffusion pump (Edwards model 203 B, rated at 50 liters per second with a water baffle) maintains the pressure in this tube between 2×10^{-6} and 5×10^{-5} mm Hg. An Edwards liquid air cold trap is placed between the water baffle and the gun chamber. The outer tube shown in Fig. 5 forms an intermediate pressure chamber separating the inner gun chamber from the test section of the low density tunnel. A similar diffusion pump, water baffle and cold trap system is used to maintain the pressure in this chamber at 10^{-4} to 10^{-3} mm Hg, while the test section pressure may be typically in the range from 1 - 100 microns Hg. The inner and outer chambers can be isolated from the diffusion pumps by gravity-operated butterfly valves in the event of a power failure.

The electron beam passes through a 2 mm diameter nozzle, which is 12.5 mm long, into the intermediate chamber, and from there the beam exits into the test section through a 15 mm long nozzle with a 1 mm diameter hole. Careful alignment and focusing of the beam is necessary to allow it to pass

through both nozzles. This alignment is achieved with a set of eight electrostatic deflection plates within the inner chamber. Independent controls are provided for shifting or tilting the beam in two perpendicular planes.

The cathode potential is supplied by an NJE high-voltage regulated DC power supply and may be varied between 0 and 30 kilovolts (for all experiments described in this report, the cathode potential was 17.5 kilovolts), and the beam current was nominally held between 100 and 200 microamperes. The anode is kept at ground potential while the grid and lens voltages are obtained from a voltage divider circuit. A separate, regulated 400 volt DC power supply furnishes the deflection plate voltages. A schematic of the gun and associated circuitry is shown in Fig. 6.

3.3 The Spectrometer

The success of an experiment of this type depends upon the availability of a sensitive (required because of the low light output at low gas densities), high dispersion spectrograph (enough dispersion to separate all of the lines in the rotational spectrum, a total range of about 25 Å). The instrument was originally designed by Marsden to fulfill the above mentioned requirements, and is described in detail in Ref. 16. It is an Ebert type scanning spectrometer, using a Bausch and Lomb replica grating 102 mm square with 1200 rulings per mm blazed for 3500 A° in second order. The spherical mirror has a focal length of 750 mm. This, together with the size of the grating, gives the instrument an optical f number (f equals focal length divided by the effective grating diameter) of 6.6. The instrument was used in second order, with a dispersion of 4.7 Å per mm. The slits are curved to provide sharp resolution over the full slit length, see Fastie (Ref. 36). A schematic of the instrument is given in Fig. 7.

The light passing through the entrance slit is focussed by the spherical mirror into a parallel beam of light incident on the grating. Spectrally resolved light from the grating is then focused by the mirror on the plane of the exit slit. Rotation of the grating (via the grating drive motor and lever arm) causes the resolved spectrum to move past the exit slit and the intensity of the lines is measured by a photomultiplier placed behind the slit. For the experiments discussed in this report, the entrance slit width was 0.004 inches (100 microns) and height was 0.300 inches, while the exit slit width was .006 inches. As discussed by Marsden (Ref. 16), with these slit dimensions, all lines with $K' > 3$ should be resolved with no contribution (or rotational line overlap) from neighboring lines. Lines $K' = 1, 2$, however, may be affected by the presence of its neighbor (since line spacing decreases with decreasing K'). The experimental results presented in Section IV seem to bear out this conclusion.

The photomultiplier used to measure the line intensities is an uncooled EMI type 9502 S, having an S-11 spectral response (a peak at 4000 Å). The dark current as recorded on a Keithley 414 micro-microameter was found to be $1.5 \rightarrow 2.0 \times 10^{-10}$ amperes at 1500 volts.

Careful alignment of the grating and slits was accomplished using light sources of mercury, hydrogen and nitrogen. Proper slit alignment is critical for experiments at low temperatures where only a few spectral lines are recorded. These lines have low K' values and small spacing, for example, $\Delta\lambda$ for $K' = 1$ to $K' = 2$ is only 0.67 Å. Thus, the entrance and exit slits

must be carefully aligned to minimize the amount of line overlap at low values of K'. This was accomplished by removing the photomultiplier at the exit slit, and visually watching various lines from the light sources pass by the slit as the grating was rotated by hand using the micrometer drive. Any non-alignment of entrance and exit slits could be observed by a "rolling" of the emission line as it passed by the exit slit. The exit slit was then rotated until the emission line jumped sharply into and out of the slit. Proper alignment seems to have been achieved in this manner, as can be seen from the spectral data shown in Section IV.

3.4 Experimental Setup

The complete experimental arrangement is shown schematically in Fig. 8, which shows a top view of the system. The fluorescence from the beam is focused onto the entrance slit of the spectrometer with a K-24 aerial camera lens. It should be noted that the entrance slit is parallel to the beam (i.e. beam vertical, slit vertical). This focusing lens, which has a focal length of 7 inches, and an optical f number of 2.5, is attached on a bar support which is part of the electron gun assembly. Thus, the lens moves with the beam as it is traversed axially (or radially) in the free jet. The lens-to-beam and lens-to-slit distances were approximately 9 and 3¼ inches respectively, giving a magnification of about 4. Thus, the .00¾ inch wide entrance slit, when imaged on the 1 mm wide electron beam is only .001 inch in width and about 2 mm in height. This defines the "point" or elemental volume in the beam fluorescence where the measurements were made.

The spectrometer and grating drive motor assembly rested on a specially constructed traversing table which rode on ball bushings. This table allowed the spectrometer to "track" the beam, i.e. to "track" the beam image formed by the focusing lens, to keep this image on the spectrometer entrance slit. The lead screws for this table were similar to those for the electron gun traversing mechanism atop the tunnel test section, 8 Acme threads per inch. Graduated dials on the lead screws were marked in thousandths of an inch for both traversing assemblies.

Several photographic views of the experimental apparatus can be seen in Fig. 9(a) through 9(d). The first photo shows the electron gun and associated vacuum system mounted on its traversing assembly atop the tunnel test section. This assembly moves on a sliding O-ring seal preventing leaks from occurring in the test section. Also seen in the photo is the mechanical backing pump for the diffusion pumps, also mounted atop the low density tunnel. A view of the spectrometer and traversing table in position at the test section window is given in Fig. 9(b). The traversing table lead screws and ball bushing supports can be seen, along with the grating drive motor mounted directly on the table. Figure 9(c) shows a general view of the associated instrumentation, including the high voltage power supply, photo-multiplier power supply, micro-microammeter, etc. The final photograph shows an internal view of the tunnel test section, as viewed from the opposite side of the tunnel from the spectrometer. The bottom of the electron gun chamber with the automatic door and the beam collector cup are clearly seen. In position are the focusing lens described above, and the shock holder model mounted on the test section traversing mechanism. The nozzle seen in the photograph is an orifice type with an exit diameter of 5 mm.

The system was aligned optically in the following manner: the traversing table was properly aligned with the tunnel to assure parallel movement with the electron beam. The spectrometer was mounted on the table and leveled. A tungsten lamp was then used to backlight the spectrometer with the exit slit removed. An image of the entrance slit was formed (via the focusing lens) on a ground glass screen inside the tunnel test section. A plumb line was suspended from the automatic door at the bottom of the gun assembly, in line with the electron beam. The entrance slit image was then focused on the ground glass at the plumb line, and the spectrograph height was adjusted to insure correct focusing and alignment with the centerline of the tunnel. This was accomplished by moving the plumb line close to the exit orifice of the nozzle under study, and eyeball centering was used. The gun assembly was then traversed along the centerline of the tunnel, tracked by the spectrometer, to insure proper focusing for the full length of travel. This procedure was followed with the installation of every nozzle, and was felt to be accurate to less than .010 inch.

The output of the photomultiplier was amplified by a Keithley 414 micro-microammeter and fed into a Tektronix 514 storage oscilloscope. During the experimental runs the spectrometer was centered on the beam by observing the output on the micro-microammeter dial. Using one line of the spectrum, the output was maximized as the entrance slit image was traversed back and forth across the beam fluorescence (i.e. traversing the spectrometer with its traversing table). Since the beam width was about 1 mm total, and the slit image width only .001 inch, this gave a rather broad plateau of intensity of about .020 inch. The maximum part of this plateau was considered as the beam center and the spectrometer was aligned with this. After some experience with numerous runs, this maximum was found to be trackable to within about .005 inch.

The time constant, or response speed, of the Keithley amplifier varied with the scale range being used. However, for most of the experiments the range was about 10^{-9} to 10^{-7} amperes, giving a time constant of about .07 seconds to 63% of final current. Several grating scanning speeds were employed in the early experiments to determine the optimum speed needed to obtain accurate spectra, and enough data points for any given free jet or shock wave setup. The final speed chosen gave a dwell time at the peak of each line of about 2 seconds, much larger than the time constant of the amplifier. These results will be discussed in Section IV.

Before actual spectral data was taken during a run, a photograph of the flow was taken using a Polaroid camera mounted on the opposite side of the test section. In this way, a visual examination of the flow field could be made to insure proper flow conditions, etc. This beam visualization technique is described by Rothe (Ref. 37), and consists in traversing the electron beam parallel to itself down the centerline of the jet. The camera shutter was left open and the flow conditions then are "painted" on fast Polaroid film. Photographs of underexpanded jets and shock waves are shown in Section IV.

IV. EXPERIMENTAL RESULTS

The experimental program consisted of a systematic survey of under-expanded nitrogen jets issuing from a room temperature source, using the electron beam probe to obtain rotational temperature distributions. A number of sonic orifices and stagnation pressures were used in the investigation to allow a large variation in flow properties. Several shock waves were investigated, covering the Mach number range from about $M \approx 4$ to 15. For these runs, a shock holder model was inserted in the free jet before the first Mach disc (Ref. 35). In addition to temperature measurements, density profiles were obtained for both free jets and shock waves using a photomultiplier optical system designed by Rothe (Refs. 35, 38). The results of the measurements are given in the present Section of this report, it being divided into three separate subsections. A discussion of the results and conclusions will be presented in Section V.

4.1 Calibration Runs

After the spectrometer was optically aligned with the beam-lens system (as described in Section III), a number of measurements were made at room temperature to give an indication of the accuracy and scatter of the rotational temperature data. Room temperature bottled nitrogen (Linde) was admitted directly into the tunnel test section through a large diameter side port. One oil booster pump was used to maintain a quiescent nitrogen ambient condition in the chamber at a fixed pressure, P_∞. The temperature of the nitrogen in the test section was monitored with a copper-constantan thermocouple, with the output read directly on °F on a Brown Instruments potentiometer. The electron beam was then turned on, and a rotational spectra was obtained - the thermocouple output being continuously monitored during the time interval required for a spectral scan. As described previously, the grating speed was such that the entire R-branch spectrum was obtained (for this room temperature condition) in approximately 5 minutes. The electron beam current was also monitored during this interval on a microampere meter measuring the collector cup current. If the current varied by more than 5% during this time, the run was discarded (this procedure was used throughout all experiments). A sweep speed of about 10 seconds per division was used on the oscilloscope, giving sufficient resolution such that all the line heights could be measured accurately. Thus, about 3 photographs of the scope face were needed for a given spectral trace. At the end of the each sweep, the grating drive motor was stopped momentarily while the scope was re-triggered, then the spectral trace was resumed, etc. This momentary interruption in the grating scan did not affect the data, as will be seen from both the actual spectral photographs and the line heights used in the straight line slope technique.

These calibration runs were performed at test section pressures ranging from about 10 to 125 microns Hg. The pressures were measured with a cold trapped mercury McLeod gauge mounted outside of the tunnel. The run conditions are summarized in the following table:

Run No.	P_∞ μ Hg.	Beam current μA at 17.5 KeV	T°K Thermocouple	T_R°K Spectra
1	9.8	190	305	304
2	23	155	302	298
3	38	155	303	305
4	39	160	303	295
5	48	155	301	300
6	128	140	301	298

Figure 10 shows a typical spectrum obtained at room temperature conditions. Eighteen rotational lines in the R branch are seen, with the spacing between lines increasing with increasing K', and $K'_{max.}$ being about K' = 7. Owing to the nuclear spin properties of the nitrogen molecule, the alternate line intensities are predicted to be in the ratio of 2.1 on the K'(K'+1) log plots at the same value of the ordinate (Ref. 32). These half-intensity lines correspond to even values of K' as shown in the figure. For all data reduction, the heights of these lines were multiplied by two for use in the slope technique, shown, for example, in Fig. 10 for the same spectrum indicating a T_R = 298°K. It is seen that the points are linear with K'(K'+1) showing a Boltzmann distribution to exist in the ground state molecule. In addition the even K' lines fall in line with the odd K' lines, indicating an alternating intensity ratio close to the theoretical figure of 2. There was some question about the value of this ratio previously (Ref. 16), but careful slit alignment minimized line overlap that would have affected this ratio experimentally, and the factor of 2 now seems to be correctly measured.

Figure 11 shows the linear plot of log intensity vs. K'(K'+1) used to obtain the T_R values for the room temperature calibration runs. It can be seen from the data that a scatter of about $\pm$ 2.5% exists in the present data at 300°K, which is in general agreement with Muntz's (Ref. 14) results. There is some indication from the log plots that the first two points may be high. This could be due to the overlap of neighboring lines at the low K' values (this was mentioned in Section III in the discussion of spectrometer slit dimensions). There is, however, another source that may contribute to the apparently higher intensity of these lines. Since the P branch doubles back upon itself (to form the bandhead at 3914 Å), it may be expected that a number of the lightly populated higher K' lines of this branch may be in the approximate wave length region of the low K' lines of the R branch under study. These would contribute to the measured intensity of the R branch lines. This was discussed by Marsden (Ref. 16) for conditions of 500°K, where the overlapping P branch lines may contribute 20% of the measured R intensities for the first 3 lines. A similar calculation was performed for 300°K, and as shown below, the intensity overlap at this temperature is extremely small:

R Branch		P Branch		I_P/I_R at 300°K
K'	Å	K'	Å	
1	3909.71	26	3909.82	.011
2	3909.04	27	3909.17	.016
3	3908.30	28	3908.45	.0028
4	3907.53	29	3907.67	.0045
5	3906.70	30	3906.85	.001

The P branch intensity contribution will be even less than the above values at the low temperatures encountered in free jets, since the high K' levels will have no appreciable population. Examination of the straight line log plots for a large number of experimental runs at room temperature, indicated that the measured intensities of the first two lines seemed to be about 5% high. Since this value is larger than P branch contribution predicted above, it can be taken as a possible indication of the amount of rotational line overlap due to slit geometry as discussed in Section III.

Individual rotational lines were scanned with a rapid sweep on the oscilloscope to obtain line profiles. Figure 12 shows such a trace for the K' = 3 line. The sweep speed is one second per division, indicating a dwell time at the peak height of about two seconds (see Section III). This grating scan speed was used throughout the experimental program.

4.2 Free Jet Studies

A large number of nitrogen free jets were investigated using the electron beam probe, and both temperature and density measurements were obtained. The stagnation pressure and orifice exit diameter was varied to obtain flow conditions where the rotational degree of freedom was expected to depart from equilibrium in the expansion on the basis of Knuth's calculations (Ref. 13). The parameter $(P_o d)$, where P_o is the stagnation pressure in torr, and d is the orifice exit diameter in mm, was varied from

$$(P_o d) = 15 \text{ torr-mm} \quad \text{to} \quad (P_o d) = 480 \text{ torr-mm} \quad .$$

These values correspond to Reynolds numbers based on the sonic exit conditions at the orifice, of

$$Re_{d^*} = 290 \text{ to } 9{,}320 \quad .$$

A large contoured nozzle, 47.5 mm in diameter was used for measurements in the very low x/d range. Several orifice type nozzles having much smaller exit diameters were machined, and were attached to the large contoured nozzle inside the test section. This arrangement can be seen in Fig. 9(d), which shows the 5 mm diameter orifice in place. These small nozzles were machined with a very thin wall at the end, thus the nozzles acted as orifices, as follows:

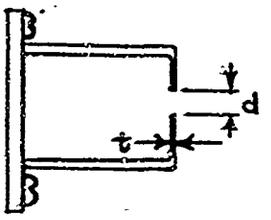

Diameter d	thickness t	t/d
2 mm	.0025 inch	.032
5 mm	.0055 inch	.0275
15 mm	.013 inch	.022

The data presented by Ashkenas and Sherman (Ref. 6) for orifices having similar t/d ratios indicate an effective orifice discharge coefficient of about 1 for values of Re_{d^*} greater than 100. Thus, the d value used in the x/d correlation is the actual exit diameter of the orifice, given above.

The experiments were performed as follows (see Fig.8): bottled, room temperature nitrogen was admitted through flow metering valves into the stagnation chamber of the tunnel after the oil booster pumps had evacuated the test section to about 1 micron Hg. Sufficient time was allowed for the flow to stabilize and both the stagnation pressure (P_o) and test section pressure (P_∞) were measured with the mercury McLeod gauge. The electron beam was turned on, and a photograph of the flow field was obtained with a Polaroid camera as described by Rothe (Ref. 37). The beam was then traversed down the centerline of the jet, being tracked by the spectrometer on its traversing table. At numerous points along the jet centerline, rotational spectra were obtained as described in Section 4.1. Again, the beam current was continually monitored to insure a variation of less than 5% in the beam current during the grating scan. This proved to be an upper limit, since for the majority of the data points, the beam current fluctuations were only about 1%, and in most cases, not discernable at all on the microampere meter. For the larger values of ($P_o d$), about 15 data points were taken along the jet centerline. In addition, several radial temperature distributions were obtained in the jet by traversing the electron gun radially outward from the centerline. Again, the beam was tracked by the spectrometer which was traversed backwards away from the tunnel to keep the beam focused on the entrance slit. The stagnation temperature was monitored by a copper-constantan thermocouple during the run. Since it took about 3 minutes to obtain a complete spectral scan near the nozzle orifice (i.e. $T_R \approx 200^\circ K$ for example), and about 1-1/2 minutes to obtain a spectral scan further down the jet at low temperatures (i.e. about 20 $^\circ K$ or so), a complete jet centerline survey could be completed in approximately 1-1/2 to 2 hours, including flow visualization.

The important flow parameters of the nitrogen free jet runs are tabulated below:

$P_o d$ torr-mm	d mm	P_o torr	P_∞ μ Hg.	P_o/P_∞	x/d last	Re_d*	x_M/d
15	5	3	2.2	1,365	7.5	290	25
	15	1.05	5.2	202	5		9.5
40	2	20.5	2.1	9,770	19	775	66
	5	8	4	2,000	15		30
80	2	40	3.4	11,780	22	1550	72
	5	16	6.7	2,390	17.5		33
250	2	128	9.8	13,080	32	4850	76
	5	50	21	2,380	22.5		32
480	2	240	18.5	13,000	38	9320	76
	5	94	52	1,810	20		28

where x_M/d is the theoretical distance to the first Mach disc, and x/d_{last} is the position where the last spectral data was taken for each run.

The jets observed covered a wide range of pressure ratios and in all cases the last spectral data point was taken well before the occurrence of the first Mach disc as predicted theoretically (Ref. 6). Actually the last data point for each run was determined by the local density in the jet, the optical system becoming light limited at low densities (i.e. the spectral trace became quite noisy, since the photomultiplier output was nearing the dark current level). In general, this light limiting point occurred at densities equivalent to a pressure of about 5 microns Hg at room temperature. It may be noted that the density measurements to be discussed later indicated that the first Mach disc is quite diffuse for low values of$(P_o d)$.

It is of interest to examine the photographs of the flow field, and these are shown in Fig. 13 for various values of $(P_o d)$. For small $(P_o d)$, the entire flow field is quite diffuse and the free jets do not seem at all well defined. At the larger $(P_o d)$ values (and consequently higher pressure ratios), the jets become very sharply defined and the barrel shock quite clear. The complete travel of the beam is about six inches giving an indication of the first Mach cell size. The slight uneveness in the quality of the photos is due to the fact that the electron beam traversing screw was turned by hand.

Examples of spectral records from which the values of rotational temperature were obtained are presented in Fig. 14 for a large number of temperatures (i.e. positions along the free jet centerline, for example) and indicate the quality of the data. In all records, the oscilloscope sweep speed is about 10 seconds per division. Readily apparent in the data is the intensity maximum shift to lower K' values as the temperature decreases (Section II), indicating the low population of the higher rotational levels. The number of

rotational lines obtained varies from about 20 at 300 °K to 5 at about 10 °K. The alternating intensity of adjacent lines is apparent in all of the photographs. For each data point along the jet centerline at a given $(P_o d)$ value, the spectral data was analyzed as discussed in Section II, and the rotational temperature, T_R, was obtained.

A number of log slopes plots are presented in Fig. 15 for representative data points along the centerline of a free jet. The slope of the linear portion was used to obtain T_R. In some cases, the higher J' lines are seen to depart from this linear curve. This phenomenon is discussed in Section V.

The final rotational temperature data is plotted in Fig. 16 as function of distance down the jet centerline, x/d. For all values of $(P_o d)$, the T_R values fall on the $\gamma = 1.4$ isentropic temperature curve at small values of x/d. The data shows a gradual departure from this curve, and in the low $(P_o d)$ case, the rotational temperature seems to freeze at a relatively high value in the jet. The scatter is seen to be quite small for both orifice diameters used in each $(P_o d)$ curve. These results will be discussed in Section V, but it can be said from a cursory observation of Fig. 16, that as $(P_o d)$ is increased, the rotational temperature follows the isentropic $\gamma = 1.4$ curve to lower temperatures, as would be expected for a non-equilibrium phenomena.

For all of the free jet experiments, the measured centerline temperatures departed from the isentropic curve at different locations, depending on the value of $(P_o d)$. The measurements obtained at the lowest value of $P_o d$ = 15 torr-mm, for example, depart at about 85 °K. At the highest value of $P_o d$ = 480 torr-mm, the data seems to depart at approximately 50 °K, as can be seen from Fig. 16. A comparison of the experimental data obtained near the orifice (i.e. at small x/d) before departure from the isentropic curve, is shown in Fig. 17 where data points from all orifices and $(P_o d)$ values are plotted vs. x/d. The agreement with the isentropic prediction is quite good and the scatter obtained (about ± 3%) is comparable to the scatter obtained in the room temperature calibration runs discussed in Section 4.1.

A typical radial temperature distribution is shown in Fig. 18 at an x/d of 0.3 for $(P_o d)$ = 250 torr-mm. The temperature distribution in the center of the jet is seen to be quite flat, and the increase in rotational temperature in the barrel shock is very apparent.

As a check on whether the diffuse Mach disc (as shown in flow photos) at low $(P_o d)$ values may be contributing to the departure of the rotational temperature from the $\gamma = 1.4$ curve, a series of runs were undertaken in which the density distribution in the free jets was obtained. The optical instrument used is discussed in detail by Rothe (Refs. 35, 38), and will only be described briefly here. It consists of a photomultiplier housing mounted to the electron gun assembly (i.e. mounted to the same bar used to hold the focusing lens in the spectrometer experiments), so that it traverses with the beam. The entrance slit to the housing was focused perpendicular to the beam (i.e. beam vertical, slit horizontal) so that all of the fluorescence surrounding the beam would be gathered. Light fibres (from the American Optical Company) were used to guide the radiation from the entrance slit to an interference filter directly ahead of the photomultiplier face. An uncooled EMI 9502 S photomultiplier was used (similar to that in the spectrometer), in conjunction with an interference filter of 100 Å half-width centered at 3900 Å. The instrument was calibrated in the tunnel test section at room temperature in a quiescent nitrogen atmos-

phere, to obtain a curve of light output versus nitrogen density (pressure). The photomultiplier current was read on the Keithley micro-microammeter. This calibration data is shown in Fig. 19 and is seen to be linear to at least 120 microns pressure.

Using this instrument, a number of free jets were surveyed to obtain centerline density distributions for the 5 mm diameter orifice. This data, which is shown in Fig. 20, was obtained using the calibration curve of Fig. 19. The scatter is seen to be quite small, and the density distribution generally follows the isentropic curve. For low ($P_o d$) values, the density leaves this isentropic curve and begins to increase well ahead of the theoretical Mach disc location. This is an indication that this Mach disc is not at all well defined (as seen in Fig. 13) at low densities, but becomes sharper as the density is increased at higher ($P_o d$) values.

By comparing Figs. 16 and 20, it is seen that the last spectral data point was taken before the density begins to depart from the isentropic curve. In fact, the rotational temperatures show marked departures from equilibrium while the density still follows the isentropic curve: (i.e. the density drops off approximately as $(x/d)^{-2}$ (Ref. 6)). This comparison was carried out for the most conservative case, since the 2 mm diameter orifice, having much larger pressure ratios, has Mach disc locations farther downstream (over twice as far downstream as the 5 mm nozzle in most cases: see table for free jet runs). Thus, the Mach disc does not appear to contribute to the overall departure of the rotational temperature from the isentropic curve.

A more comprehensive discussion of these results is presented in Section V.

4.3 Shock Wave Studies

During the course of the experimental program, a shock holder was inserted in the free jet ahead of the first Mach disc so that shock structure data could be obtained for a wide range of Mach numbers. This shock holder consists of a hollow, diverging cone with a 2-inch diameter opening at the front, see Ref. 35. A sliding conical plug is used to partially close the rear opening, producing a standing shock wave ahead of the holder. The leading edge of the holder has two sets of slits, 1/8 inch wide by 1/2 inch long. One set of slits allows the electron beam to pass vertically down through the shock holder, and the other set enables the beam fluorescence to be gathered by the focusing lens. The shock holder, can be seen mounted in the test section in Fig. 9(d). Both rotational spectra and density measurements were obtained through the shock waves at closely spaced intervals of x/d. The shock wave runs are listed below:

$P_o d$ torr-cm	d cm	P_o torr	P_∞ μ Hg.	Shock-holder Leading Edge x/d	$\gamma = 1.4$ Mach No.
23	47.5	0.490	19	2	3.9
295	5	59	22	17.5	11
480	2	242	21.5	34.8	15

As in the free jet experiments, flow visualization photos were taken at the start of each run. These are shown in Fig. 21. It can be seen from the photos that the shock wave is not plane. This is due to the fact that the free jet flow is similar to flow from a source near the orifice, (Ref. 6) and the curved shock then is normal to the local flow streamlines, being perpendicular to the shock holder only near the jet centerline, where the shock profile data were obtained.

Using the photomultiplier-interference filter assembly described in the previous section, density profiles were obtained along the jet centerline and through the shock wave. These are given in Fig. 22 for the $M_s = 4$ and 11 shocks. The density drops off similar to the isentropic curve, then increases through the shock front towards the post shock value. Similar shock density profiles have been reported by Robben and Talbot (Ref. 39). When the electron beam was near the shock holder, and at times behind the leading edge, the light gathered by the focusing lens was diminished due to the presence of the shock holder. To account for this, an occulation calibration was carried out in quiescent nitrogen (no shock wave), the fluorescence being measured as the beam moved close to the shock holder. This calibration curve is shown in Fig. 23. The data agrees extremely well with a point source theoretical curve reported by Rothe (Ref. 38). This calibration factor was used to obtain the final density data shown in Fig. 22.

With the spectrometer setup as previously described, rotational spectra were obtained along the jet centerline through the shock front. The log slope plots are non-linear, indicating a non-Boltzmann distribution in population of the rotational levels existing in the nitrogen molecule before excitation by beam electrons. This effect seems to be a direct function of shock strength. The deviation from linearity is small for the $M = 4$ shock, but exceedingly strong for the $M = 15$ shock. Robben and Talbot (Ref. 40) report, for example, essentially no deviation at $M = 1.7$, but a much stronger deviation at $M = 13$. Figure 24 shows the log slope distribution through a shock wave for the three cases investigated, $M = 4$, 11 and 15. In all cases, the log slope is non-linear in the center of the shock front, and becomes linear again in the high temperature region at the tail of the shock wave. Thus, a Boltzmann distribution is regained in the post shock conditions. This non-Boltzmann effect would go undetected in density measurements alone.

Since the factor (G) is a function of rotational temperature, T_R, a difficulty arises when a non-linear log slope plot is obtained as to what value of T_R should be used for the calculation of (G). Since the plots given in Fig. 24 are meant to be representative of the non-Boltzmann effect with increasing shock strength, only one value of (G) (i.e. one value of assumed T_R) was used for each slope. To obtain actual temperatures from different slopes of the same log plot, detailed iterations using various assumed values of T_R are needed. This procedure will be discussed in Section V. Thus, for the log plots in Fig. 24, the following values of assumed T_R (i.e. to compute (G)) were used: (the circled points denote positions in front of the shock, ① , to positions behind the shock, i.e. ⑧ , see Fig. 27).

M	Point Number	Assumed T_R °K for Log Plot
4	①	100
	2	100
	3	100
	4	150
	⑤	300
11	①	20
	2	20
	3	100
	4	100
	5	150
	6	200
	⑦	225
15	①	20
	2	30
	3	125
	4	125
	5	200
	6	200
	7	200
	⑧	250

As pointed out by Marsden (Ref. 16), there is an approximate one-to-one relationship between the line intensities in the rotational spectrum and the rotational energy distribution. Thus, from the plots in Fig. 24, it appears that the lower rotational levels have a population reflecting the temperature ahead of the shock, while the higher rotational levels are populated according to the temperature behind the shock wave. Robben and Talbot (Ref. 40), for example, found it was possible to represent their results approximately by the merging of two rotational distribution functions corresponding to temperatures upstream and downstream of the shock wave.

V. DISCUSSION AND CONCLUSIONS

The rotational temperature measurements obtained in underexpanded jets indicate that the electron beam fluorescence probe can be used with some degree of confidence as a diagnostic tool at low temperatures. As noted in Fig. 17, for example, the rotational temperature values obtained experimentally agree with the predicted centerline isentropic distribution down to about 50 ^{o}K for high values of $(P_o d)$. For all of the experiments, the measured rotational temperatures departed from equilibrium, the degree of departure depending on the value of $(P_o d)$. However, as noted earlier, the trend of the rotational temperature measurements with increasing $(P_o d)$ is such that the experimental results follow more closely the isentropic curve to lower temperatures. This is to be expected, since at higher densities (higher $P_o d$ values here), collisions become more frequent and the rotational degree of freedom is more apt to follow the translational degree to lower temperatures.

The appearance of the rotational temperature versus x/d curves, Fig. 16, (i.e. slow departure of rotation from equilibrium with subsequent tendency to freeze) is typical of vibrational non-equilibrium in expansion flows, for example, and as noted, the trend with pressure, $(P_o d)$, is correct. In addition, for each value of $(P_o d)$, two different orifice diameters were used, so that for a given Reynolds number, i.e. given $(P_o d)$, different flow densities would be obtained (a factor of 2-1/2 in the densities). As can be seen from the small scatter for each $(P_o d)$ value, the data scales in a binary fashion. The possibility of Mach disc interference with the free jet rotational temperature measurements should be considered if measurements are made far downstream. However, the density distributions shown in Fig. 20 seem to rule out this possibility for the present results. Even at distances (x/d) where there are large departures of rotational temperature from equilibrium, the density continues to follow the isentropic curve, decreasing approximately as $(x/d)^{-2}$.

It is of interest to compare the results of the present investigation with the only other published rotational temperature measurements in under-expanded jets, those of Robben and Talbot (Ref. 21). Their experimental setup was somewhat similar to that shown in Fig. 8, with their electron beam vertical, but their spectrometer slit horizontal (i.e. across the beam). A number of measurements were made at several values of $(P_o d)$, but none were carried out as extensively for a given $(P_o d)$ value as those reported here. In addition, their electron beam probe was used at a high beam current (approximately 5 milliamperes) as compared to about 100 microamps in the present investigation. Figure 25 shows the University of California T_R results compared with those obtained at Toronto. The comparison for similar $(P_o d)$ values is quite good for the two different investigations, but in general it can be said their measurements somewhat are higher than those reported here. Robben and Talbot report high T_R data for all of their experiments, even those performed at subsonic Mach numbers. The reason for this is not clearly brought out in the reference. It is seen that all of their data lies fairly close to the isentropic curve, and they have concluded that the electron beam technique is in error at low temperatures since their measured rotational temperatures are above the predicted isentropic values. For example, when the isentropic temperature is predicted as 10 ^{o}K, their T_R value obtained from spectral data is about 13 ^{o}K, or 30% high. This is then referred to as a calibration point, i.e. T_R data must be multiplied by 0.70 to obtain correct values in this temperature range. However, the present data shows that the measured rotational

temperature can have numerous values depending on the value of ($P_o d$), when the isentropic prediction is 10 °K.

Robben and Talbot (Ref. 21) do point out one possible source of error associated with the electron beam technique, this is the effect of secondary electrons on the measured rotational temperature (i.e. the electrons stripped from N_2 to yield N_2^+ by collisions with the primary beam electrons). These secondary electrons will, in general, have much lower energies than those in the primary beam (Ref.14), but their actual energy distribution and direction are unknown.

Excitation to the excited ion state by secondary electrons may arise from direct excitation of the ground state molecule (similar to primary excitation) or excitation of the ground state ion. The potential energy curves schematically diagrammed in Section II (and given in detail in Ref. 31) show that electron energies in excess of 18.7 eV are needed to excite the ground state nitrogen molecule (N_2 $X^1\Sigma$) to the excited ion state (N_2^+ $B^2\Sigma$) while electrons with energies in excess of 3.1 eV are needed to excite the ground state ion (N_2^+ $X^2\Sigma$) to the excited ion state. Thus, as pointed out by Muntz (Ref. 14) for single collisions, secondaries with energies below 3.1 eV cannot produce any excitation. In addition, Muntz calculated that the secondary excitation of ground state ions (i.e. for electrons with energies in excess of 3.1 eV) may be neglected. For electrons with energies in excess of 18.7 eV, say in the 100 eV range, Muntz indicated that there could be a large contribution to the observed emission owing to direct excitation of the ground state molecule by these electrons. If this excitation is different in nature than the primary excitation (i.e. as suggested by Robben and Talbot (Ref. 21) that these excitations may not obey the optical selection rules), an error could be associated with the rotational temperature measurements.

The fluorescence excited by secondary electrons is confined to a halo surrounding the beam of primary electrons. Experiments performed by Muntz, Abel and Maguire (Ref. 17) in helium indicate the presence of a large number of secondary electrons, which appear to be concentrated near the center of the beam. As pointed out in Ref. 17, the contribution of secondary electrons to the emission excited by an electron beam must be determined as a function of radial distance from the beam axis for each gas. Thus, the magnitude of a possible error in the measurements may depend on how much of the halo is observed. The University of California experiments, with the slit perpendicualr to the beam, would gather more of this halo emission. Robben and Talbot report that their measurements seemed to show smaller errors when the spectrometer slit length was reduced (i.e. less halo observed). For the experimental data reported here, this "effective heating" due to possible secondary electrons is not apparent since the experimental temperatures agree with the isentropic curve down to low temperatures. This could be due to the fact that the spectrometer slit is parallel to the beam (i.e. views a narrow slice along the beam axis) and only a small portion of the halo within the optical cone is observed. A study of the excitation processes due to secondary electrons is needed to more fully understand the electron beam technique at low temperatures and densities.

There is, however, another trend that can be observed in the present rotational temperature data obtained in free jets. As seen in Fig. 15, the log slope plots of rotational line intensities are linear, using the majority of observed rotational lines at each data point. However, the higher K' rotational lines (those lightly populated) always indicated a higher intensity than was consistent with this straight line. This effect was also noted by

Robben and Talbot (Ref. 21) in a number of their published log plots. For a given rotational temperature as obtained from the straight line slope, it is always the higher rotational lines that show this apparent discrepancy of over population. Careful examination of all of the free jet spectral data obtained in this investigation indicated that the higher rotational levels seemed to depart from a Boltzmann equilibrium with the lower rotational levels in the expansion. This departure can be depicted in the following way: define a rotational "temperature" $\tilde{T}_{R_{K'}}$ based on the slope for each rotational line K' referred to the K' = 1 line as shown schematically

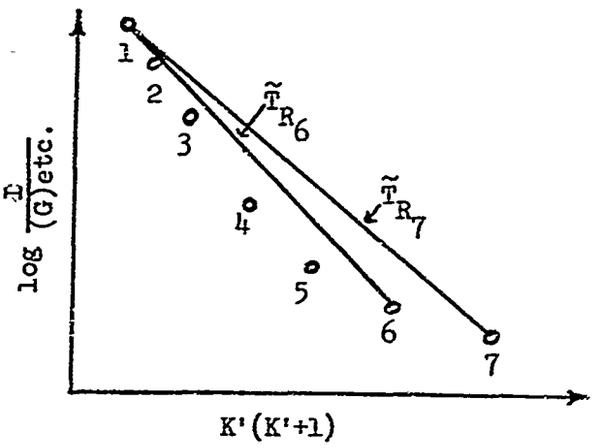

For a linear plot, (i.e. Boltzmann distribution in population of rotational levels), all $\tilde{T}_{R_{K'}}$ are equal and equal to the rotational temperature T_R. Thus, $\tilde{T}_{R_{K'}}$ is an indication of the population of a particular level referred to the lowest rotational level. These "temperatures" have been obtained from the spectral log plots (similar to those shown in Fig. 15) and plotted in Fig. 26. Again, where possible for each (P_od) value, results from two different orifices have been plotted, showing the same binary scaling as before. A general trend for each (P_od) curve seems to be a gradual peeling away of the $\tilde{T}_{R_{K'}}$ values for the higher levels during the expansion. The data indicates for example, that $\tilde{T}_{R_5}$ peels away at about 17°K, and the $\tilde{T}_{R_7}$ data peels away at approximately 40°K. Above this peeling away point for each K', these rotational lines lie on the linear portion of the log plot. It can be seen for example, that for P_od = 15 torr-mm, the K' = 7,5,3 points never depart, since the data does not go below 40°K (seemingly the $\tilde{T}_{R_7}$ departure point). Again for P_od = 80 torr-mm the K' = 5,3 curves never depart since the data is higher than 17°K (seemingly the $\tilde{T}_{R_5}$ departure point).

It may be surmised that there is no reason to expect that there would not be a departure from a Boltzmann distribution in a rapid expansion. A greater amount of theoretical and experimental work has been devoted to this problem for the case of vibrationally relaxing flows. The calculations of Treanor (Ref. 10), for example, indicate the possibility of a non-Boltzmann population distribution in vibrational levels during expansion. However, experimental results of vibrational relaxation, such as those of Hurle, Russo and Hall (Ref. 11), have as yet not confirmed this. In addition, the electron beam measurements of vibrational relaxation in arc-tunnel nozzles reported by Sebacher and Duckett (Ref. 19) and Petrie (Ref. 20) seem to agree with the results obtained using a line-reversal technique employed in Ref. 11. Further-

more, in the electron beam measurements, a Boltzmann distribution in vibration is assumed in order to relate the relative intensities of vibrational band systems to the vibrational temperature.

This aspect of the rotational temperature measurements leads to the possibility that the apparent rotational non-Boltzmann distribution indicated during the expansion process may be produced by the electron beam itself, perhaps by secondary electrons in some way. The author has found no studies or computations concerning the relaxation of individual levels. This would, of course, require the individual transition probabilities of each level to be known, so that a separate rate equation could be applied to each level during a relaxation process.

There is a possible way to determine experimentally whether or not this departure from a Boltzmann distribution is caused by the beam or is due to the expansion process. This would constitute shooting an electron beam into a chamber of stagnant low temperature nitrogen, in equilibrium, with its condensate at a very low temperature (say 30°K) and obtaining a rotational spectra. The log slope plot of the line intensities should reveal any non-Boltzmann effects due to secondary electrons. In addition, the rotational temperature obtained can be compared to the known temperature as a calibration check on the accuracy of this technique at low temperatures. An experiment of this type has been reported by Williams (Ref. 39) where an electron beam was used in conjunction with a liquid nitrogen cooled chamber. Temperatures as low as 80°K were obtained, with the beam fluorescence being monitored by a set of narrow pass-band filters within a single-vibration-rotation band, as originally described by Muntz and Abel (Ref. 40). Unfortunately, the reduction of data with this technique utilizes an assumed Boltzmann distribution in rotation. However, it has been reported to the author that additional experiments using a high dispersion spectrograph to monitor the beam fluorescence are being planned.

The shock wave profiles presented in Fig. 24 can also be represented by a $T_{RK'}$ for each rotational line. In order to make these more detailed calculations of "temperatures" for a non-linear log plot, iterations with (G), using various assumed values of T_R were employed. For the $T_{RK'}$ values representing the higher rotational levels (i.e. $K' > 9$), the T_R values given in Section IV were used to compute (G). For the lower levels, complete iterations using appropriate T_R guesses yielded more accurate results for these $T_{RK'}$ values. The results are shown in Fig. 27. The spread of "temperatures" $T_{RK'}$ is small for $M = 4$, since the departure from linearity in the log plot is small. However, as the Mach number increases, the spreading is readily apparent due to the highly non-linear log plots. For all three cases, a Boltzmann distribution (i.e. all $T_{RK'}$ are equal) is regained in tail of the shock wave.

Since the rotational energy distribution in the shock waves are markedly non-Boltzmann, one may suspect that this effect could be felt upstream of the shock and perturb the rotational distribution in the jet, possibly leading to the apparent non-Boltzmann effect discussed earlier. Robben and Talbot (Ref. 41), for example, have shown from their results that the average local temperature was found to precede the density profile through the shock wave by an amount which increased with Mach number. However, the presence of a shock wave in the flow did not affect this apparent non-Boltzmann distribution in the jet, as can be seen from Fig. 27(c). For the given ($P_o d$) flow condition, the position of the Mach disc is predicted to be at $x_M/d = 28$ and $x_M/d = 76$ for

P_o = 94 torr and P_o = 240 torr respectively. The two sets of results, however, agree very well. In addition, the presence of the M = 15 shock caused by the shock holder at x/d = 35 for the P_o = 240 torr case did not change the T_{R_K} distribution. Within the experimental scatter, the T_{R_K} curves with the shock wave present agree with the pure jet results. This seems to indicate that the presence of a shock (either the Mach disc or a shock caused by the shock holder) did not influence this apparent non-Boltzmann distribution in the expansion.

Another interesting aspect of the shock wave structure is the density profile data presented in Fig. 22, which indicates that the beam fluorescence probe can be used to measure shock wave thickness. To compare the shock thickness obtained for the M = 3.9 and M = 11.5 shock waves presented in Fig 22, reference will be made to the procedure of Robben and Talbot (Ref. 42). A maximum slope thickness δ_m was obtained by drawing a straight line through the maximum slope of the density profile, and measuring the distance between the intersections of this line with the extrapolations of the upstream and downstream flow conditions, i.e.:

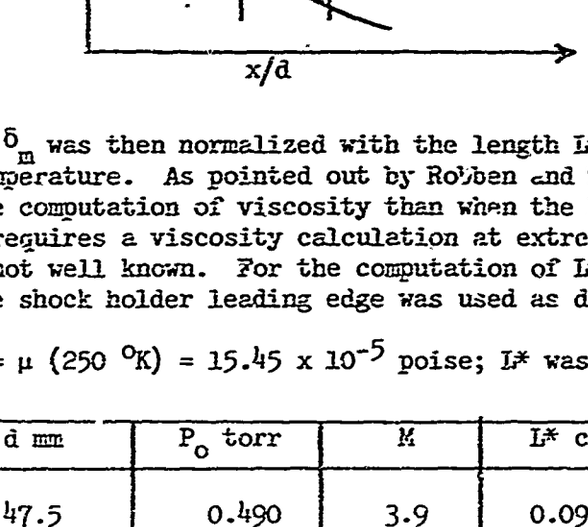

This length δ_m was then normalized with the length $L^* = \mu(T^*)/\rho u$, where T* is the sonic temperature. As pointed out by Robben and Talbot, using T* allows a more accurate computation of viscosity than when the local mean free path is used, which requires a viscosity calculation at extremely low temperatures, where it is not well known. For the computation of L*, the isentropic Mach number at the shock holder leading edge was used as discussed in Section 3.3.

Using $\mu(T^*) = \mu\ (250\ ^oK) = 15.45 \times 10^{-5}$ poise; L* was computed as:

d mm	P_o torr	M	L* cm
47.5	0.490	3.9	0.0987
5	59	11.5	0.0865

Referring to Fig. 22, the maximum slope thickness was obtained as:

M	Δ(x/d)	δ_m cm.	L^*/δ_m
3.9	1.93 - 1.76 = .17	0.808	0.123
11.5	17.2 - 15.2 = 2.0	1.0	0.087

To compare the values of L^*/δ_m obtained in the present study with other results, Fig. 5 from Ref. 42 is presented below with the new data added.

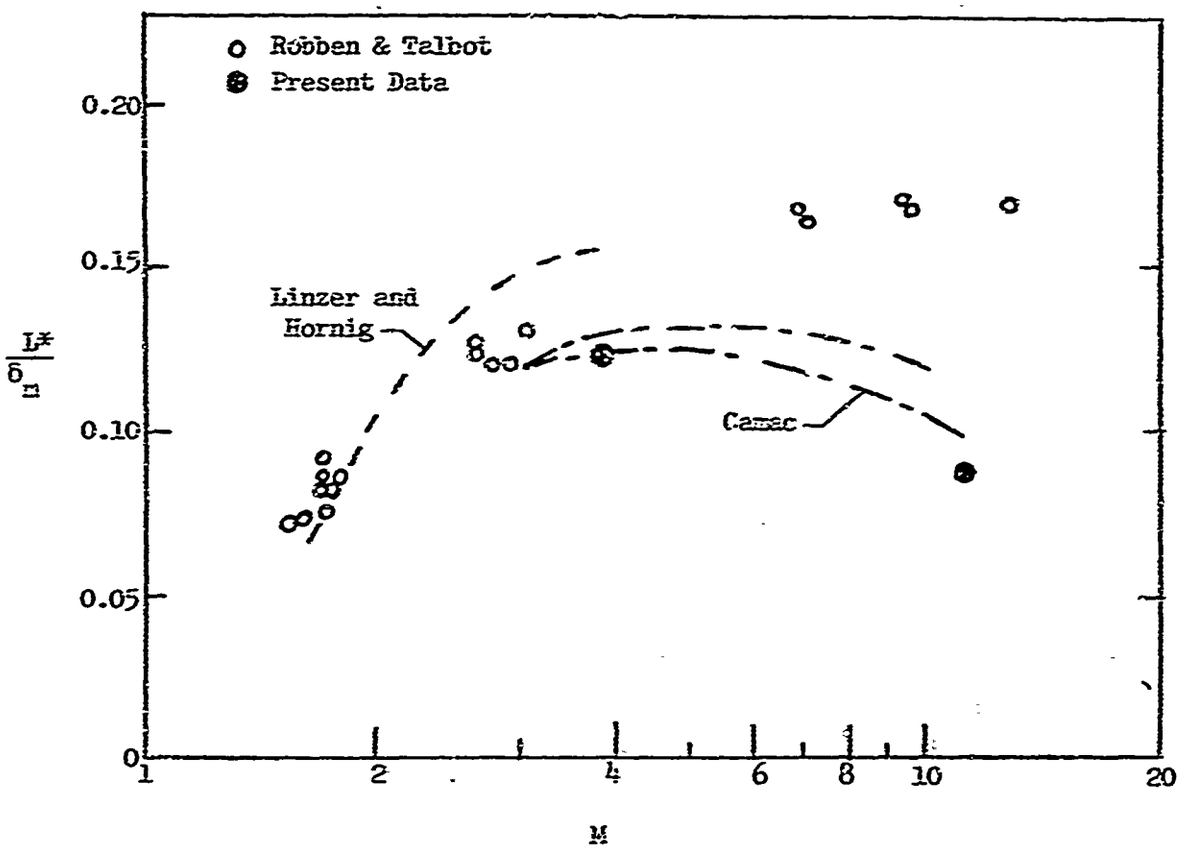

At the lower Mach number, the thickness seems to agree well with the other data. However, at M = 11.5, the present L^*/δ_m data is about 1/2 of that obtained by Robben and Talbot, but very close to that of Camac (Ref. 27) normalized with L^*. As pointed out in Ref. 42, the large discrepancy between Camac's data and that of Robben and Talbot is not clear. The indication here, however, is that the present data follows that obtained by Camac, who measured the scattered electrons from an electron beam probe in a shock tube.

One other possible source of error in the free jet temperature measurements could be condensation effects at low temperatures - that is, molecules coming together to form agglomerates consisting of large numbers of molecules. These may be expected to form, since the conditions of low temperature and pressure that exist in a free jet expanding from room temperature are well below the nitrogen triple point (i.e. 68 °K and 96.4 mm Hg). However, the pressures are so low in a free jet, that the expansion occurs such that nitrogen remains a gas to a much lower temperature than the triple point temperature indicated in the sketch.

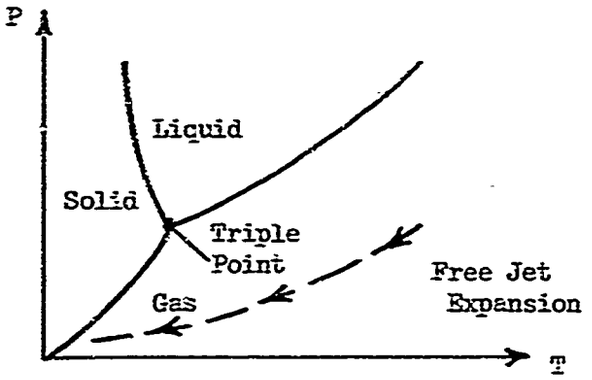

The vapor pressure of nitrogen is a strong function of temperature at these low temperatures, as shown in Fig. 28 (taken from Ref. 43). Using this figure, and the isentropic ($\gamma = 1.4$) temperature and density relations for a free jet, possible condensation points were obtained for various values of stagnation pressure. These are shown in Fig. 29.

The condensation process involves three body collisions in the formative stages (i.e. the third particle carries away the heat of sublimation, thus raising the gas temperature slightly), so will be a strong function of density (i.e. α n^2). Thus, higher stagnation pressures will foster the onset of condensation. Greene and Milne (Ref. 44), for example, report observations of polymeric species for a large number of gases, including nitrogen, in a supersonic molecular beam system expanding from room temperature. Small effects were noted at 1 atm. stagnation pressure, with more pronounced polymeric action at 5 atm. pressure. Additional skimmer experiments, performed by Bier and Hagena (Ref. 45) indicate the onset of condensation at higher stagnation pressures. With a nozzle diameter of .05 mm, an upper limiting value of ($P_o d$) = 500 torr-mm for nitrogen was found to yield non-condensed beams. This, however, means a stagnation pressure (P_o) of about 13 atm. Ashkenas and Sherman (Ref. 6) report that for stagnation pressures up to 1 atm. no condensation effect has been seen on impact probe measurements. A compilation of condensation measurements obtained in wind tunnels and arc heated nozzles is given by Cassanova and Stephenson (Ref. 46), which indicates a high degree of super-saturation at low temperatures.

Since the condensation process is a strong function of density, it may be possible to determine from the rotational temperature results if this effect is present. Again, in general the trend of decreasing T_R with increasing density seems counter to any condensation effect. A stronger point can be made once again by referring to the scaling for binary collisions existing for two nozzle diameters used at the same ($P_o d$) value. Increasing the stagnation pressure by a factor of 2-1/2 at each ($P_o d$) value does not destroy the scaling. It can be noticed from the data that for a given diameter, the ($P_o d$) curves get closer together as the pressure increases, and it may be expected that at a high enough pressure, the trend may reverse itself. That is, at very high values of ($P_o d$), the curves would show an increasing rotational temperature due to condensation effects. For a quick check on this, a number of data points were taken for ($P_o d$) = 630 and 930 torr-mm, corresponding to stagnation pressures of 815 and 1200 torr respectively (with a 0.75 mm diameter nozzle). At x/d values greater than about 25, these data agreed approximately with the

$(P_o d)$ = 480 torr mm curve shown in Fig. 16. At lower x/d values, the data increased and rose above the $(P_o d)$ = 480 curve. It should be noted that at these high pressures, the electron beam itself was scattered, leading to a very wide fluorescence. Spatial resolution was destroyed, especially with the very small nozzle, and part of the barrel shock may even have been observed at small x/d values because the size of the flow field was very small in that region. Thus, the high pressure results are inconclusive, except possibly at large values of x/d.

Thus, based on the discussion of pressure dependence, and the fact that the stagnation pressures reported for the present data were less than 240 torr (i.e. 1/3 atm.), it is felt that condensation plays no role in the rotational temperature departure from equilibrium.

The experimental rotational temperature results can be compared to rotational freezing values predicted by Knuth (Ref. 13), in which a freezing criterion similar to that used in chemically reacting and vibrationally relaxing expansions was used. The freezing point for rotational energy is defined as the point at which

$$\frac{De_R}{Dt} = \frac{e_R}{\tau_R} \tag{7}$$

where e_R is the rotational energy, and τ_R is the rotational relaxation time. If the rotational heat capacity can be considered as constant, then Eq. 7 may be rewritten

$$\left|\frac{DT}{Dt}\right| = \frac{T}{\tau_R} \tag{8}$$

If the magnitude of DT/Dt is either smaller or greater than T/τ_R, then the rotational energy may be considered as in equilibrium with translation, or frozen. The relaxation time τ_R was estimated from viscosity calculations using the Buckingham (6-Exp.) potential, and assuming a value for Z_R, the number of collisions required for rotational relaxation, i.e.

$$Z_R = \tau_R \nu \tag{9}$$

where ν is the collision frequency. Using a value of Z_R = 5.3 collisions from room temperature measurements, and employing the isentropic free jet relations, Knuth has predicted rotational freezing conditions in free jets. To compare the present experimental rotational temperature data with Knuth's predicted frozen values, a T_R freeze value is defined as the asymptote for each experimental $(P_o d)$ curve, i.e.

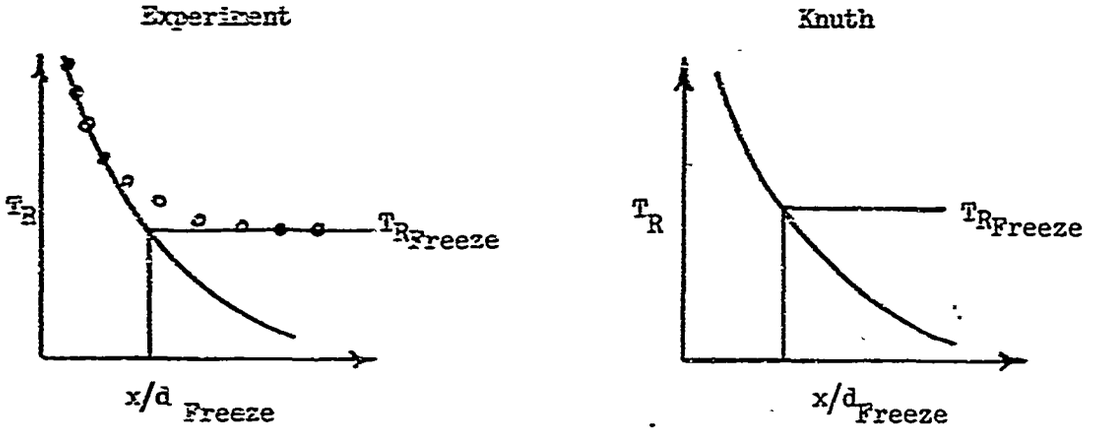

This comparison is shown in Fig. 30 for both the freeze point in the free jet (x/d freeze), and the rotational temperature at freezing (T_R freeze). It is seen that the rotational temperature results at low values of ($P_o d$), i.e. $P_o d < 50$ torr-cm, are in general agreement with Knuth's predictions use a collision number of $Z_R = 5.3$. However, at lower temperatures, typified by the higher ($P_o d$) data, a larger value of Z_R is required in the freezing criterion to match the experimental results. Using a value of $Z_R = 10$ collisions, Knuth's prediction of T_R freeze agrees more closely with the experimental values for temperature below about 20 °K.

Sufficiently far downstream of the orifice for a given stagnation pressure, the density may become low enough that translational freezing may occur, i.e. the free jet undergoes a transition to a collisionless free molecule flow. As used in the present experiments, the electron beam probe will not measure this directly, since it is the rotational energy distribution that is observed in the beam fluorescence. Computations were performed to obtain a rough estimate of where translational freezing might occur for some of the present free jet experiments. Again, the procedure discussed by Knuth (Ref. 13) was used. Using the predicted rotational freeze point as calculated by Knuth, it was assumed that the expansion proceeded from this point, now with a $\gamma = 5/3$. The "effective" source conditions of pressure and temperature, as well as "effective" source orifice diameter, were computed for this expanding $\gamma = 5/3$ gas using Knuth's relations. These equations were obtained for a given streamtube by matching conditions at the rotational freeze point for a sudden change in γ from 7/5 to 5/3. With this new expansion the translational freeze point was predicted, see Ref. 13. In addition, the prediction for terminal (i.e. freeze) Mach number for a monatomic gas was obtained from the work of Anderson, Andres, Fenn and Maise (Ref. 47). A correlation between terminal Mach number and source Knudson number was given in Ref. 47 as a linear function of $Kn_d^{-(\gamma-1)/\gamma}$ for argon free jets. Using the "effective" source values to obtain $(Kn_d)_{effective}$, the terminal Mach number was computed for the new expanding $\gamma = 5/3$ gas. The results of these computations are indicated below:

$P_o d$ torr-mm	d mm	Approx. M_{T_r} freeze Knuth	Approx M_{T_r} freeze Anderson, et al	Approx. x/d freeze Knuth
15	5	9	8.5	8
40	5	12	12	15
80	5	14.5	14	24
250	5	18	20	35

On the basis of these approximate calculations, it can be seen from referring to Fig. 16, that translational freezing may be occurring for the final few temperature points at each $P_o d$ (reference should be made to the data obtained with the 5 mm orifice). The possibility of translational freezing, then, should be considered when analyzing the rotational temperature data in Fig. 16.

Based on the experimental results, and the preceding discussions concerning the data, the following conclusions are stated:

1. Rotational nonequilibrium has been observed in underexpanded jets of room temperature nitrogen. A systematic experimental survey indicates that the rotational temperature follows the isentropic temperature curve to lower values as the density is increased.

2. The electron beam fluorescence technique may be used at low temperatures to obtain rotational temperatures in nitrogen. The scatter about the isentropic temperature down to about 70°K is comparable to room temperature scatter, approximately $\pm$ 3%.

3. Effects of secondary electrons in contributing to a systematic error in the rotational temperature measurements (i.e. "effective heating") were not observed in the present investigation.

4. Possible effects of secondary electrons may contribute to the apparent departure from a Boltzmann distribution in rotational levels measured during a rapid expansion. An experiment performed in a low temperature, stagnant gas should contribute more information on this phenomenon.

5. The population in rotational levels becomes highly non-Boltzmann in the center of shock waves. This effect becomes more pronounced as the flow Mach number is increased.

6. Measurements in free jets have shown the density to follow the isentropic curve in rotational nonequilibrium flow, following a radial source distribution. The Mach disc at low pressures was found to be very diffuse.

7. The beam fluorescence technique can be used to obtain density profiles through shock waves. The shock thickness data obtained in the present study agree quite well with the results obtained in shock tubes.

REFERENCES

1. French, J.B. — Continuum-Source Molecular Beams. AIAA Journal 3, 993-1001 (June 1965).

2. Owen, P.L. Thornhill, G.K. — The Flow in an Axially Symmetric Supersonic Jet from a Nearly Sonic Orifice into Vacuum. Aeronautical Research Council, United Kingdom, R&M 2612 (1948).

3. Love, E.S. Grigsby, C.E. Lee, L.P. Woodling, M.J. — Experimental and Theoretical Studies of Axisymmetric Free Jets. NASA TR R-6 (1959).

4. Vick, A.R. Andrews, E.H. Jr. Dennard, J.S. Craidon, C.B. — Comparisons of Experimental Free-Jet Boundaries With Theoretical Results Obtained with the Method of Characteristics. NASA TN D-2327 (1964).

5. Sherman, F.S. — Self-Similar Development of Inviscid Hypersonic Free-Jet Flows. Lockheed Rept. 6-90-63-61 (1963).

6. Ashkenas, H. Sherman, F.S. — The Structure and Utilization of Supersonic Free Jets in Low Density Wind Tunnels. Rarified Gas Dynamics, edited by J.H. deLeeuw (Academic Press, N.Y. to be published).

7. Hall, J.G. Eschenroeder, A.Q. Marrone, P.V. — Inviscid Hypersonic Air Flows With Coupled Non-Equilibrium Processes. IAS preprint 62-67 (Jan. 1962).

8. Stollery, J.L. Smith, J.E. — The Effects of Vibrational Relaxation on Hypersonic Nozzle Flows. Journal of Fluid Mechanics, Vol.13, p. 225 (1962).

9. Bray, K.N.C. — Coupling Between Atomic Recombination and Vibrational Relaxation in Expanding Gas Flows. Univ. of Southampton, Dept. of Aeronautics and Astronautics Report No. 260 (September, 1964).

10. Treanor, C.E. — Coupling of Vibration and Dissociation in Gas Dynamic Flows. AIAA Paper 65-29. 2nd Aerospace Sciences Meeting, New York (January 1965).

11. Hurle, I.R. Russo, A.L. Hall, J.G. — Spectroscopic Studies of Vibrational Non-Equilibrium in Supersonic Nozzle Flows. Journal of Chemical Physics, Vol.40, No.8, P.2076 (15 April 1964).

12. Nagamatsu, H.T. Sheer, R.E. Jr. — Vibrational Relaxation and Recombination of Nitrogen and Air in Hypersonic Nozzle Flows. AIAA Journal, 3, 1386-1391 (August 1965).

13. Knuth, E.L. — Rotational and Translational Relaxation Effects in Low-Density Hypersonic Free Jets. Univ. of California (Los Angeles) Report No. 64-53 (1964).

14. Muntz, E.P. — Measurement of Rotational Temperature, Vibrational Temperature, and Molecule Concentration, in Non-Radiating Flows of Low Density Nitrogen. Univ. of Toronto, Inst. for Aerospace Studies, UTIA Report No. 71 (1961). Also: Phys.Fluids, 5, 80 (1962).

15. Muntz, E.P. Marsden, D.J. — Electron Excitation Applied to the Experimental Investigation of Rarified Gas Flows. 3rd Int'l Rarified Gas Dynamics Symposium. Academic Press,N.Y. (1963).

16. Marsden, D.J. — The Measurement of Energy Transfer in Gas-Solid Surface Interactions Using Electron Beam Excited Emissions of Light. Univ. of Toronto, Inst. for Aerospace Studies, UTIAS Report No. 101 (1964).

17. Muntz, E.P. Abel, S.J. Maguire, B.L. — The Electron Beam Fluorescence Probe in Experimental Gas Dynamics. General Electric Space Sciences Laboratory, 1965. IEEE Conference on Aerospace. Houston, July 1965.

18. Sebacher, D.I. — Study of Collision Effects Between the Constituents of a Mixture of Helium and Nitrogen Gases when Excited by a 10-keV Electron Beam. J. Chem. Phys. 42, 1368-1372 (February 15, 1965).

19. Sebacher, D.I. Duckett, R.J. — A Spectrographic Analysis of a 1-Foot Hypersonic-Arc-Tunnel Airstream Using an Electron Beam Probe. NASA TR R-214 (December 1964).

20. Petrie, S.L. — Flow Field Analysis in a Low Density Arc-Heated Wind Tunnel. Proceedings of the 1965 Heat Transfer and Fluid Mechanics Institute. Stanford Univ. Press (1965)

21. Robben, F. Talbot, L. — Some Measurements of Rotational Temperatures in a Low Density Wind Tunnel Using Electron Beam Fluorescence. Univ. of California (Berkeley) Report No. AS-65-5(1965).

22. Sherman, F.S. — A Low Density Wind-Tunnel Study of Shock-Wave Structure and Relaxation Phenomena in Gases. NASA TN 3298 (1955).

23. Linzer, M. Hornig, D.F. — Structure of Shock Fronts in Argon and Nitrogen. Phys. Fluids, 6,1661-1668 (December 1963).

24. Ballard, H.N. Venable, D. — Shock-Front-Thickness Measurements by an Electron Beam Technique. Phys. Fluids, 1, (May-June 1958).

25. Russell, D.A. — Shock-Thickness Measurements in the Galcit 17-Inch Shock Tube. Rarified Gas Dynamics, Edited by J.H. de Leeuw. (Academic Press, N.Y. To be published).

26. Schultz-Grunow, F. Frohn, A. — Density Distribution in Shock Waves Travelling in Rarified Gases. Rarified Gas Dynamics, Edited by J.H. de Leeuw (Academic Press, N.Y. to be Published).

27. Camac, M. — Argon and Nitrogen Shock Thicknesses. AIAA Paper No. 64-35. Aerospace Sciences Meeting, New York, Jan. 1964.

28. Davidson, G. O'Neil, R. — The Fluorescence of Air and Nitrogen Excited by 50 keV Electrons. Americal Science and Engineering, Inc. Report AFCRL-64-466 (May 1964).

29. Nicholls, R.W. — Einstein A Coefficients, Oscillator Strengths and Absolute Band Strengths for the N_2 Second Positive and N_2^+ First Negative Systems. J. Atmos and Terr. Phys. 25, 218-221 (1963).

30. Gadamer, E.O. — Measurement of the Density Distribution in a Rarified Gas Flow Using the Fluorescence Induced by a Thin Electron Beam. Inst. for Aerospace Studies, Univ. of Toronto, UTIA Report No. 83 (1962).

31. Gilmore, F.R. — Potential Energy Curves for N_2, NO, O_2 and Corresponding Ions. Rand. Corporation Memorandum RM-4034-PR (1964).

32. Herzberg, G. — Molecular Spectra and Molecular Structure, I. Spectra of Diatomic Molecules. D. Van Nostrand Co., Princeton (1950).

33. Childs, W.H.J. — Perturbation and Rotation Constants of Some First Negative Nitrogen Bands. Proc. Roy.Soc. Series A, Vol. 137, No. A833, p. 641 (1932).

34. Enkenhus, K.R. — The Design, Instrumentation and Operation of the UTIA Low Density Wind Tunnel. Univ. of Toronto, Institute for Aerospace Studies, UTIA Report No. 44 (1957).

35. Rothe, D.E. Marrone, P.V. — Shock Structure Determination With an Electron Beam Probe. Univ. of Toronto, Inst. for Aerospace Studies, Annual Progress Report, Oct. 1964.

36. Fastie, W.G. — Image Forming Properties of the Ebert Monochromater. J. Opt. Soc. of America 42, 647-651 (1952).

37. Rothe, D.E. — Flow Visualization Using a Traversing Electron Beam. AIAA Journal, Vol. 3, No. 10, p-1945 (Oct. 1965).

38. Rothe, D.E. — On the Diffusive Separation of Gas Mixtures in Free Jets and Shock Waves. Presented at APS, Division of Fluid Dynamics Meeting, Cleveland, Ohio (November 1965). Also UTIAS (Toronto) Report to be published.

39. Williams, W.D. — Status of Free Stream Rotational Temperature Measurements in the Von Karman Facility. Presented at the 24th Supersonic Tunnel Association Meeting, Hawthorne, California (November 1965).

40. Muntz, E.P.
Abel, S.
The Direct Measurement of Static Temperatures in Shock Tunnel Flows. General Electric, Space Sciences Laboratory. Report No. R64SD25 (April 1964).

41. Robben, F.
Talbot, L.
An Experimental Study of the Rotational Distribution Function of Nitrogen in a Shock Wave. Univ. of California (Berkeley). Report No. AS-65-6 (1965).

42. Robben, F.
Talbot, L.
Measurement of Shock Wave Thickness by the Electron Beam Fluorescence Method. Univ. of California (Berkeley). Report No. AS-65-4 (1965).

43. French, J.B.
Muntz, E.P.
Design Study of the UTIA Low Density Plasma Tunnel. Univ. of Toronto, Inst. for Aerospace Studies.
UTIA Tech. Note No. 34 (1960).

44. Greene, F.T.
Milne, T.A.
Mass Spectrometric Detection of Polymers in Supersonic Molecular Beams. J. Chem. Phys. 39, 3150-3151 (December 1963).

45. Bier, K.
Hagena, O.
Optimum Conditions for Generating Supersonic Molecular Beams. Rarified Gas Dynamics, Edited by J. H. de Leeuw (Academic Press, N.Y. to be published).

46. Cassanova, R.A.
Stephenson, W.B.
Expansion of a Jet into Near Vacuum. Arnold Engineering Development Center, Report No. AEDC-TR-65-151 (August 1965).

47. Anderson, J.B.
Andres, R.P.
Fenn, J.B.
Maise, G.
Studies of Low Density Supersonic Jets. Presented at Fourth International Symposium on Rarified Gas Dynamics. Toronto, Ontario (July 1964).

T_R, °K \ K'	1	2	3	4	5	6	7
62	-.037	-.0295	-.017	0	.015	.0375	.061
50	-.043	-.033	-.0145	.0078	.0334	.0665	.10
40	-.053	-.034	-.0078	.025	.064	.112	.156
30	-.0675	-.0334	.0128	.0682	.135	.204	.279
20	-.0865	-.016	.078	.186	.301	.422	.551
15	-.098	.054	.169	.332	.496		
10	-.095	.138	.394	.653	.91		
8	-.075	.244	.574				

TABLE I VALUES OF $\log_{10}$ [G] AT LOW ROTATIONAL TEMPERATURES

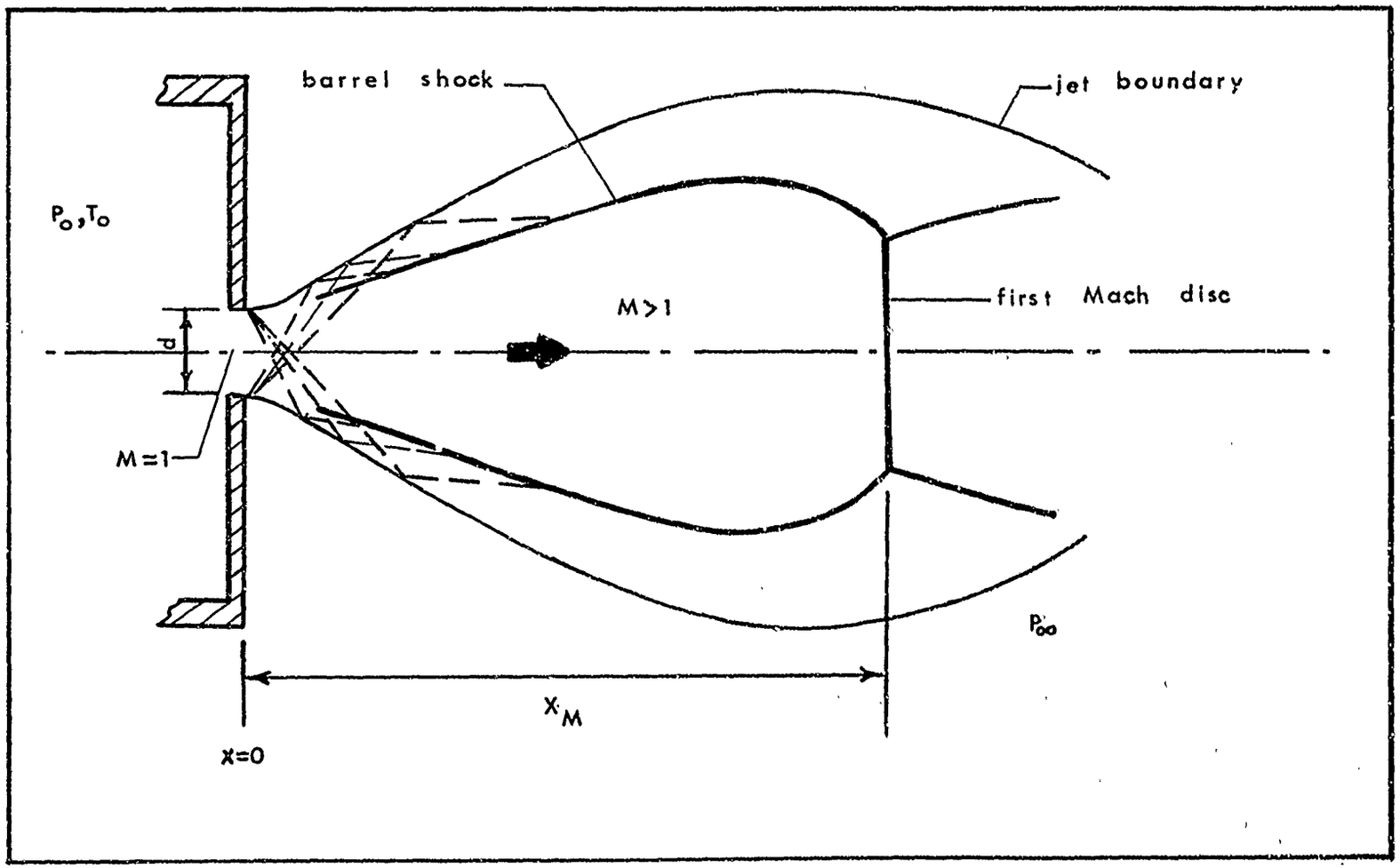

FIG. 1 SCHEMATIC OF AN UNDEREXPANDED JET ISSUING FROM A SONIC ORIFICE

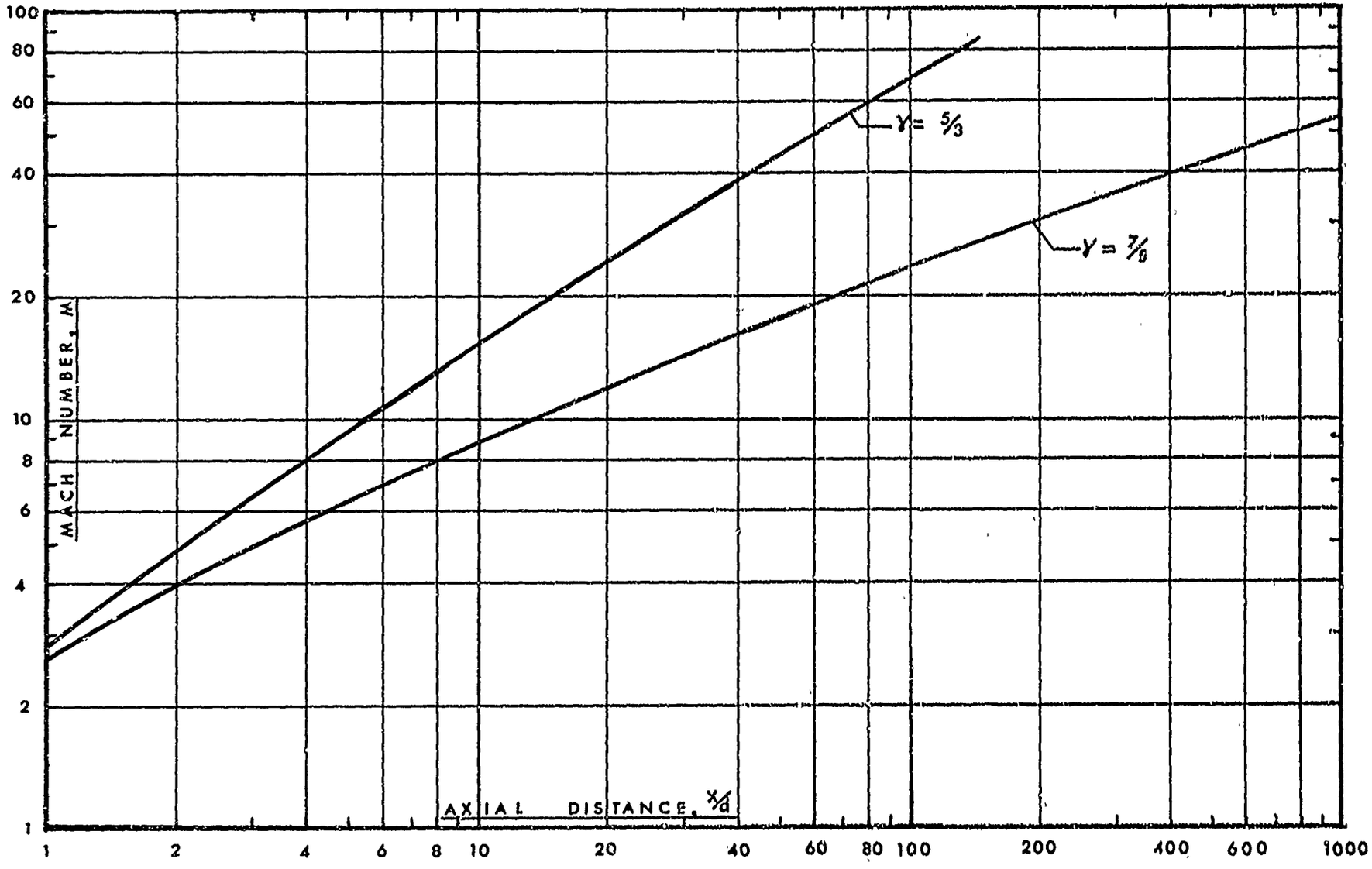

FIG. 2 MACH NUMBER DISTRIBUTION ALONG AXIS OF FREE JET

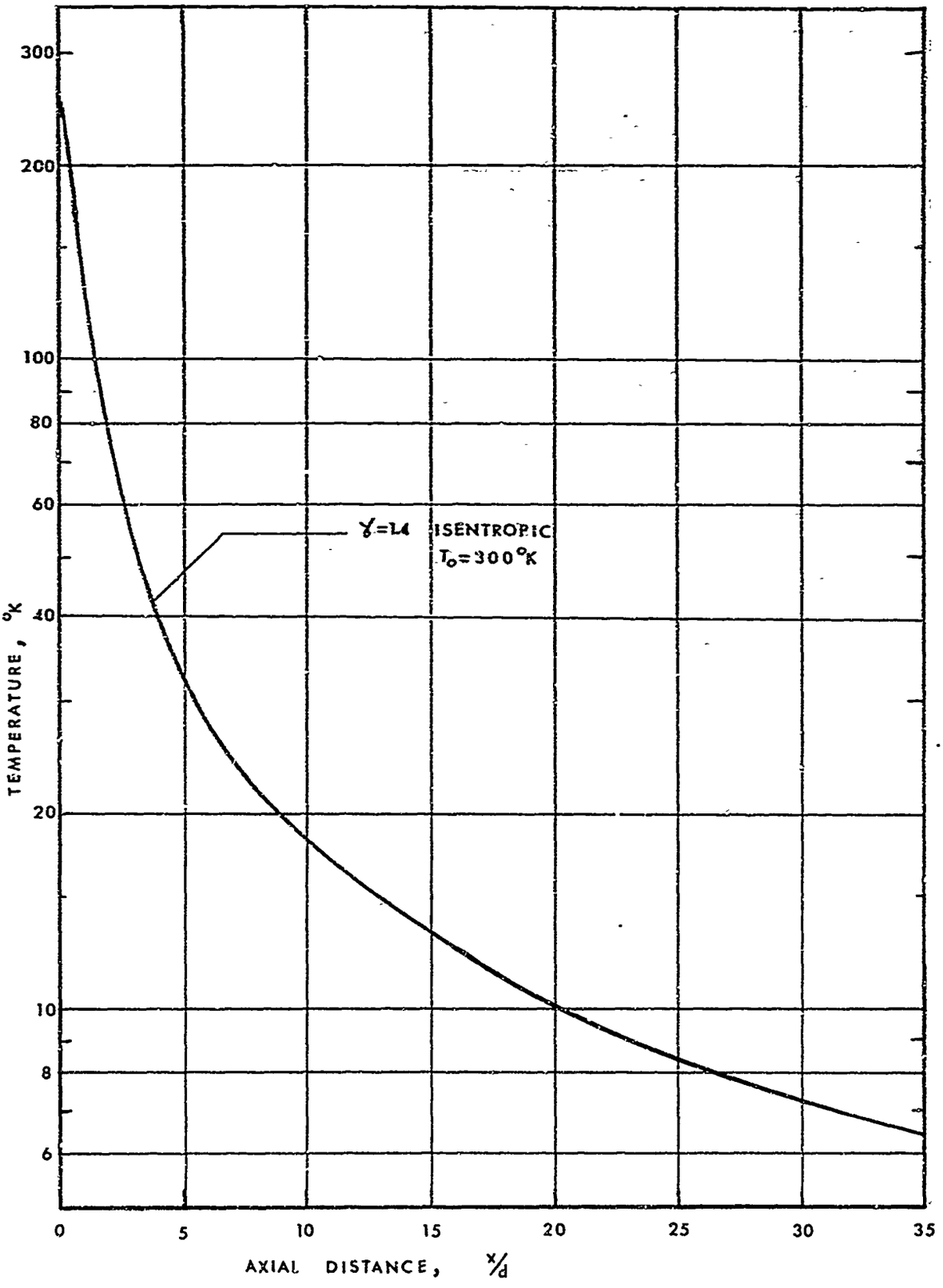

FIG. 3 TEMPERATURE DISTRIBUTION ALONG AXIS OF FREE JET

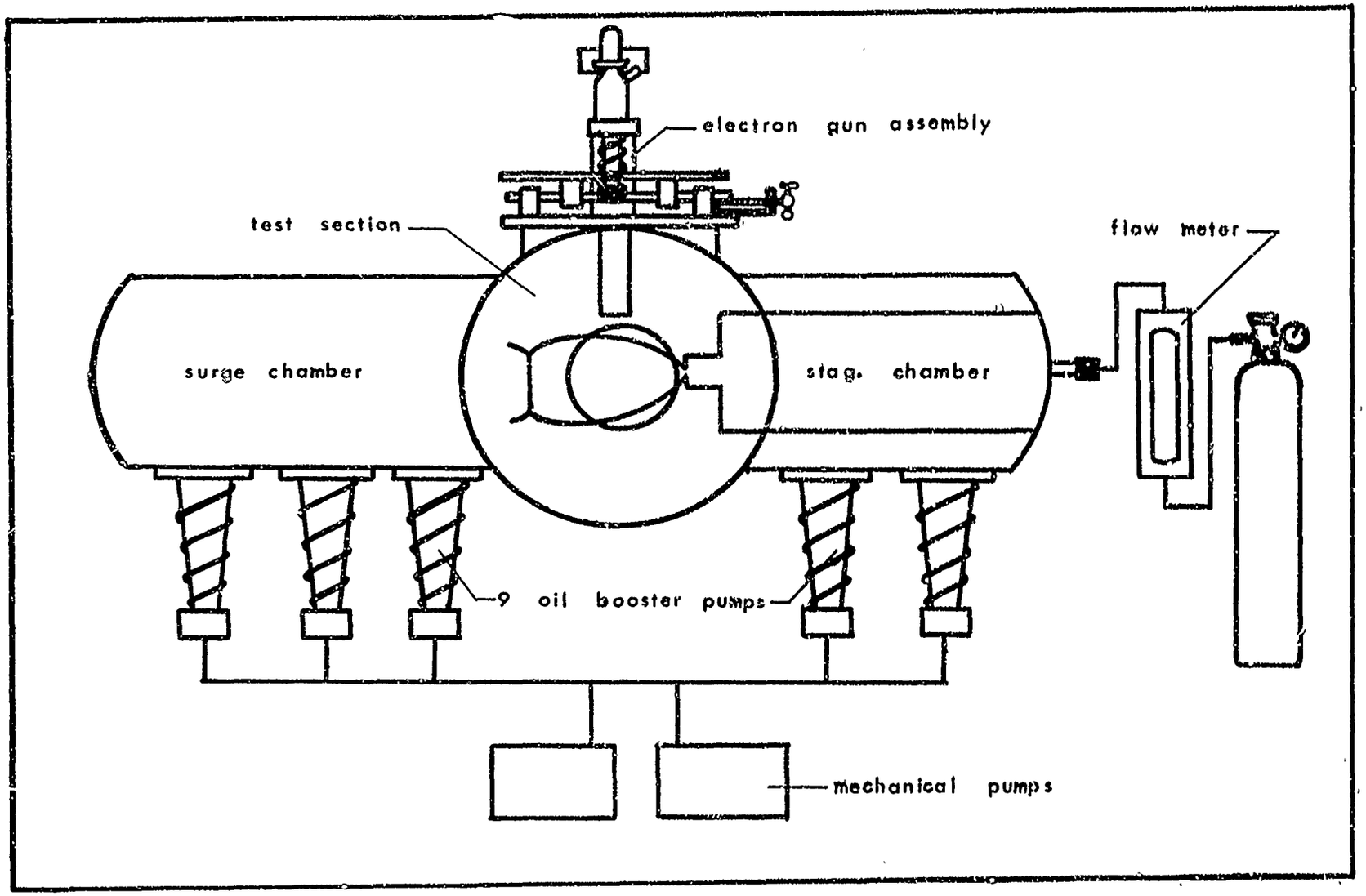

FIG. 4 SCHEMATIC OF UTIAS LOW DENSITY WIND TUNNEL

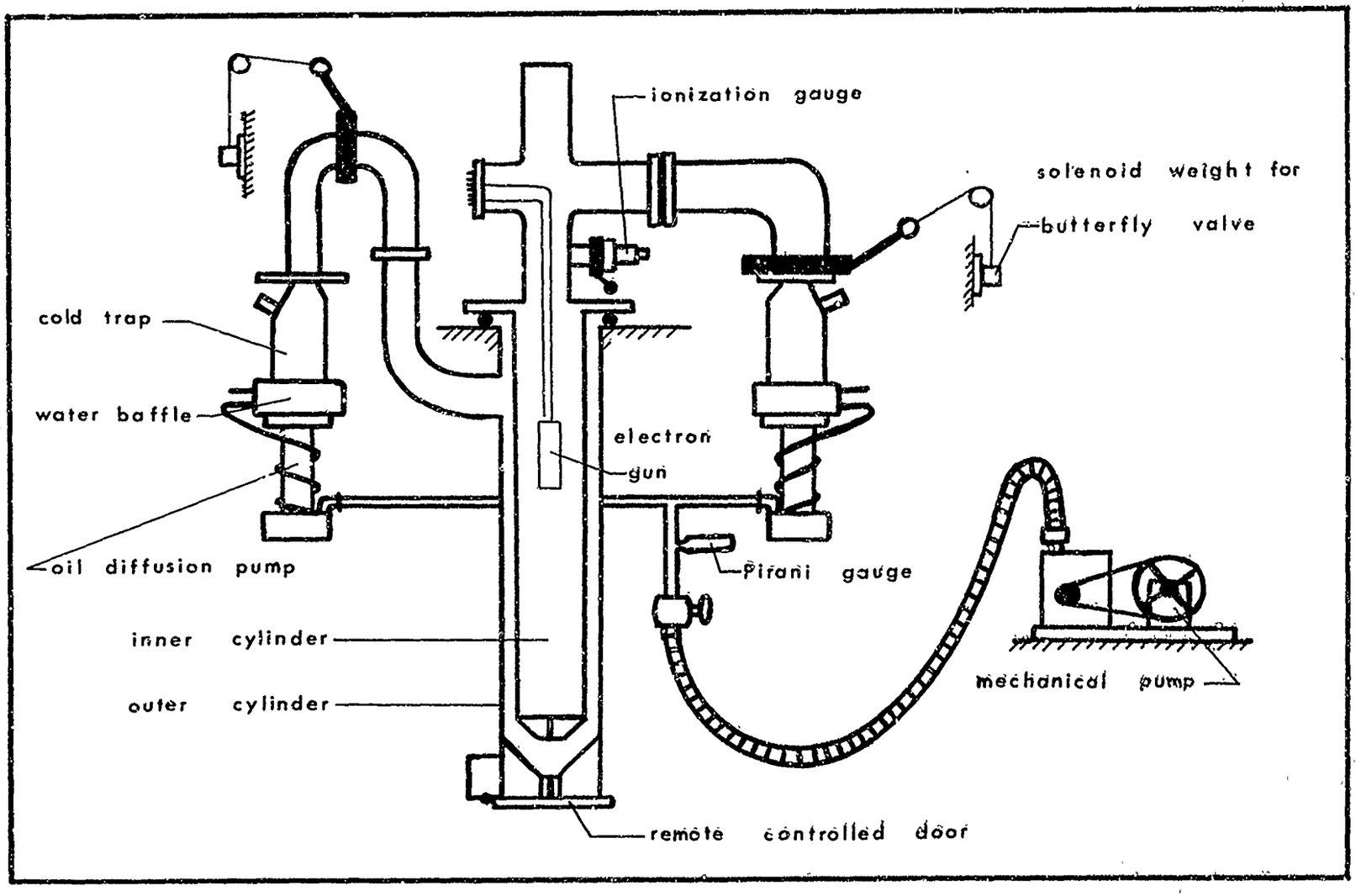

FIG. 5 SCHEMATIC OF VACUUM SYSTEM FOR THE ELECTRON GUN

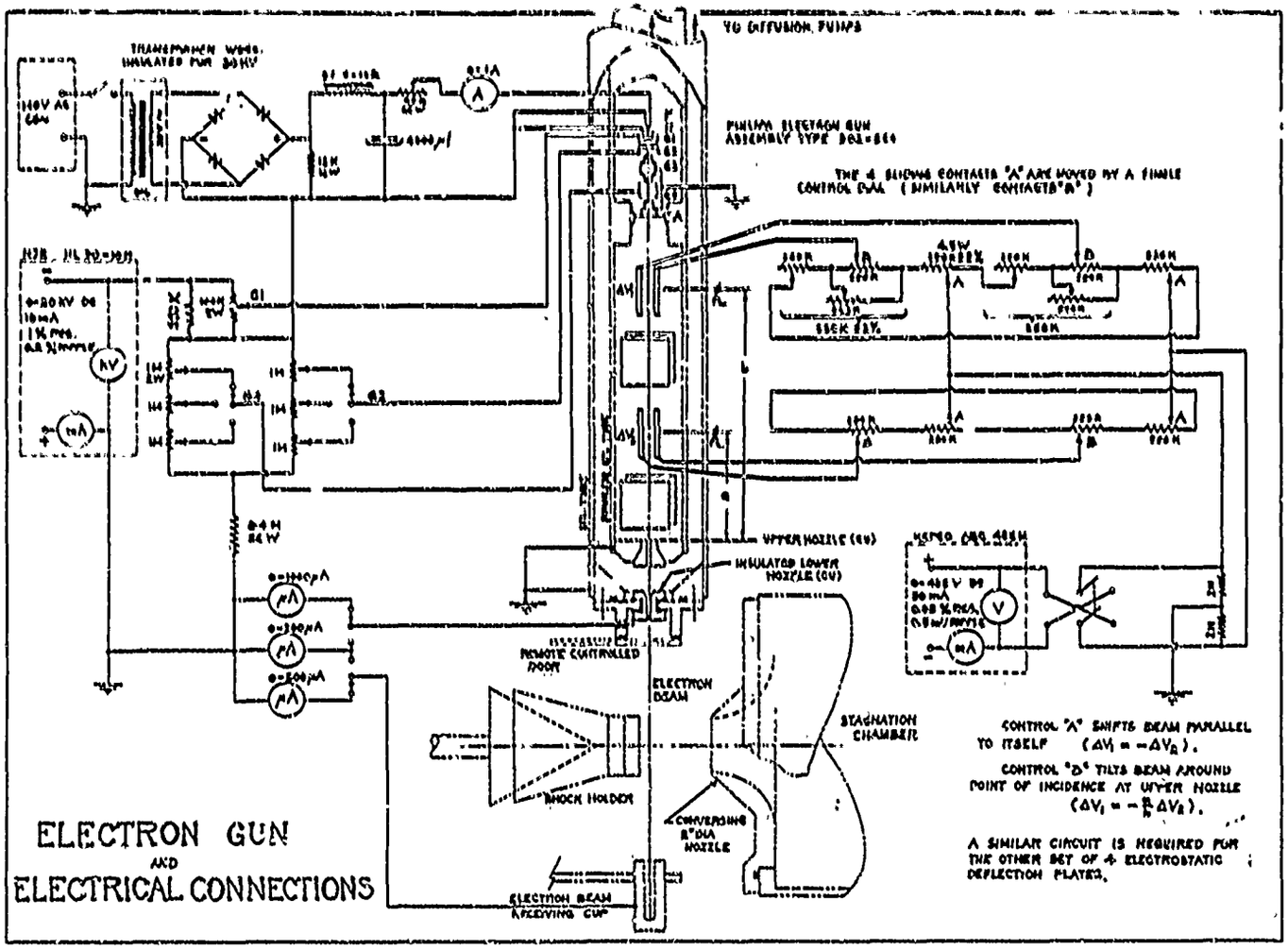

FIG. 6 ELECTRON GUN WIRING SCHEMATIC

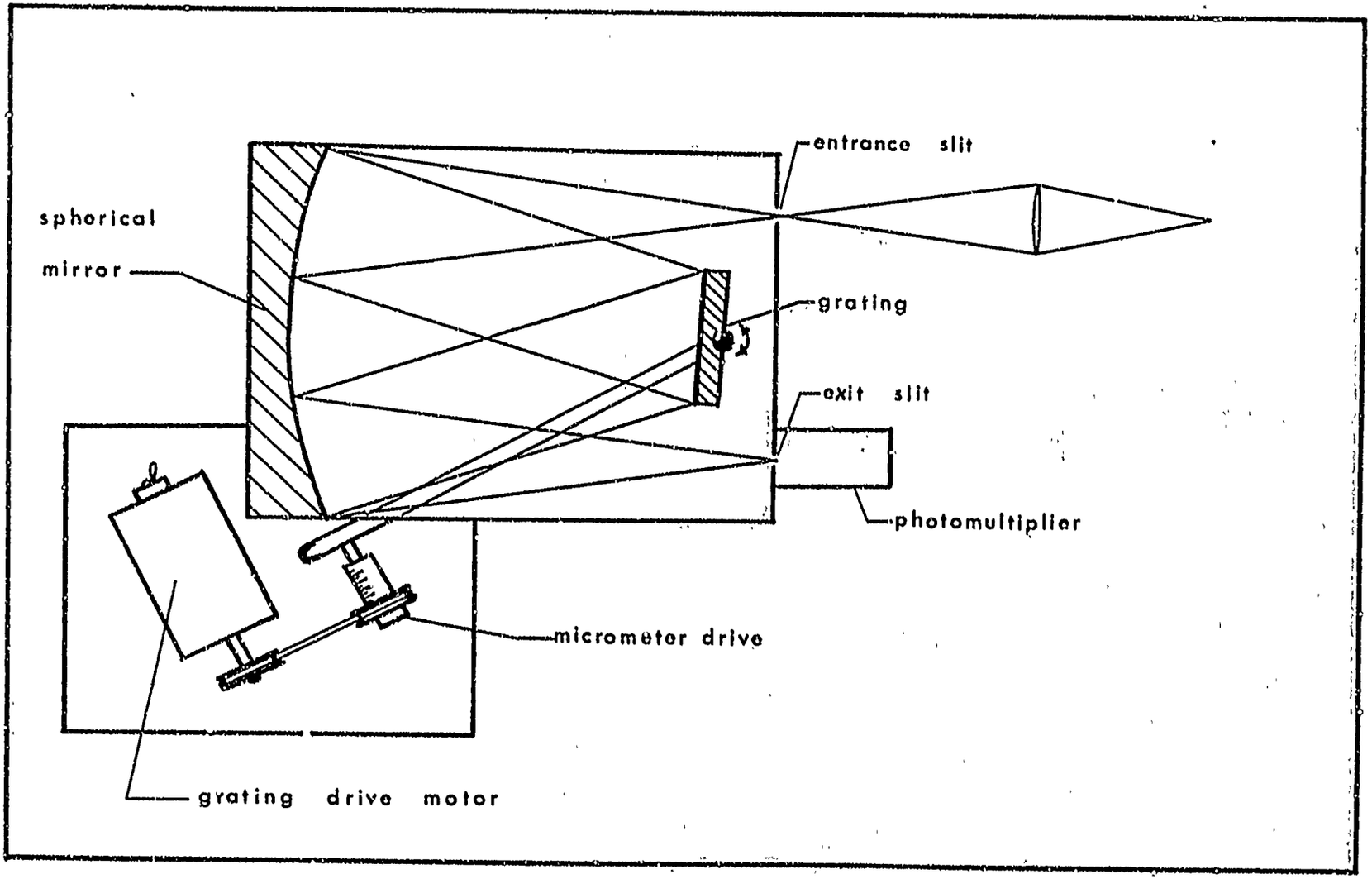

FIG. 7 SCHEMATIC OF SPECTROMETER

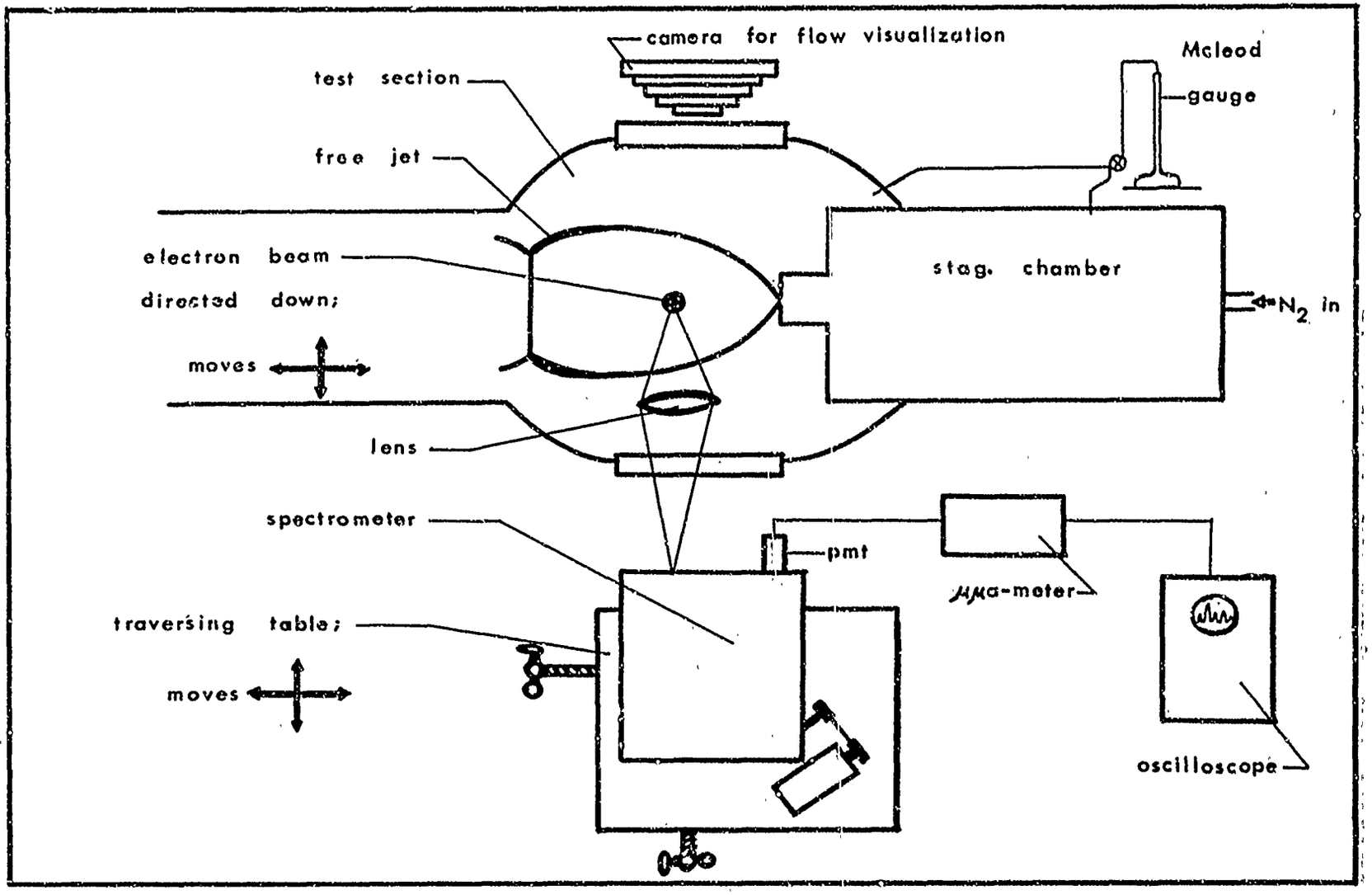

FIG. 8 TOP VIEW SCHEMATIC OF EXPERIMENTAL APPARATUS

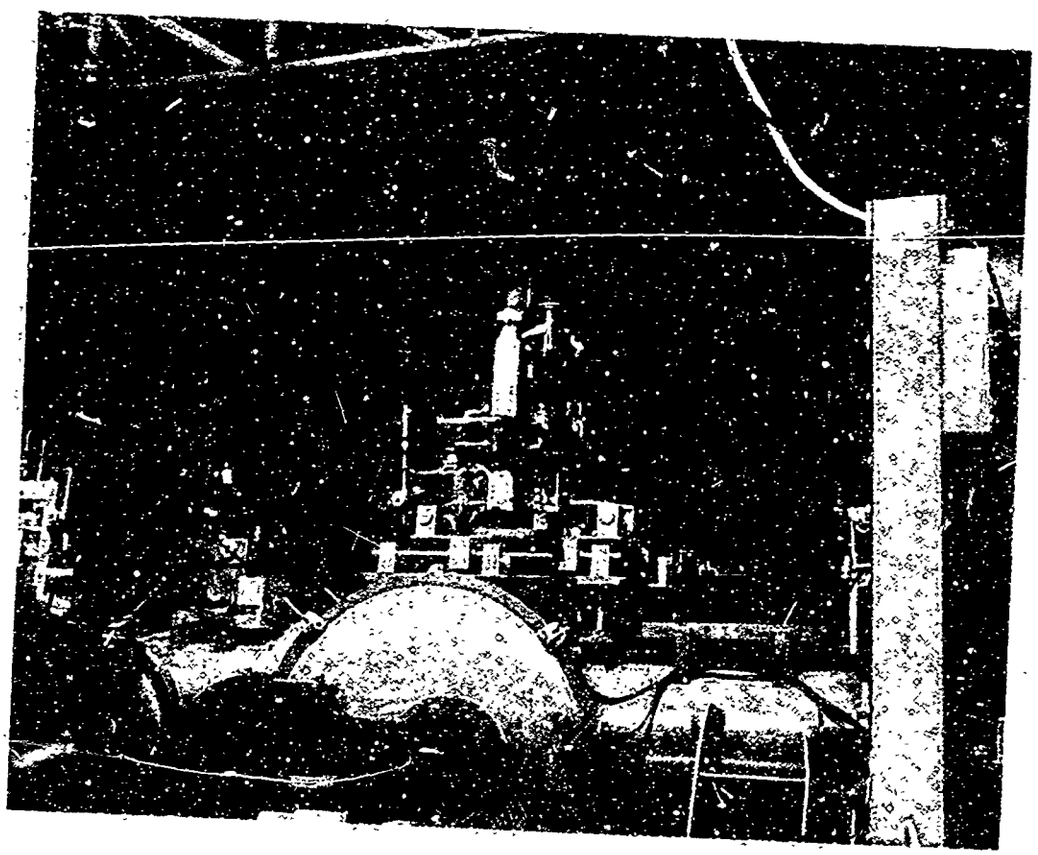

FIG. 9(a) PHOTOGRAPH OF ELECTRON GUN ASSEMBLY MOUNTED ON TEST SECTION OF LOW DENSITY TUNNEL

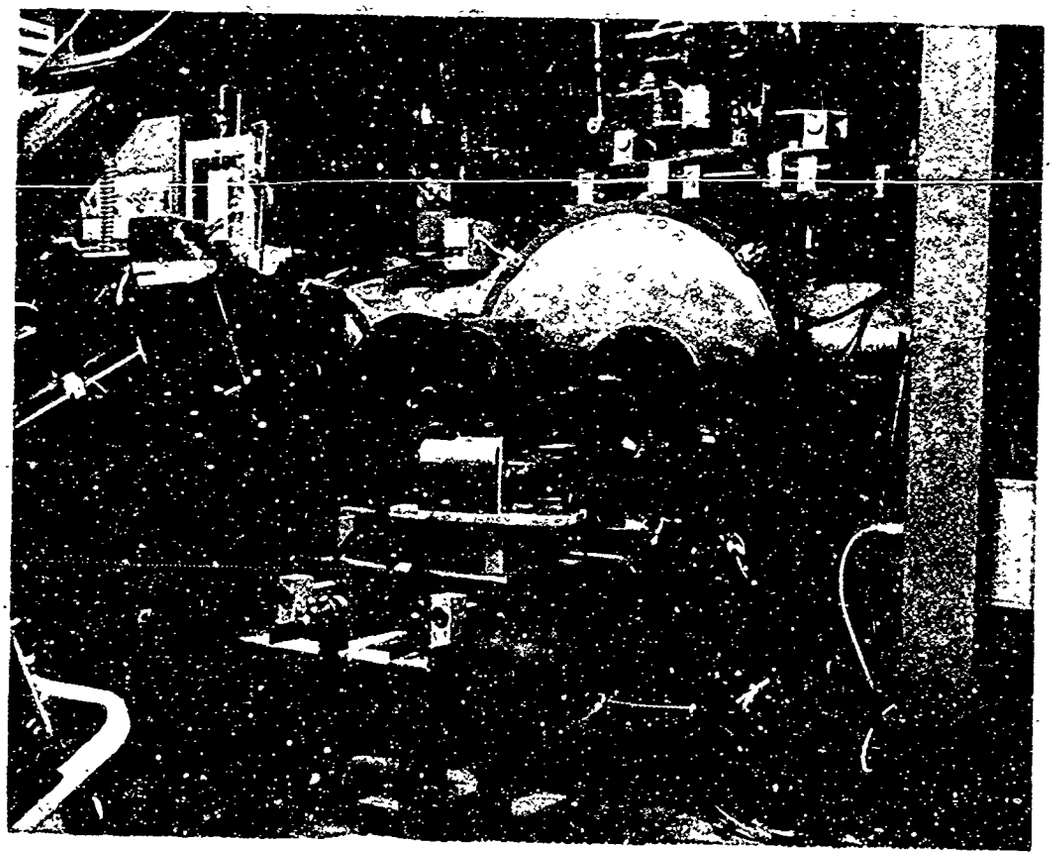

FIG. 9(b) PHOTOGRAPH OF SPECTROMETER AND TRAVERSING TABLE OUTSIDE OF TUNNEL TEST SECTION

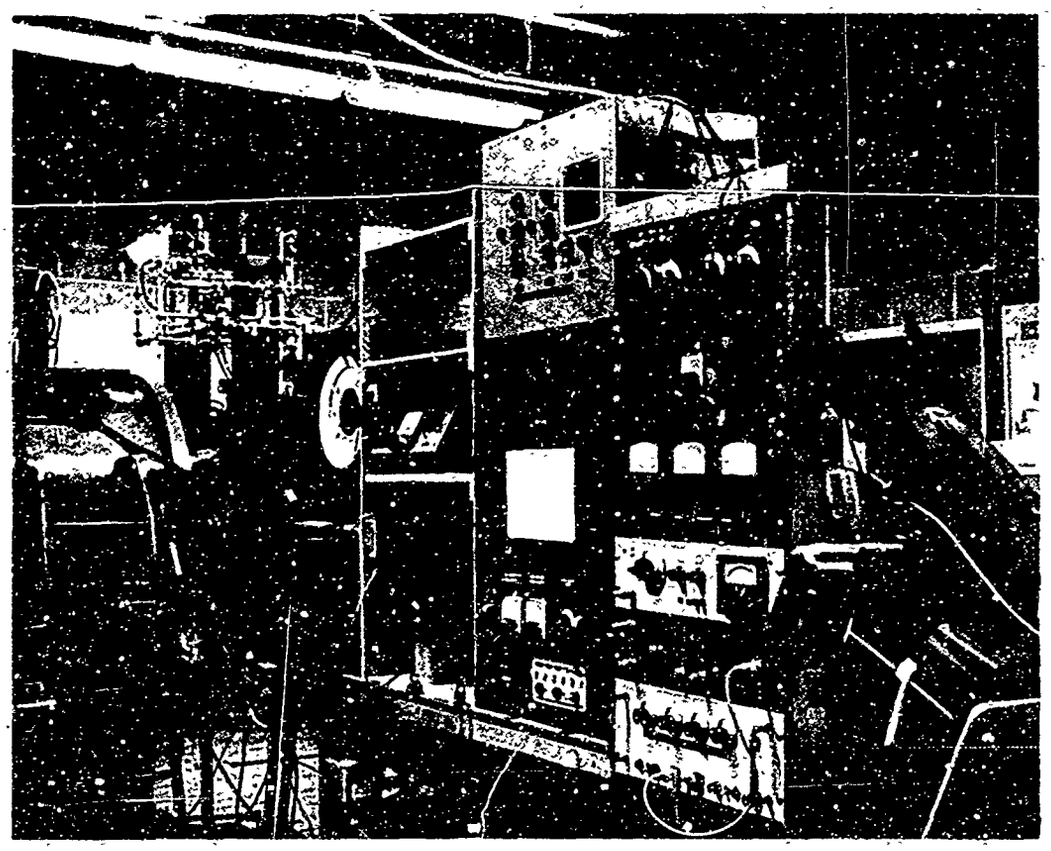

FIG. 9(c) PHOTOGRAPH OF INSTRUMENTATION SHOWING HIGH VOLTAGE SUPPLY FOR ELECTRON GUN, DEFLECTION PLATE CONTROLS AND PHOTOMULTIPLIER POWER SUPPLY.

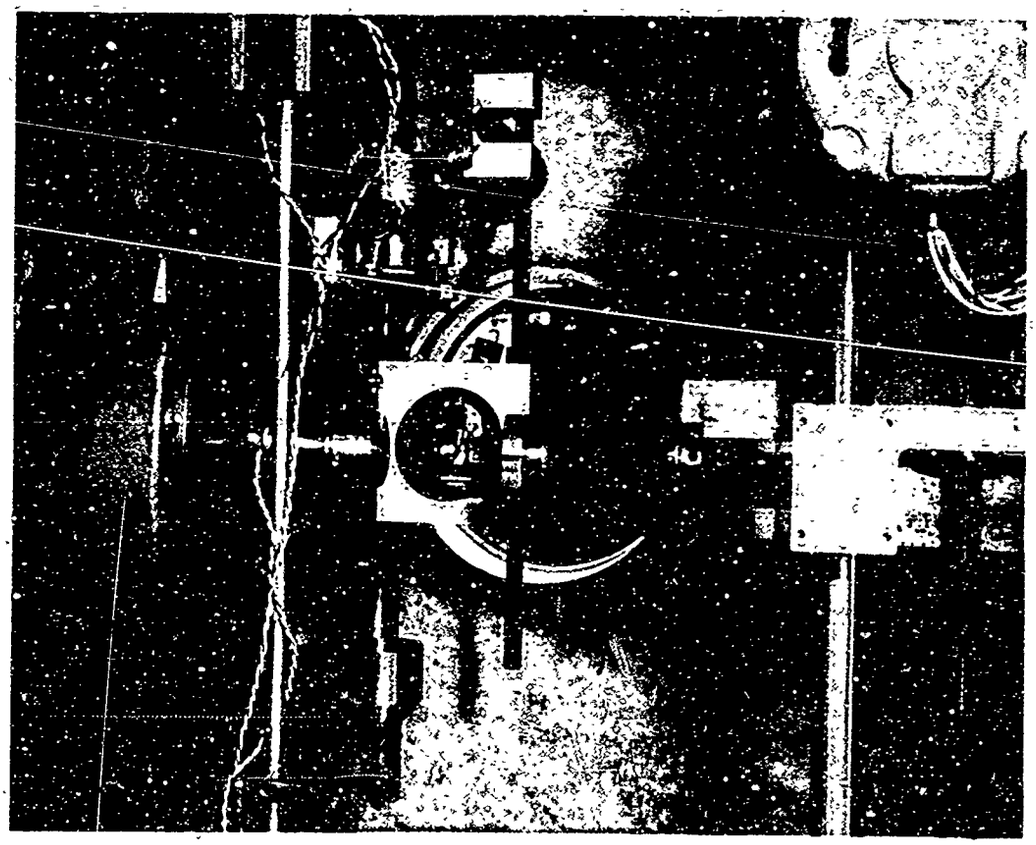

FIG. 9(d) PHOTOGRAPH OF TUNNEL TEST SECTION SHOWING SHOCK HOLDER, FOCUSSING LENS AND 5 mm. NOZZLE IN PLACE. THE REMOTE CONTROLLED DOOR AND BEAM COLLECTOR CUP ARE DIRECTLY ABOVE AND BELOW THE NOZZLE.

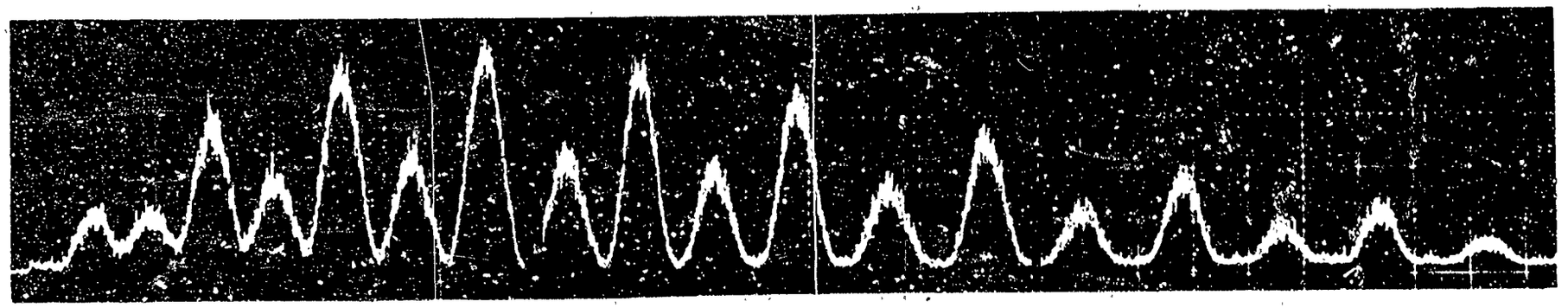

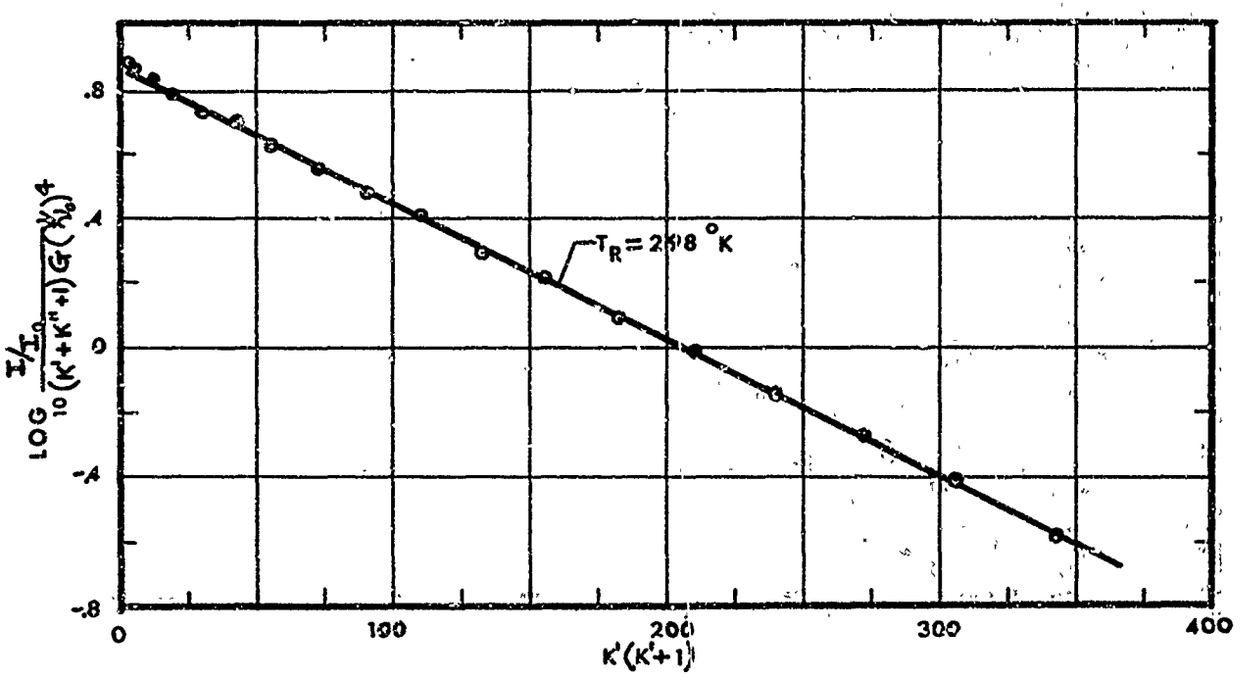

FIG. 10 ROOM TEMPERATURE R-BRANCH ROTATIONAL SPECTRUM OF N_2^+, 0-0 BAND

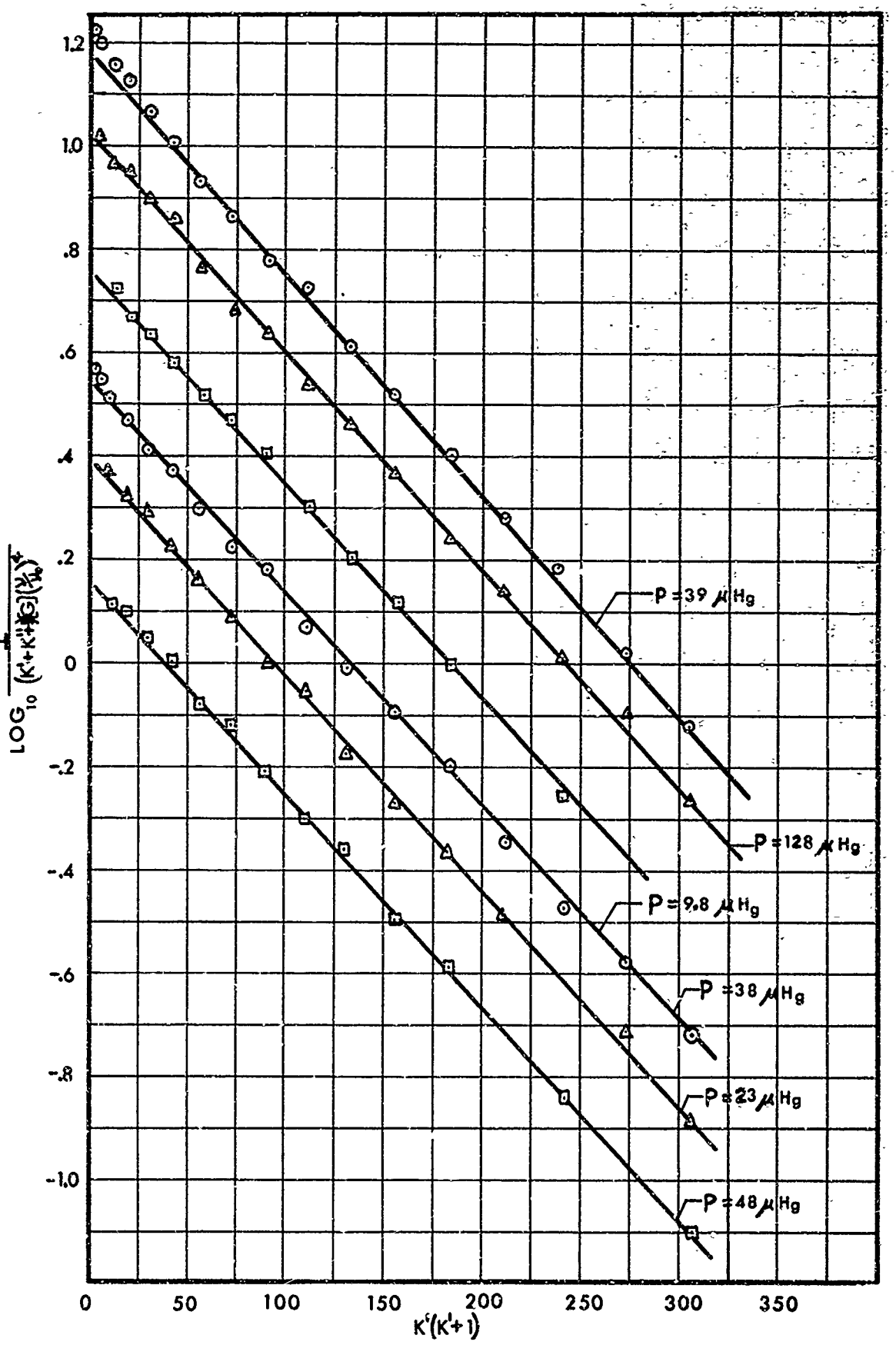

FIG. 11 LOG PLOTS OF ROOM TEMPERATURE CALIBRATION RUNS

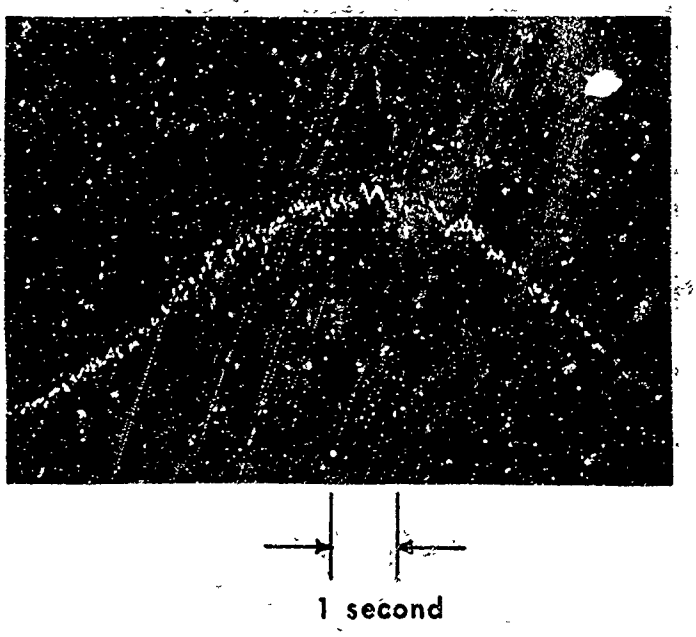

FIG. 12 LINE PROFILE FOR K' = 3

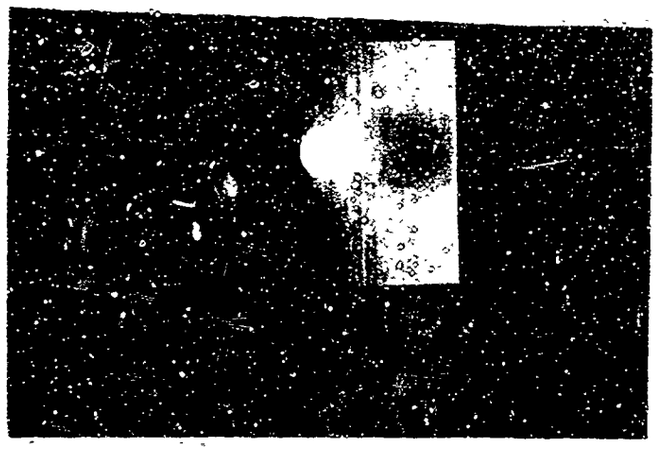

$P_o d = 15$ torr-mm

$P_o = 1.05$ torr

$d = 15$ mm

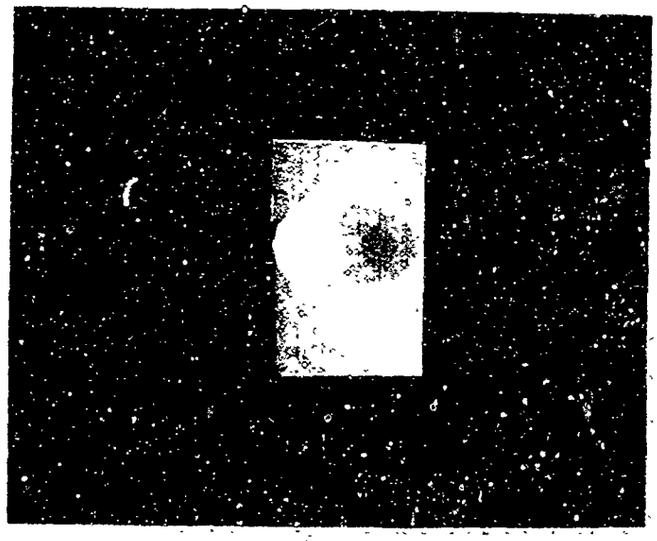

$P_o d = 40$ torr-mm

$P_o = 8$ torr

$d = 5$ mm

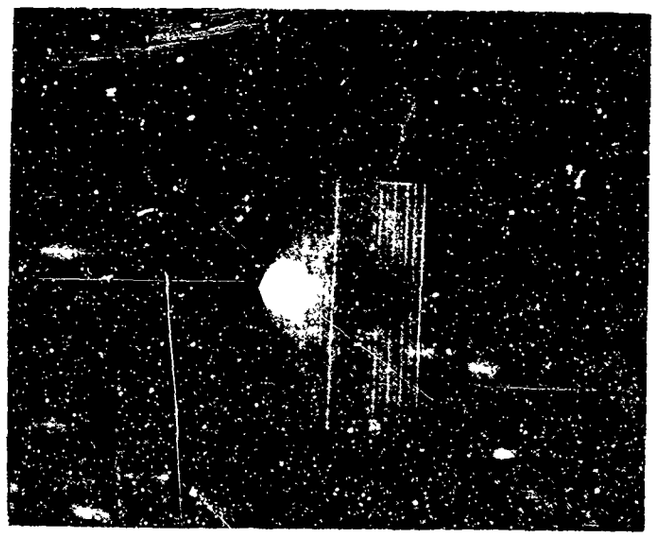

$P_o d = 80$ torr-mm

$P_o = 40$ torr

$d = 2$ mm

FIG. 13 FLOW VISUALIZATION PHOTOGRAPHS OF UNDEREXPANDED NITROGEN JETS

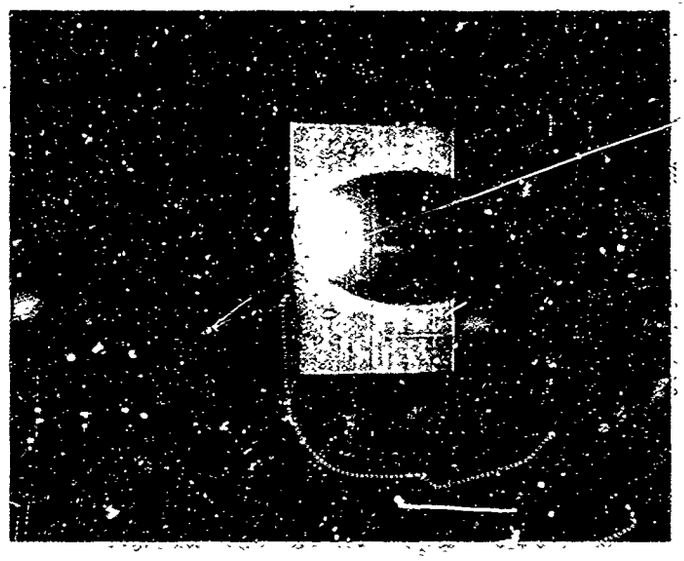

$P_o d = 230$ torr-mm

$P_o = 50$ torr

$d = 5$ mm

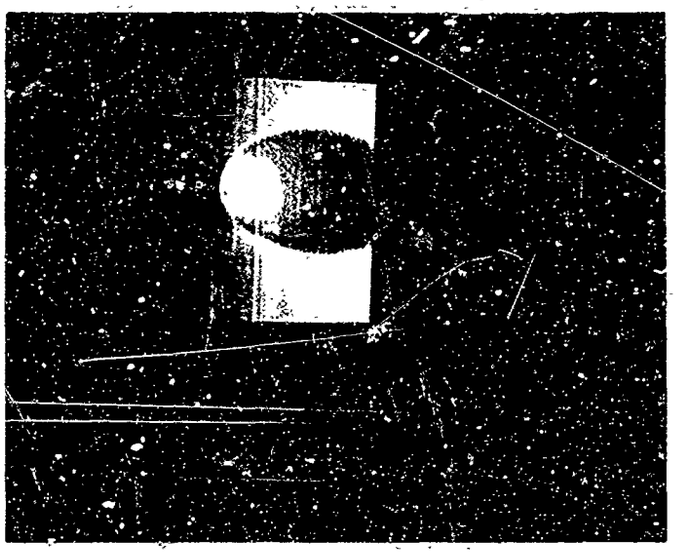

$P_o d = 480$ torr-mm

$P_o = 240$ torr

$d = 2$ mm

FIG. 13 (continued)

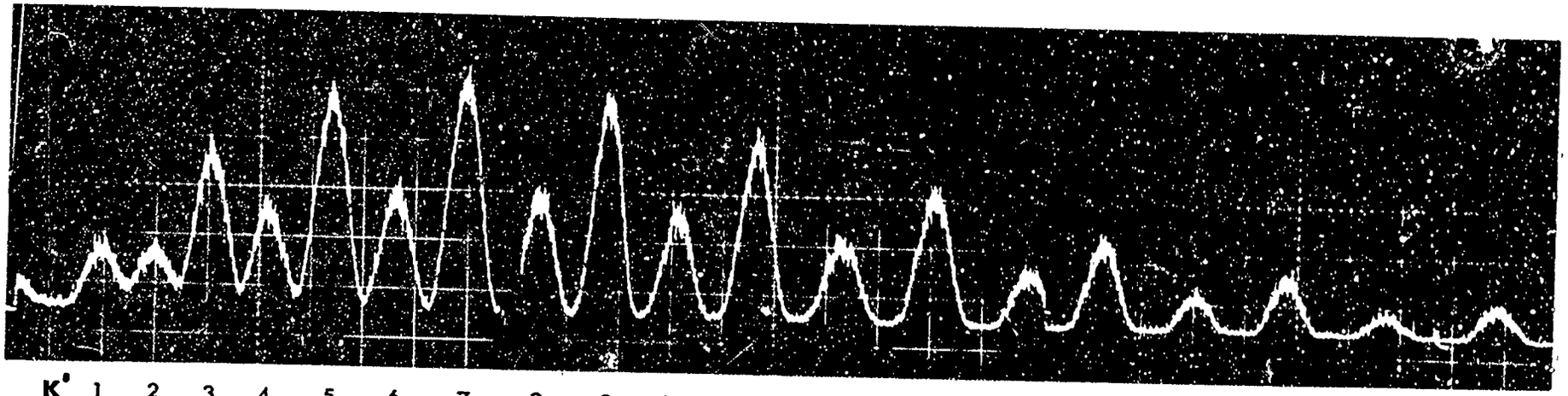

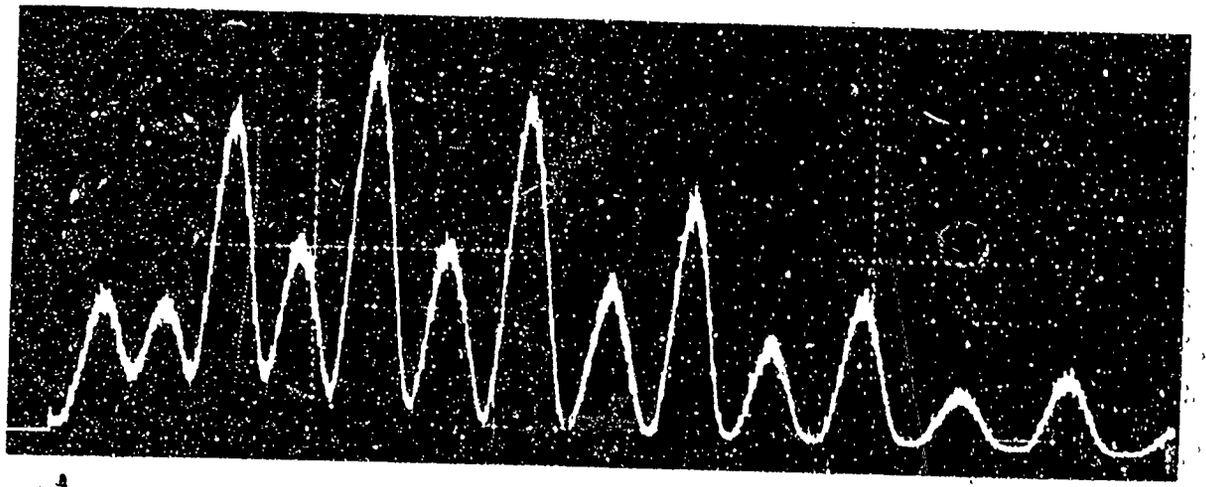

FIG. 14 R-BRANCH ROTATIONAL SPECTRA OF N_2^+, 0-0 BAND AT VARIOUS TEMPERATURES

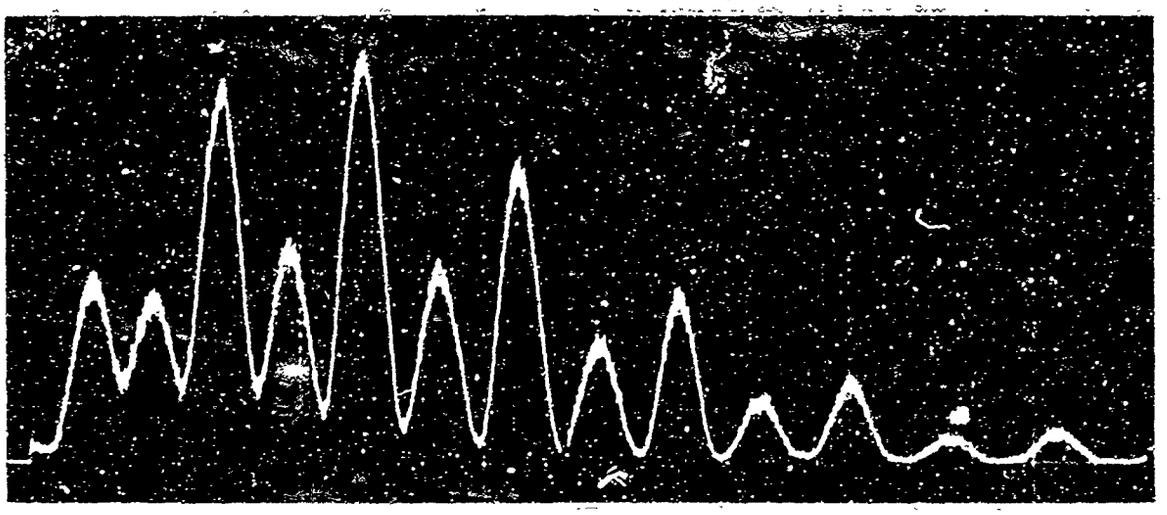

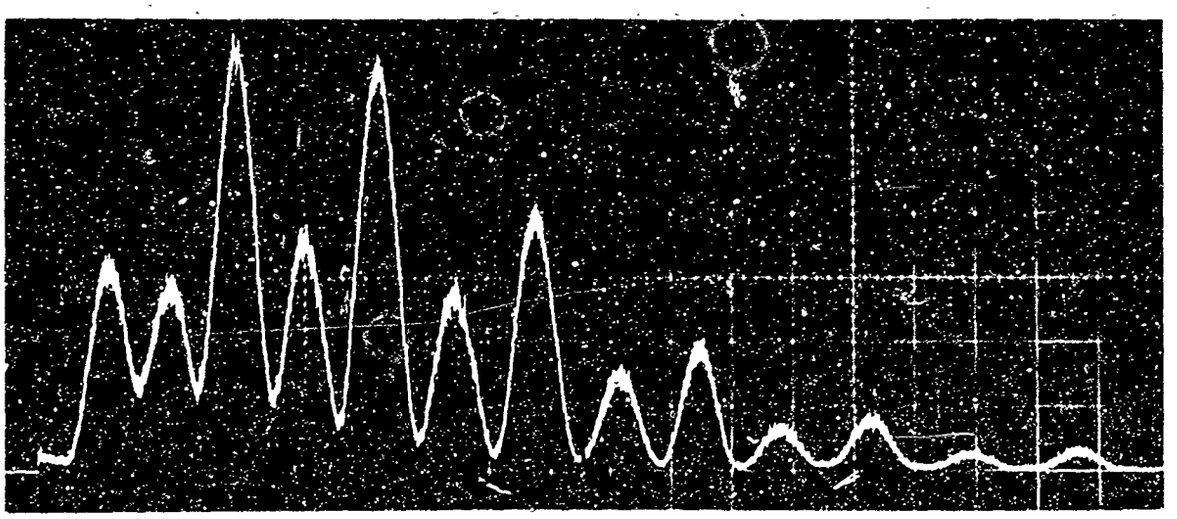

FIG. 14 (continued)

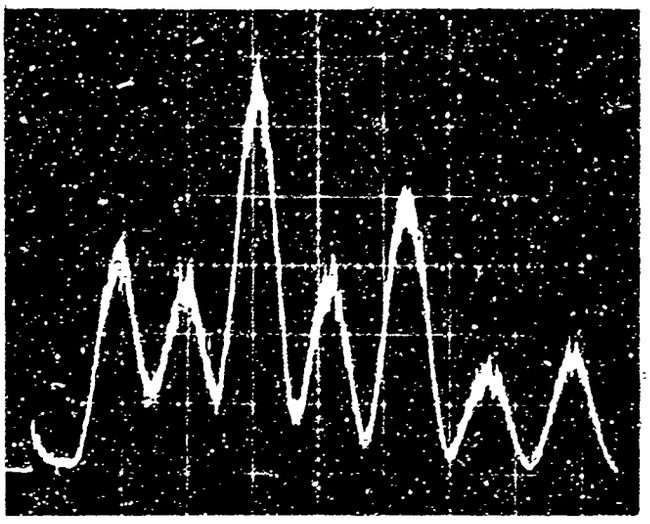

$T_R = 55\ ^\circ K$

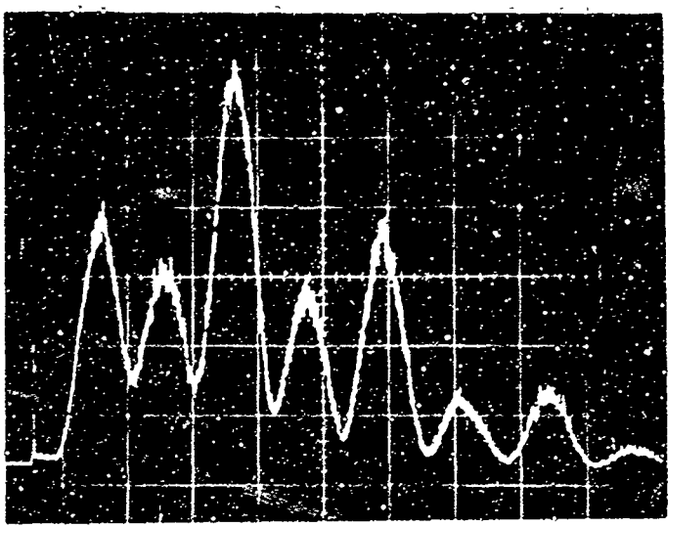

$T_R = 42\ ^\circ K$

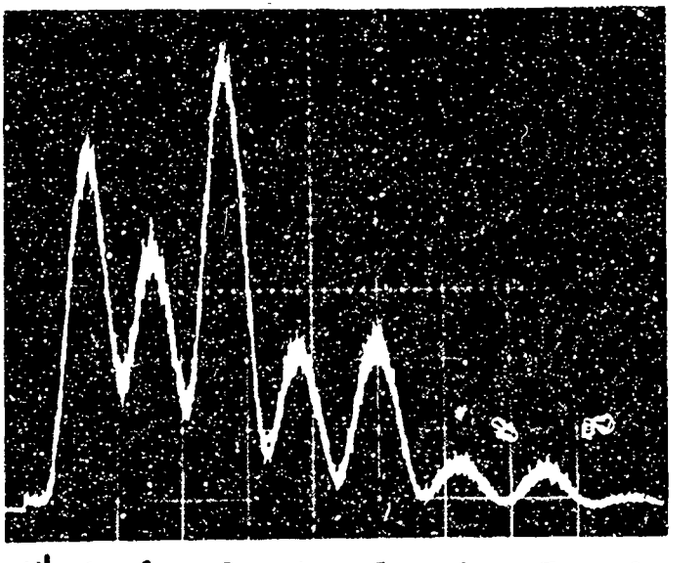

$T_R = 26\ ^\circ K$

FIG. 14 (continued)

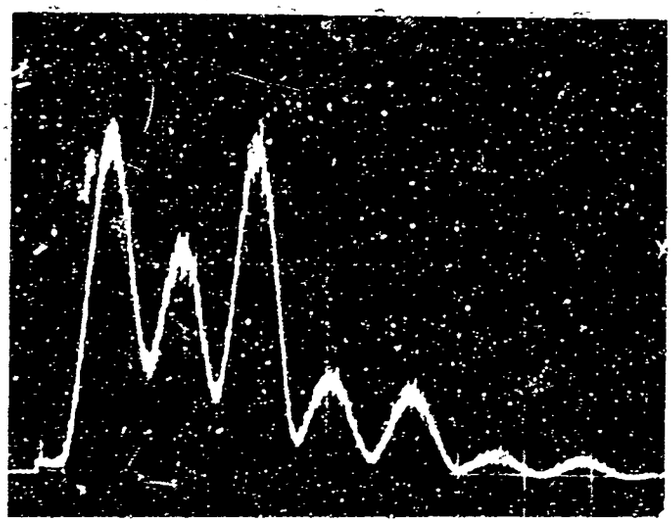

$T_R = 19\ ^\circ K$

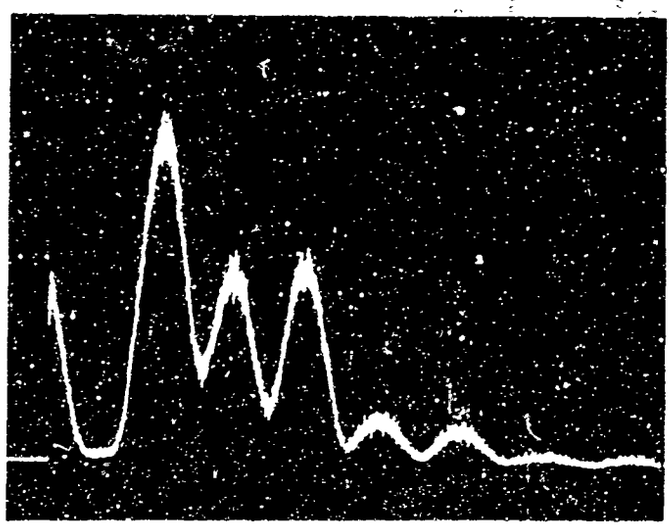

$T_R = 11\ ^\circ K$

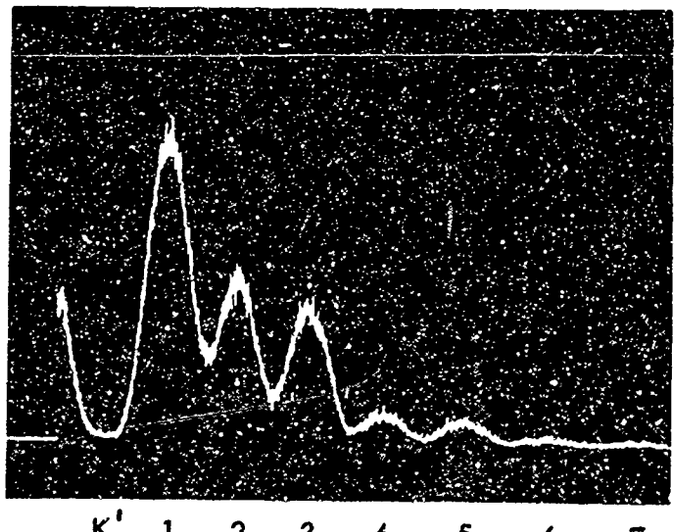

$T_R = 9\ ^\circ K$

FIG. 14 (continued)

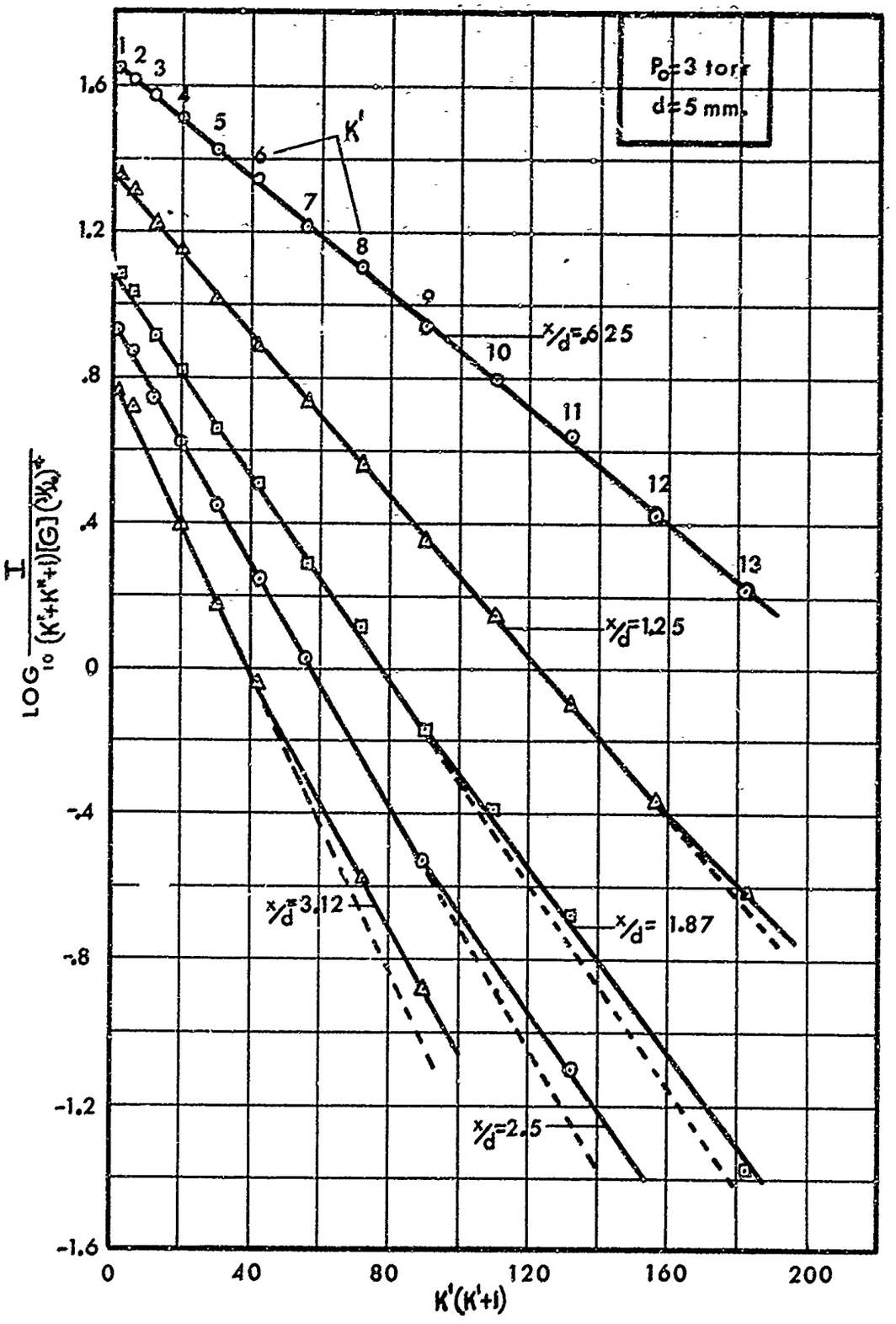

FIG. 15(a) LOG PLOTS OF INTENSITY OF FREE JET SPECTRAL DATA

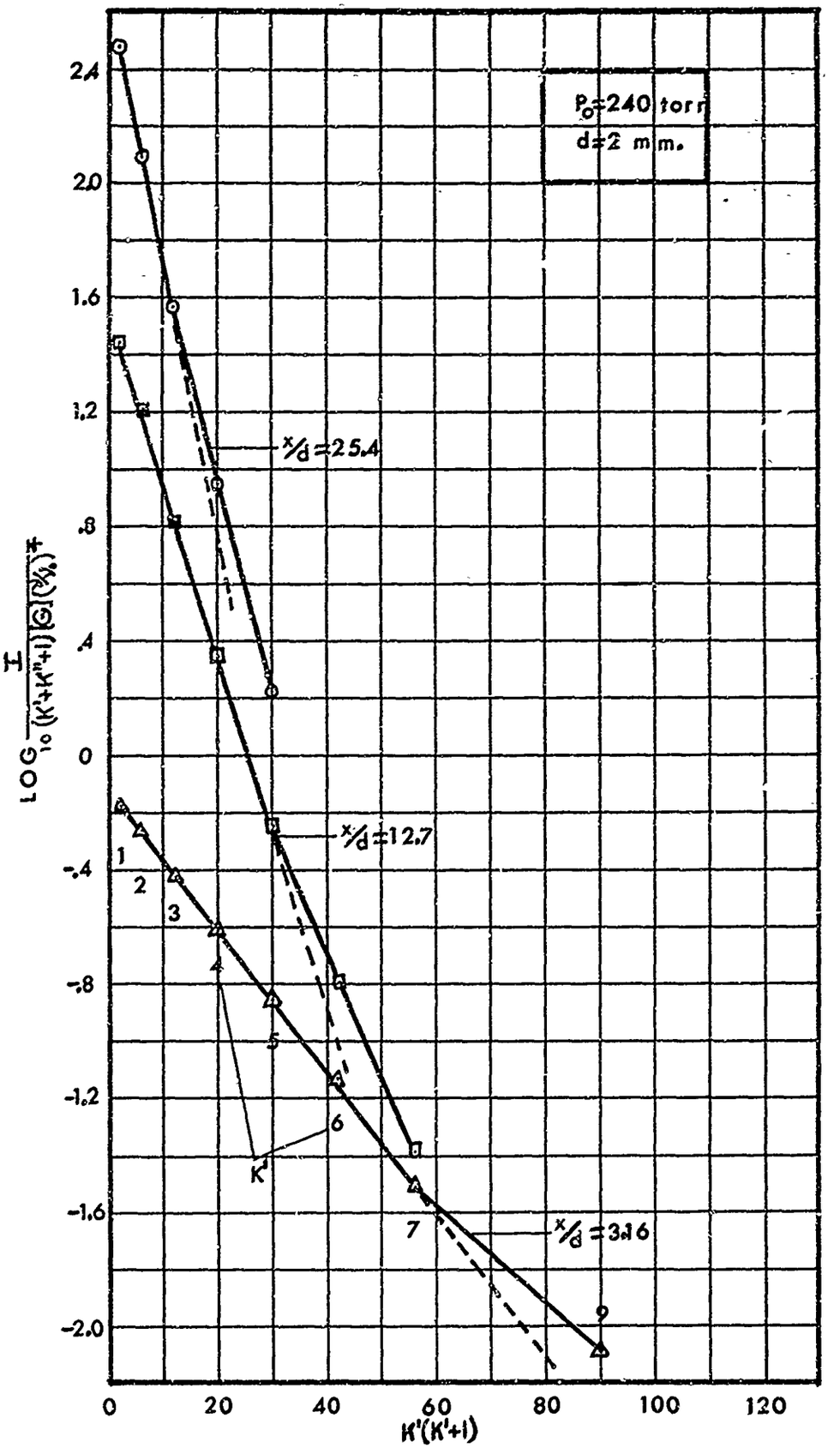

FIG. 15(b) LOG PLOTS OF INTENSITY OF FREE JET SPECTRAL DATA

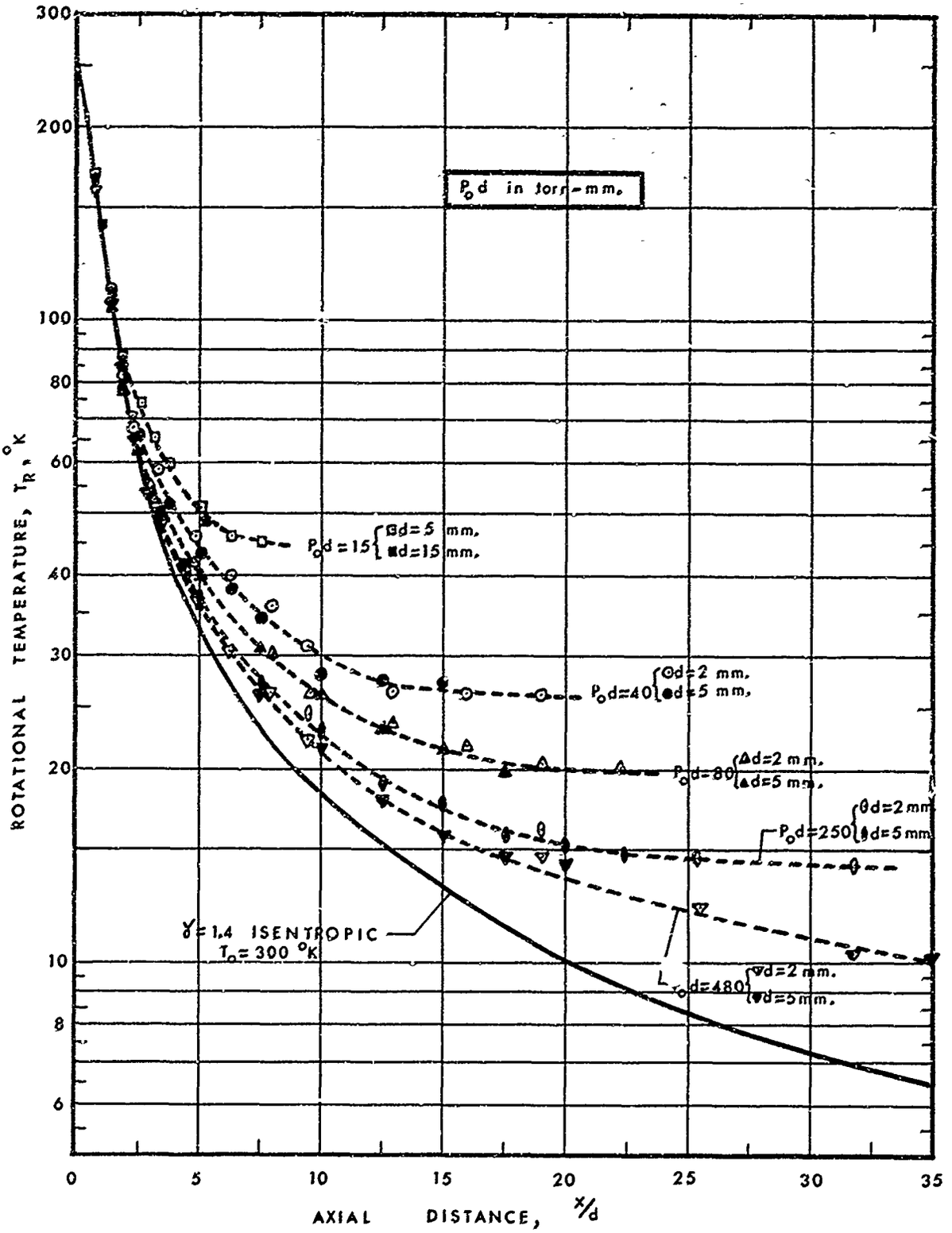

FIG. 16 ROTATIONAL TEMPERATURE DISTRIBUTION IN UNDEREXPANDED NITROGEN JETS

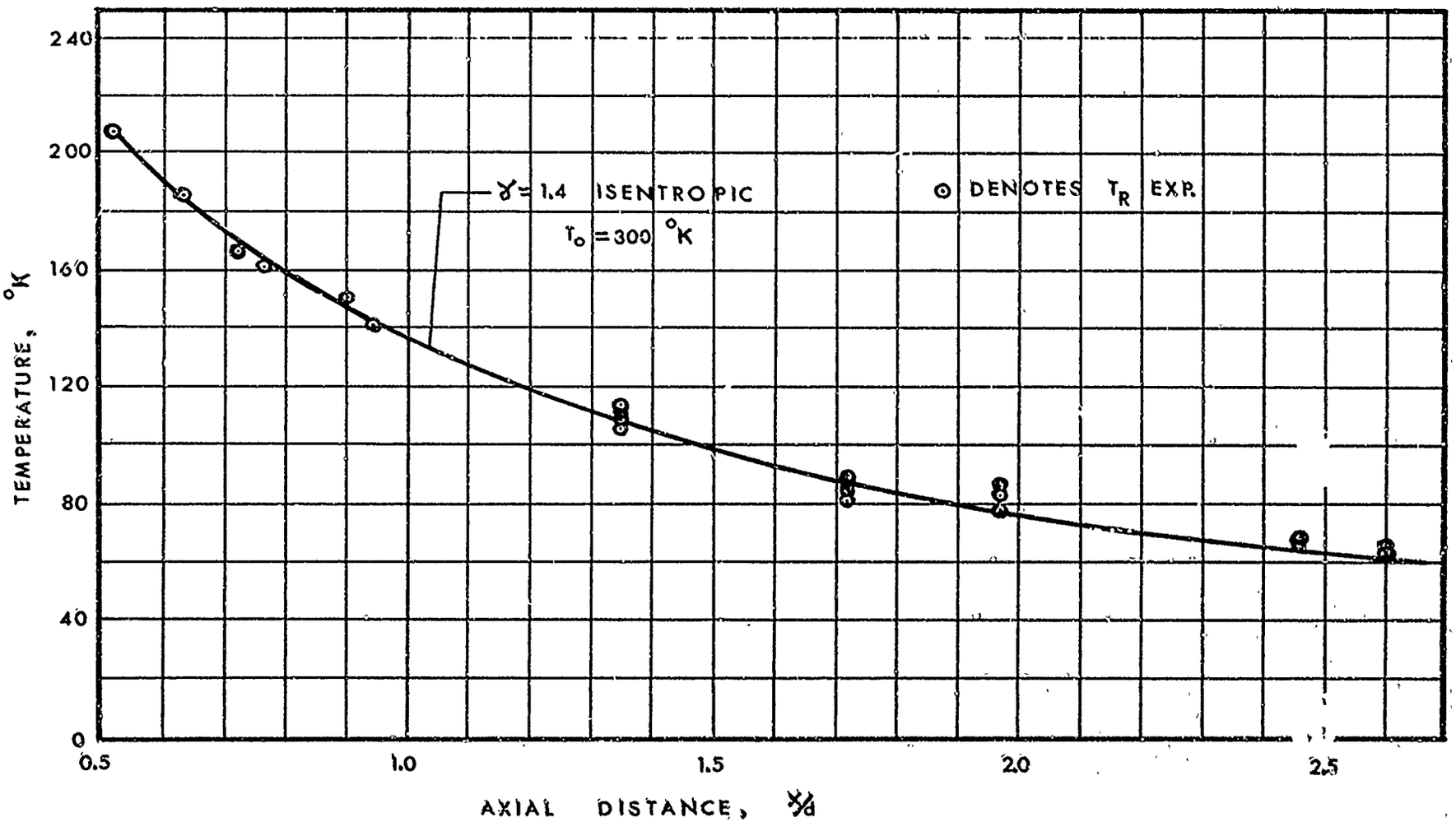

FIG. 17 ROTATIONAL TEMPERATURE MEASUREMENTS AT SMALL x/d.

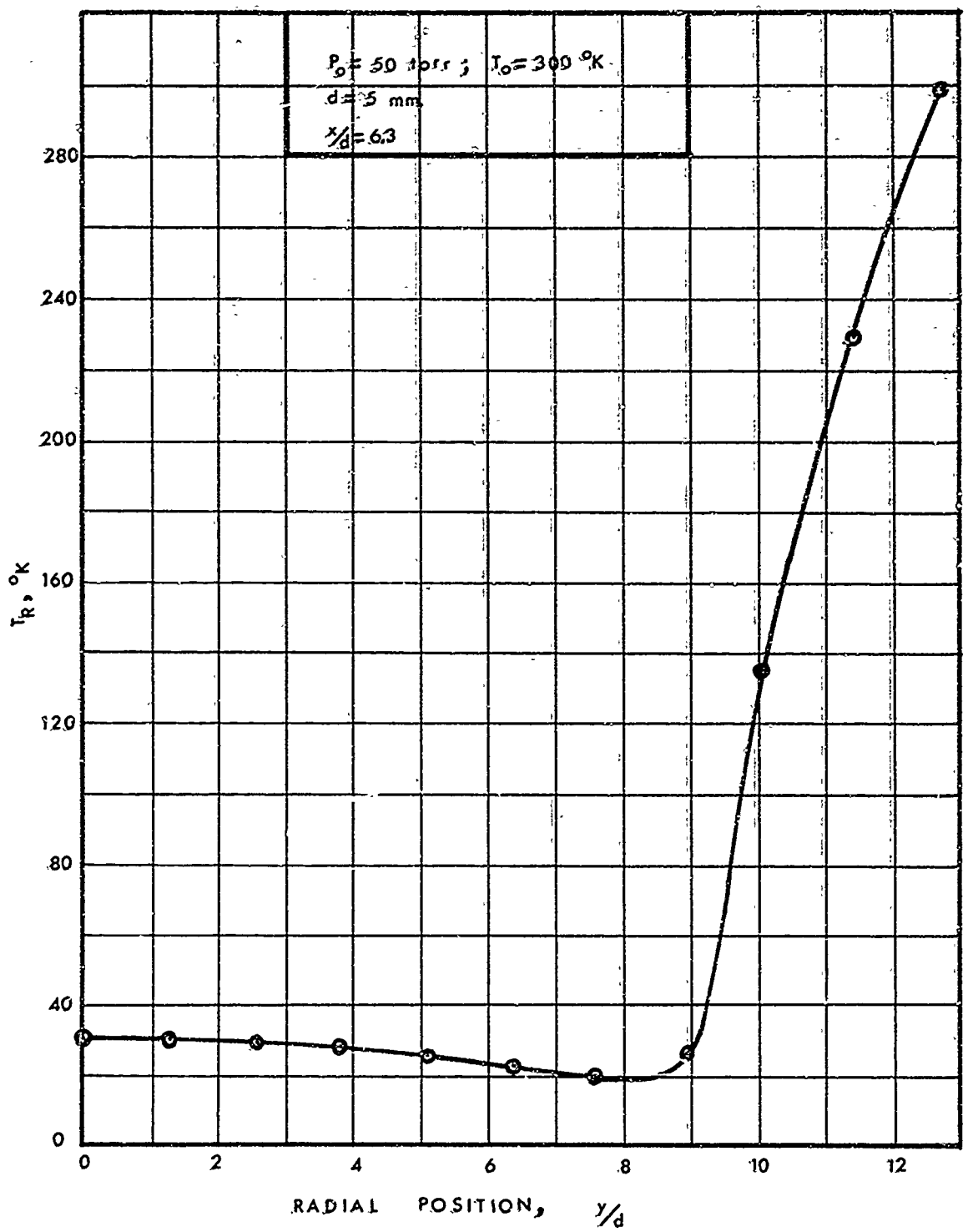

FIG. 18 RADIAL ROTATIONAL TEMPERATURE DISTRIBUTION IN NITROGEN FREE JET

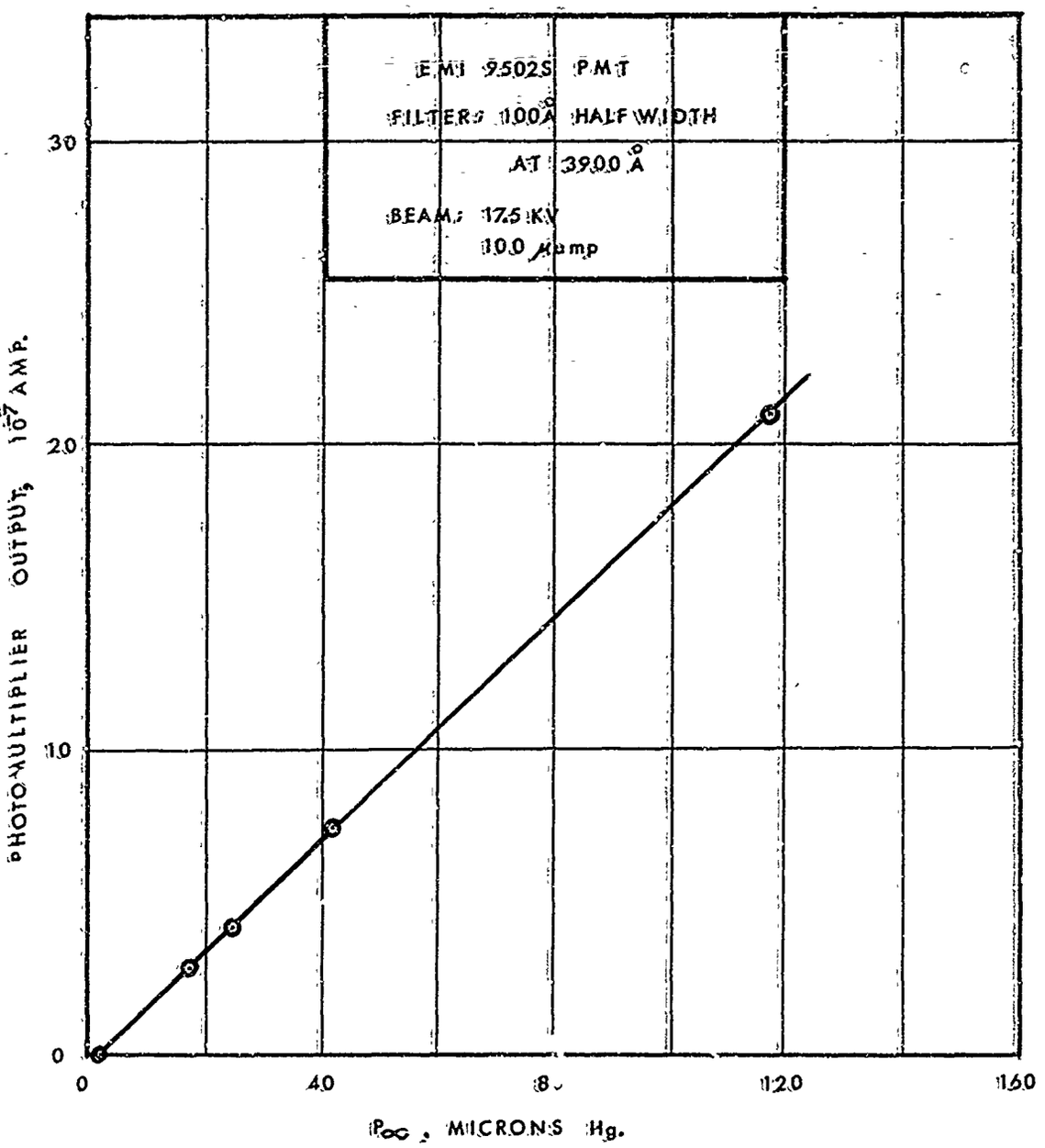

FIG. 19 PHOTOMULTIPLIER DENSITY CALIBRATION WITH ROOM TEMPERATURE NITROGEN

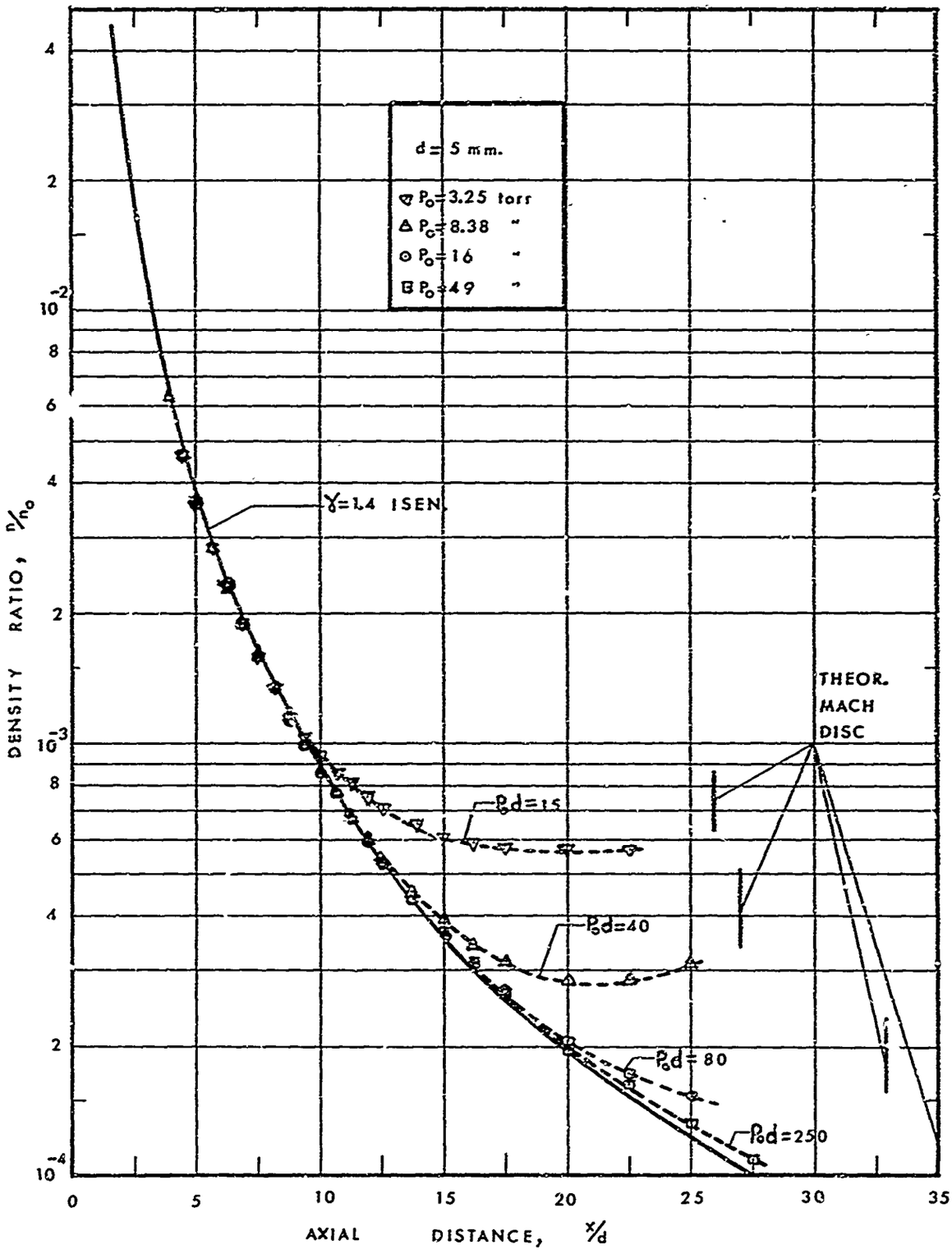

FIG. 20 DENSITY DISTRIBUTION ALONG CENTERLINE OF NITROGEN FREE JETS

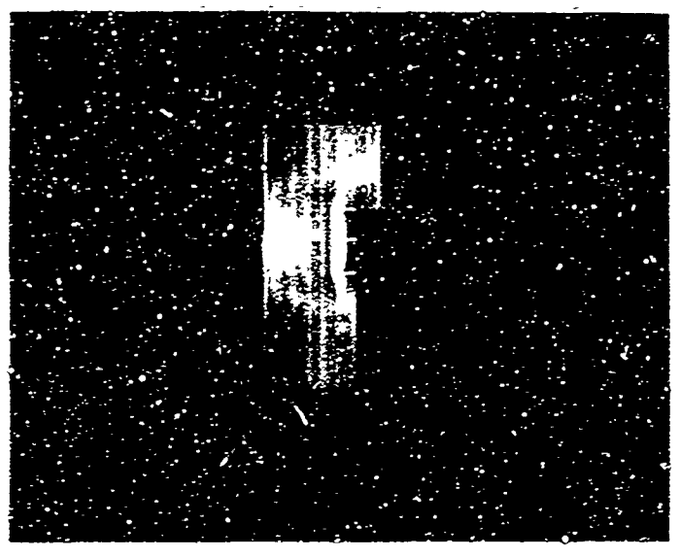

P_o=49 torr
d=47.5 mm
$\frac{x}{d}$=2 (S.H.)
M≈3.9

P_o=59 torr
d= 5 mm
$\frac{x}{d}$= 17.5 (S.H.)
M≈11

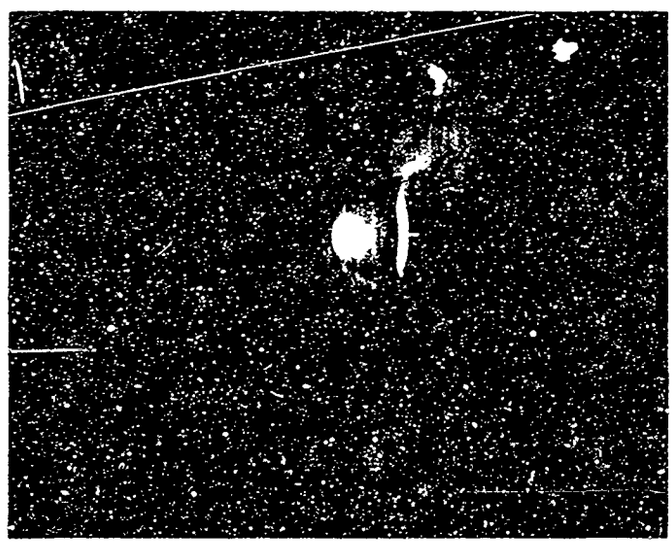

P_o=242 torr
d=2 mm
$\frac{x}{d}$=3 4.8 (S.H.)
M≈15

FIG. 21 FLOW VISUALIZATION PHOTOGRAPHS OF SHOCK HOLDER IN NITROGEN UNDEREXPANDED JETS

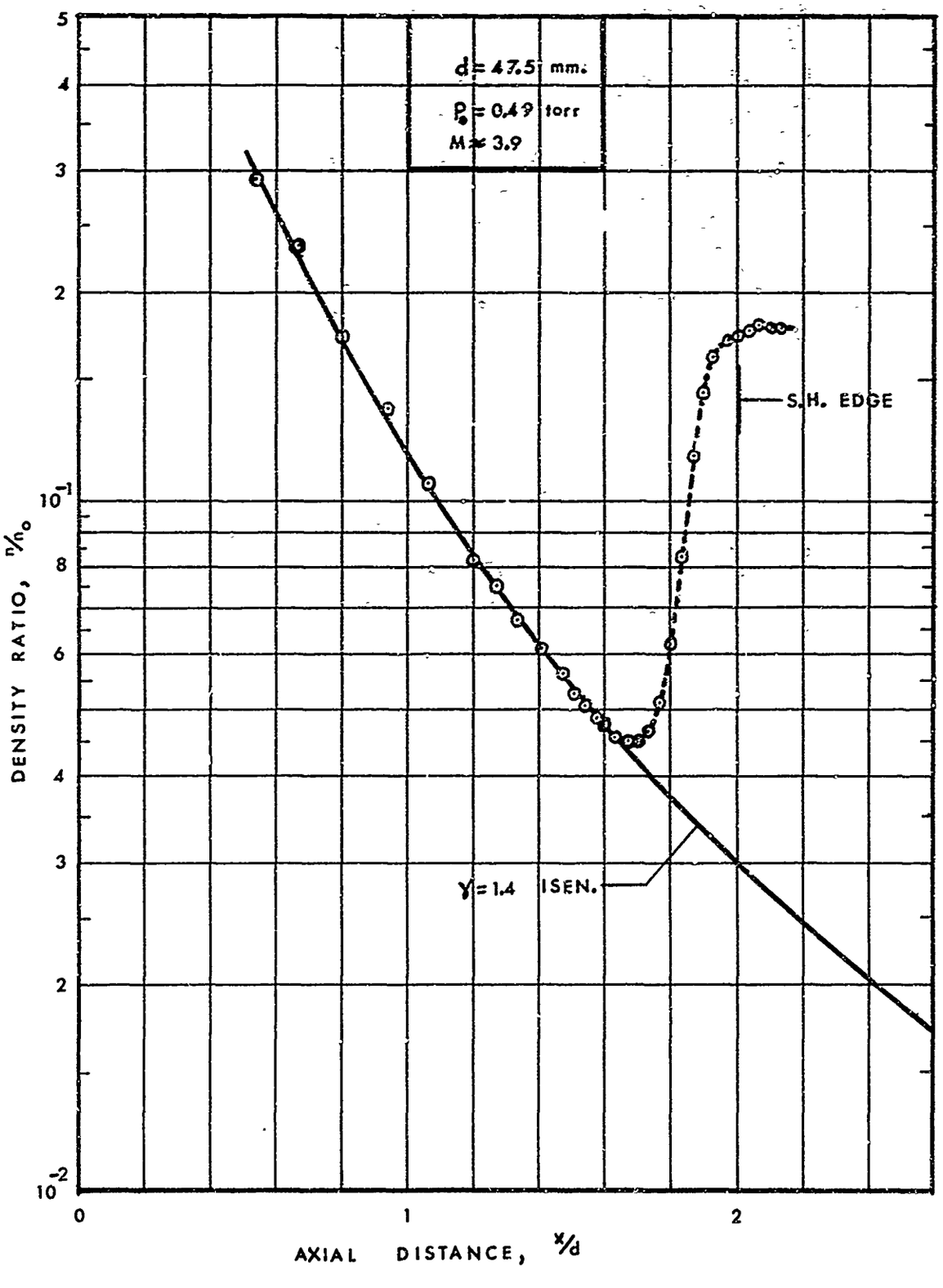

FIG. 22(a) SHOCK DENSITY PROFILE, M ≈ 3.9

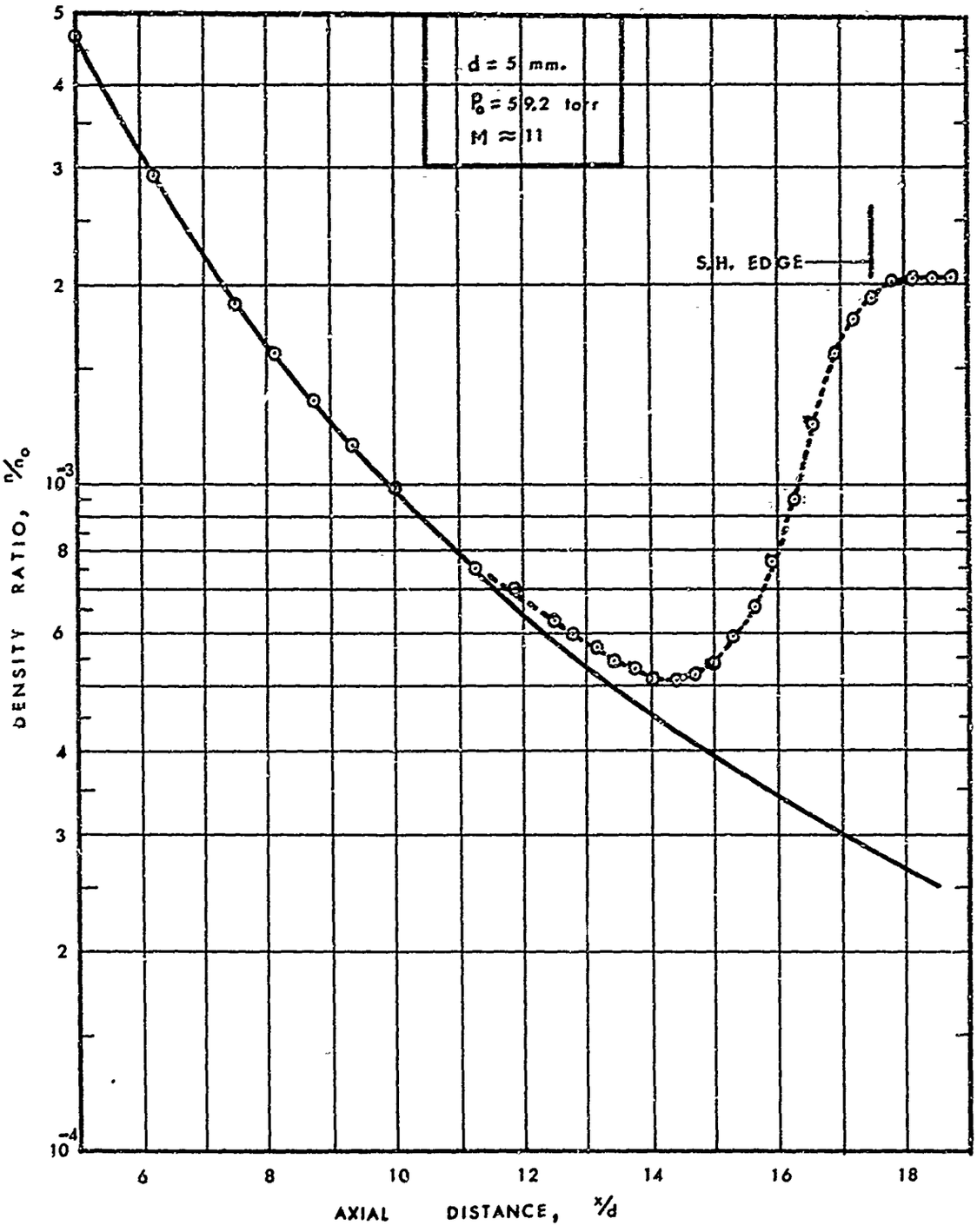

FIG. 22(b) SHOCK DENSITY PROFILE, M ≈ 11

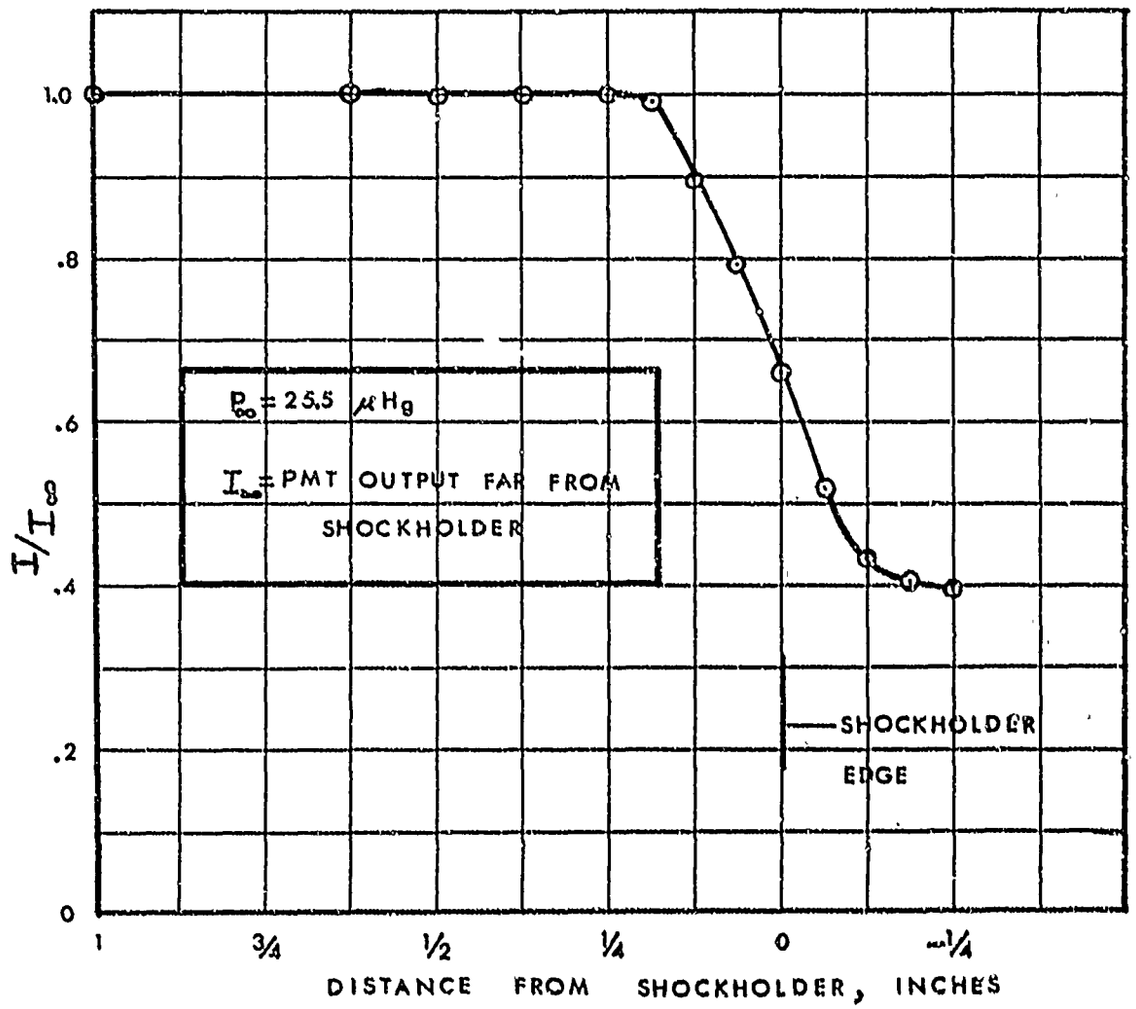

FIG. 23 SHOCK HOLDER OCCULATION CALIBRATION WITH ROOM TEMPERATURE NITROGEN

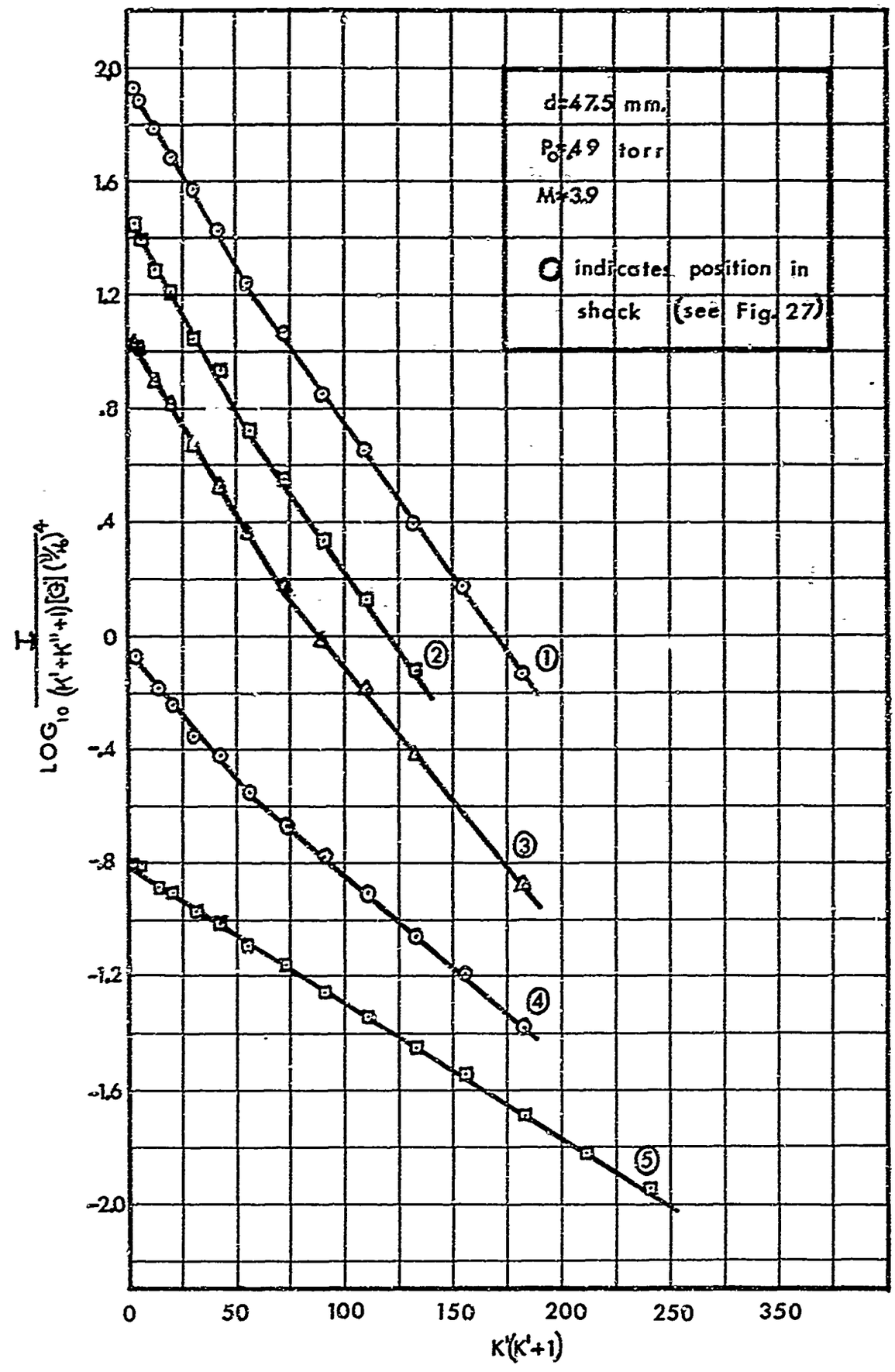

FIG. 24(a) LOG PLOTS OF INTENSITY, M ≈ 3.9

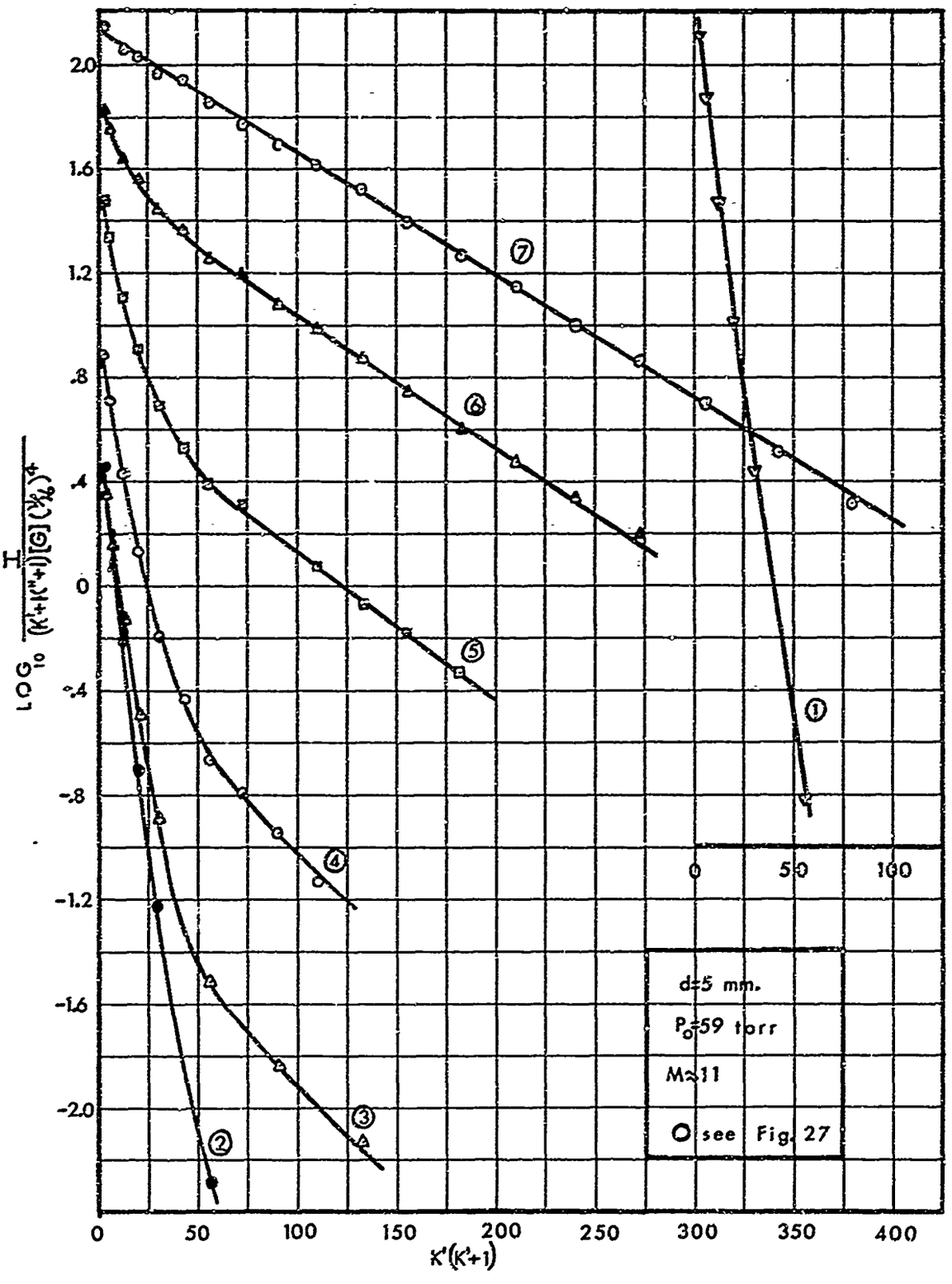

FIG. 24(b) LOG PLOTS OF INTENSITY, M ≈ 11

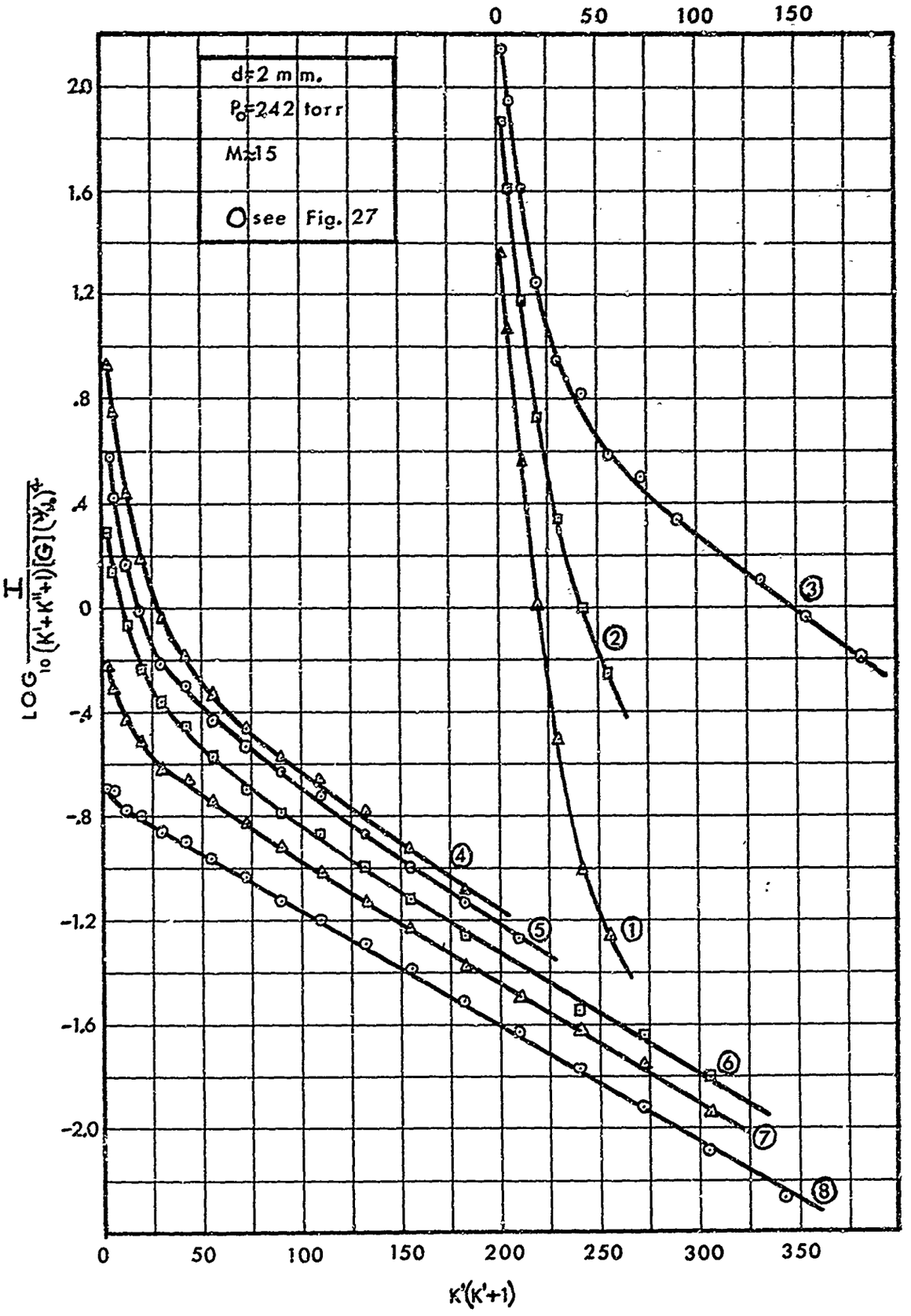

FIG. 24(c) LOG PLOTS OF INTENSITY, M ≈ 15

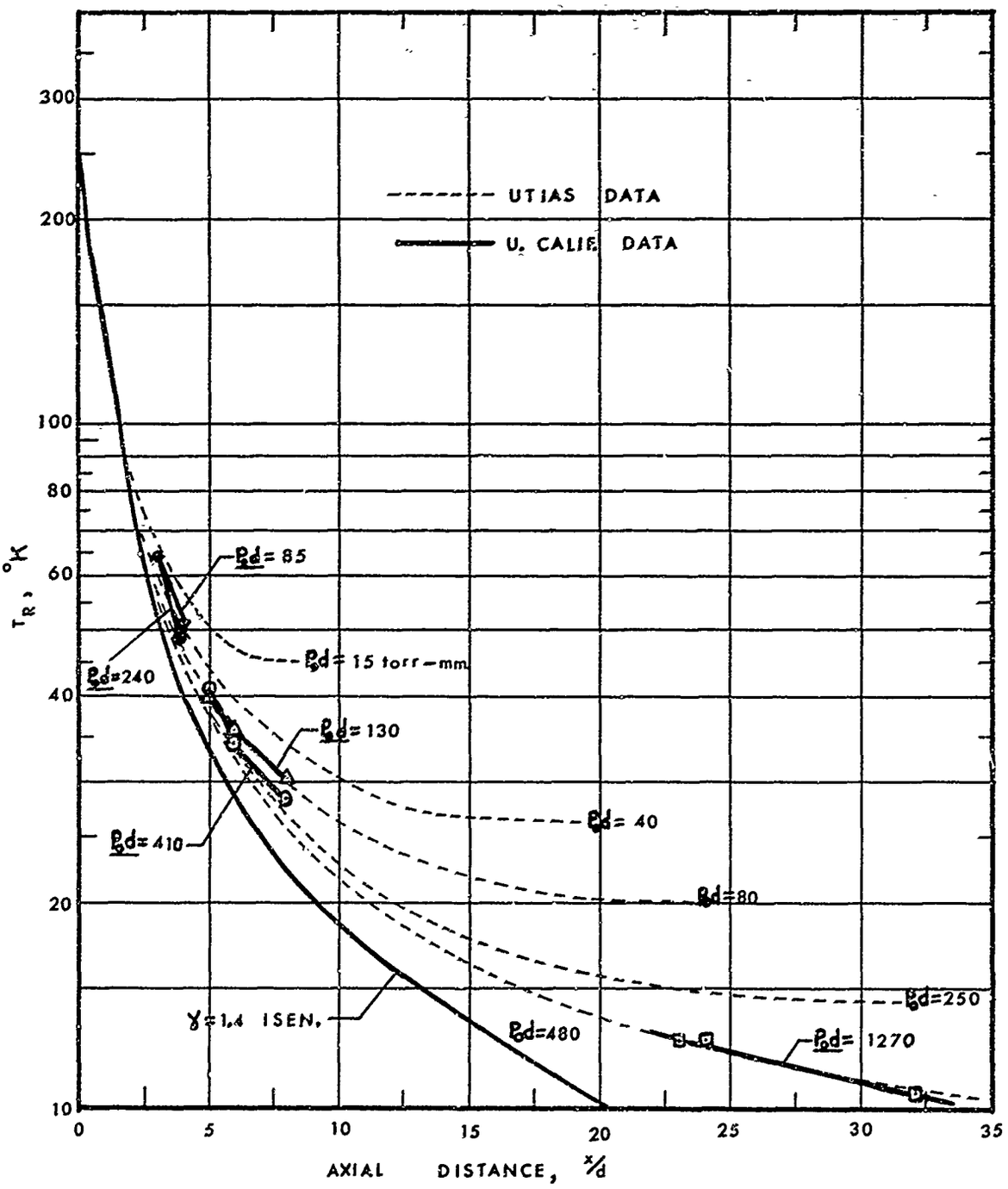

FIG. 25 COMPARISON OF UTIAS AND U. CALIF. ROTATIONAL TEMPERATURE MEASUREMENTS

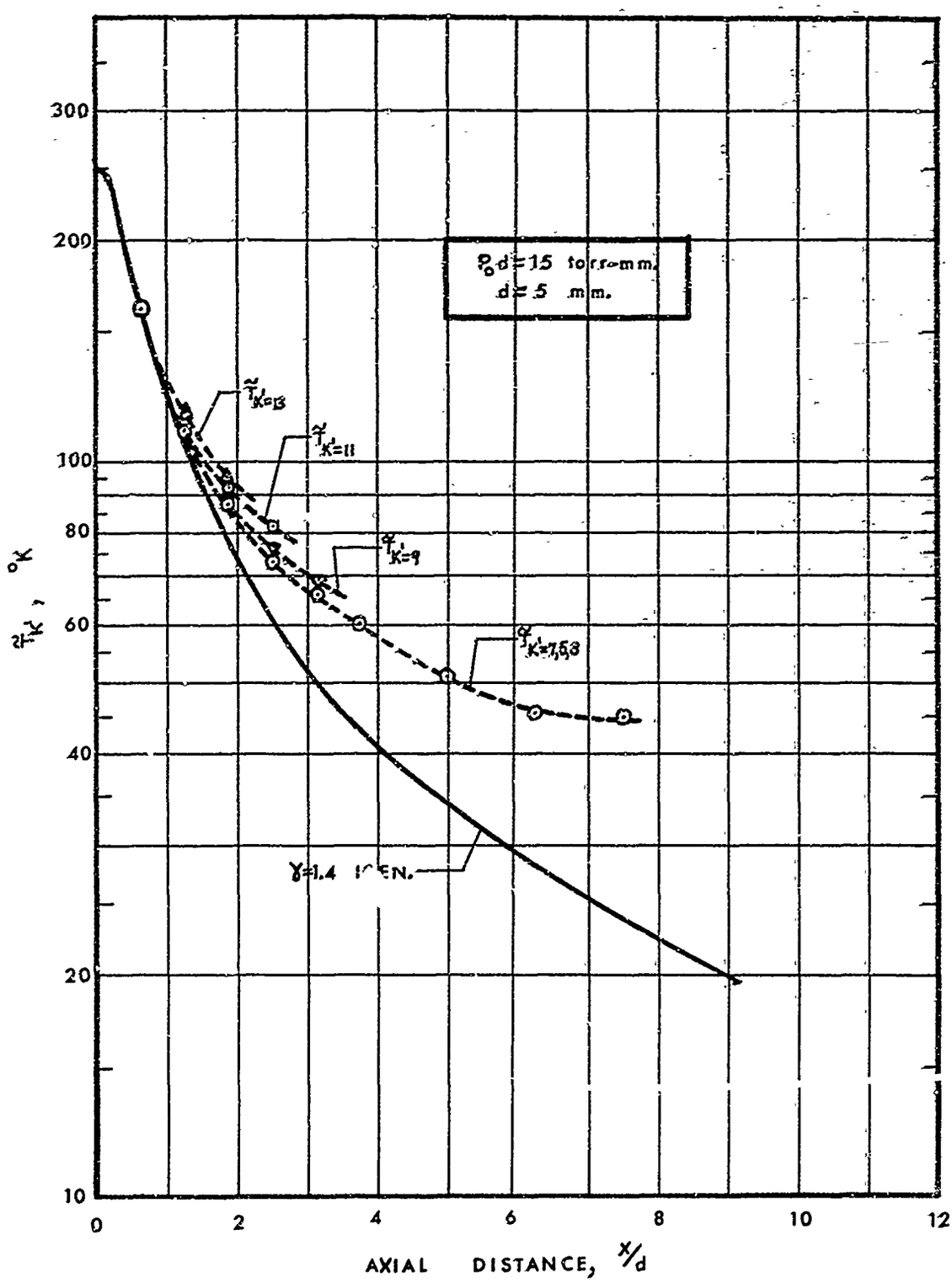

FIG. 26(a) TEMPERATURE DISTRIBUTION IN EXPANSION

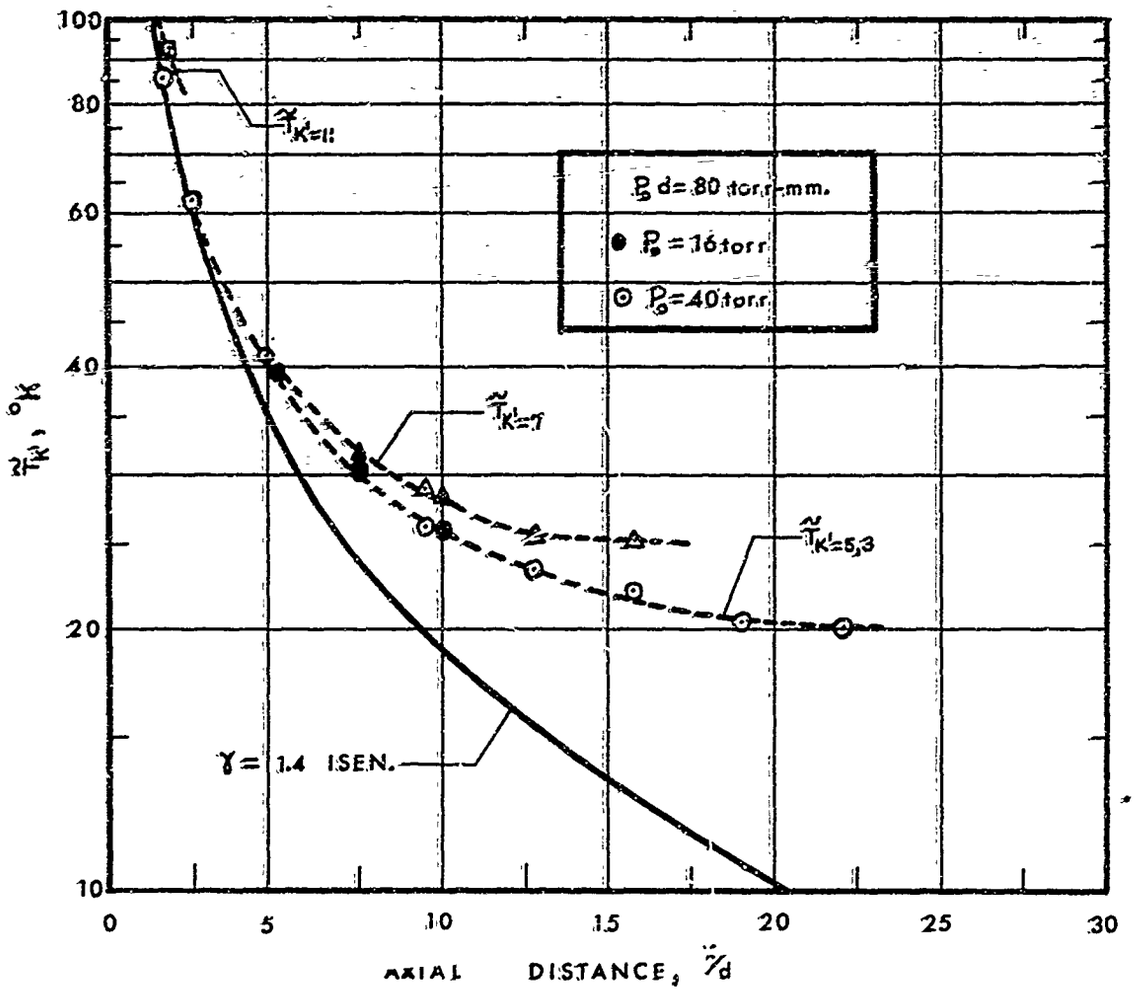

FIG. 26(b) TEMPERATURE DISTRIBUTION IN EXPANSION

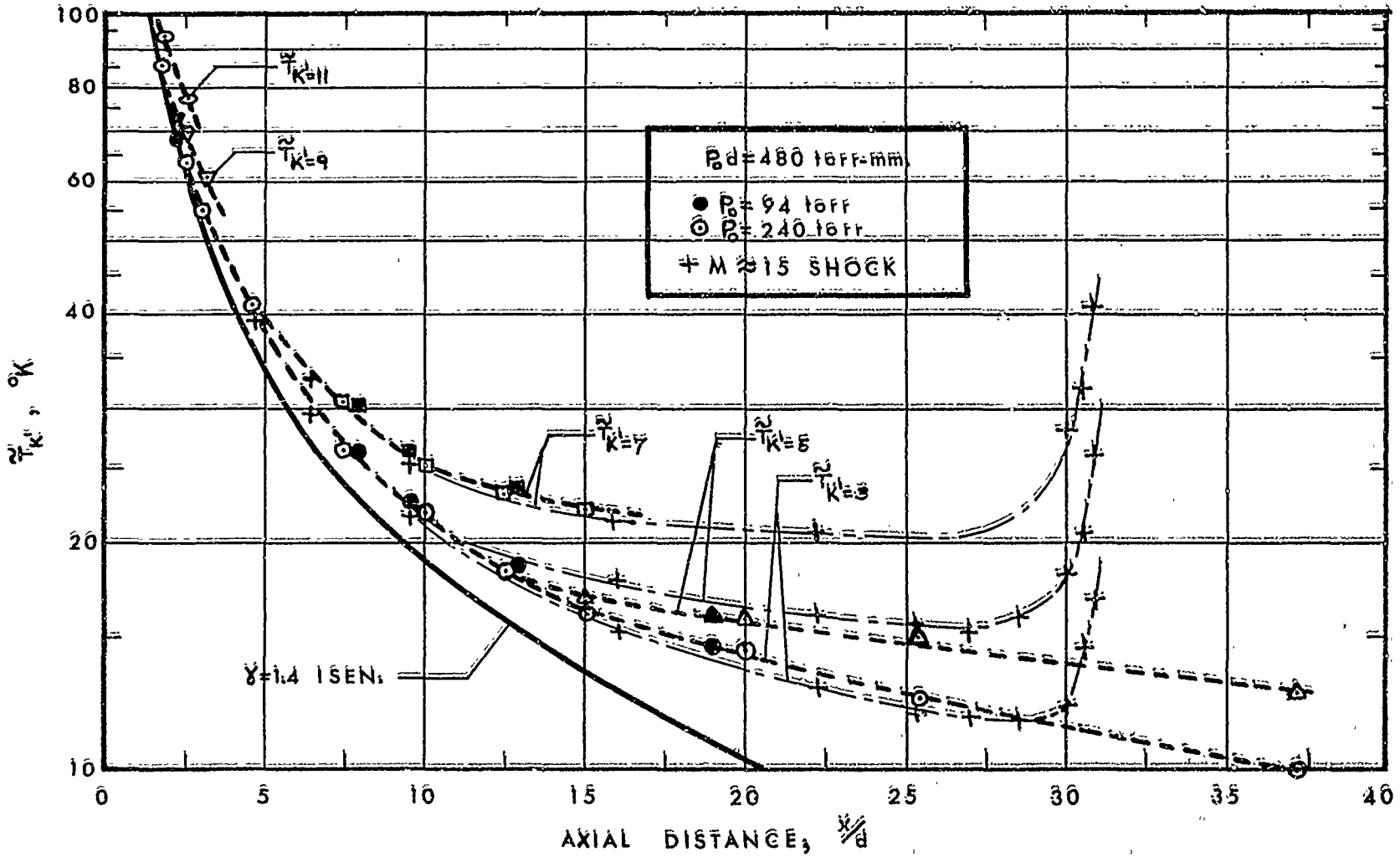

FIG. 26(c) TEMPERATURE DISTRIBUTION IN EXPANSION

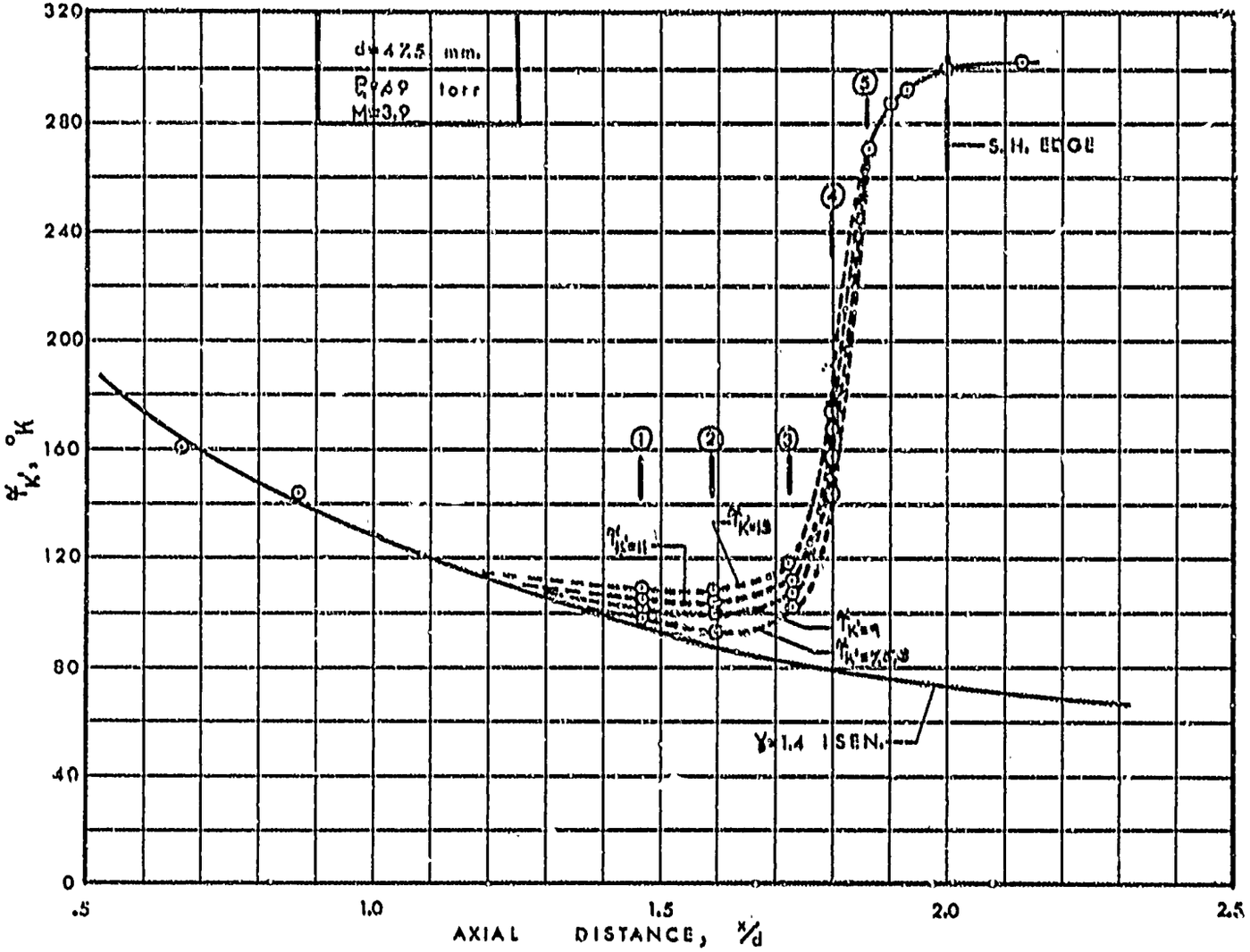

FIG. 27(a) SHOCK WAVE TEMPERATURE PROFILE, M ≈ 3.9

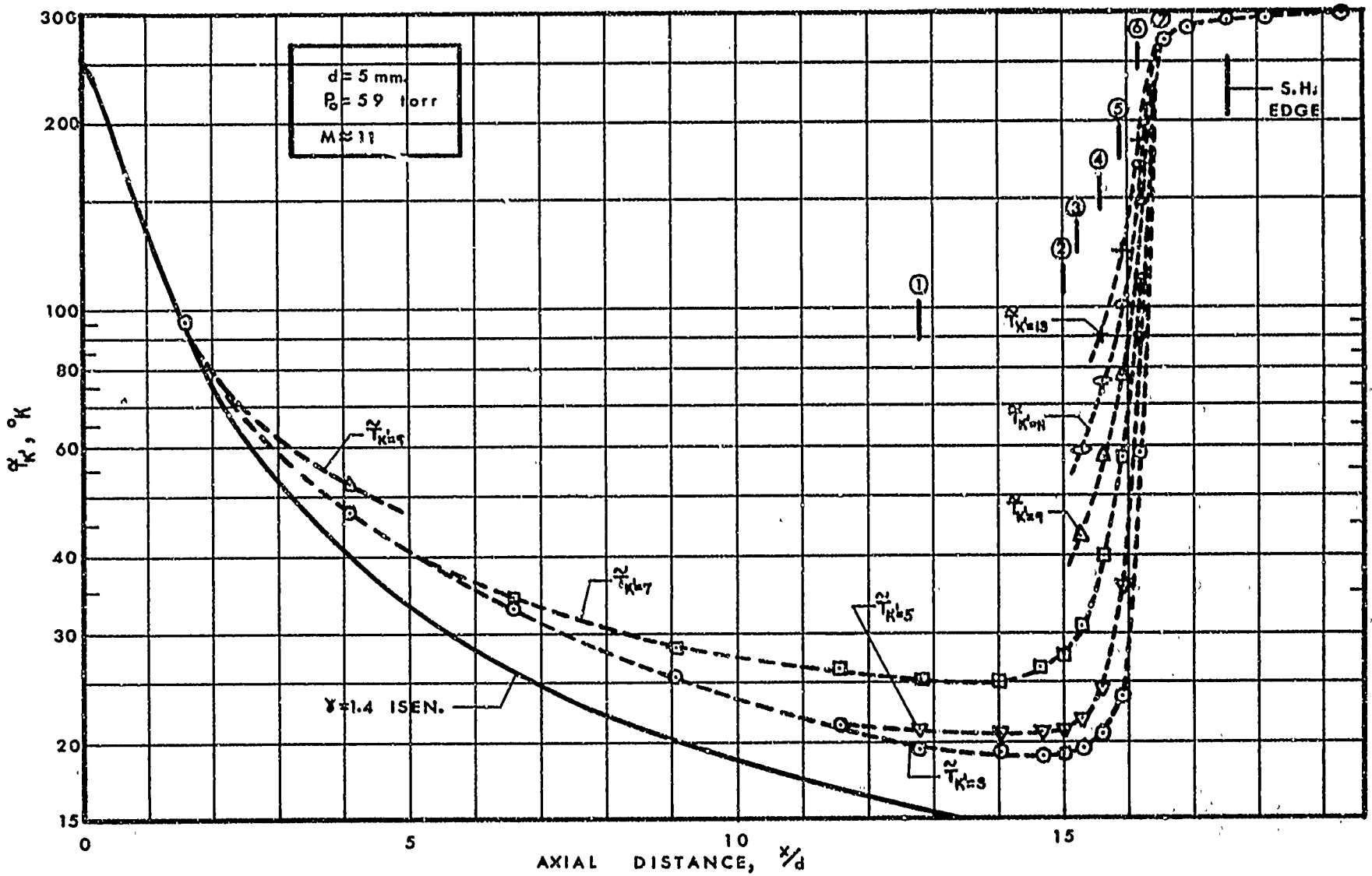

FIG. 27(b) SHOCK WAVE TEMPERATURE PROFILE, M ≈ 11

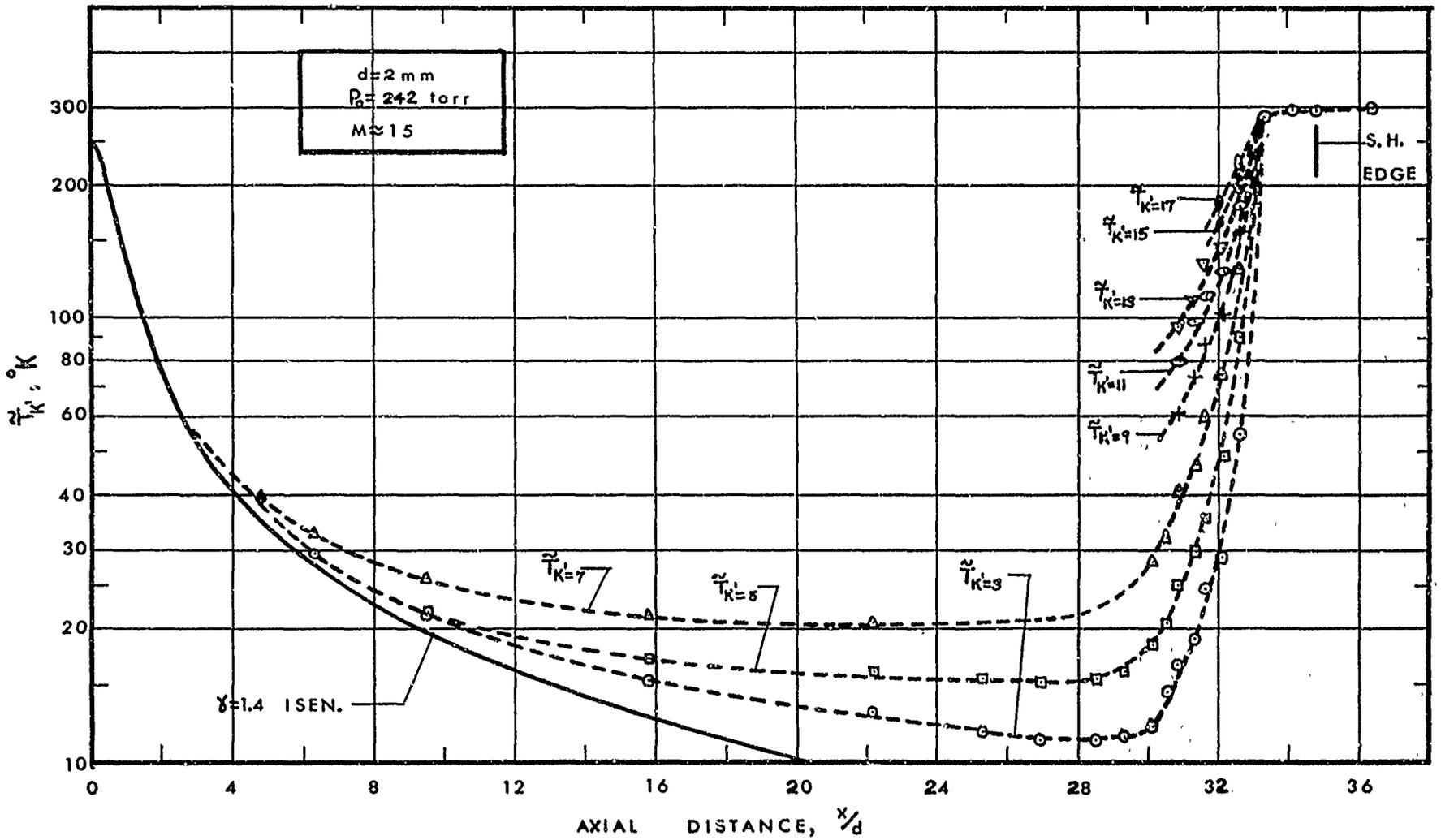

FIG. 27(c) SHOCK WAVE TEMPERATURE PROFILE, M ≈ 15

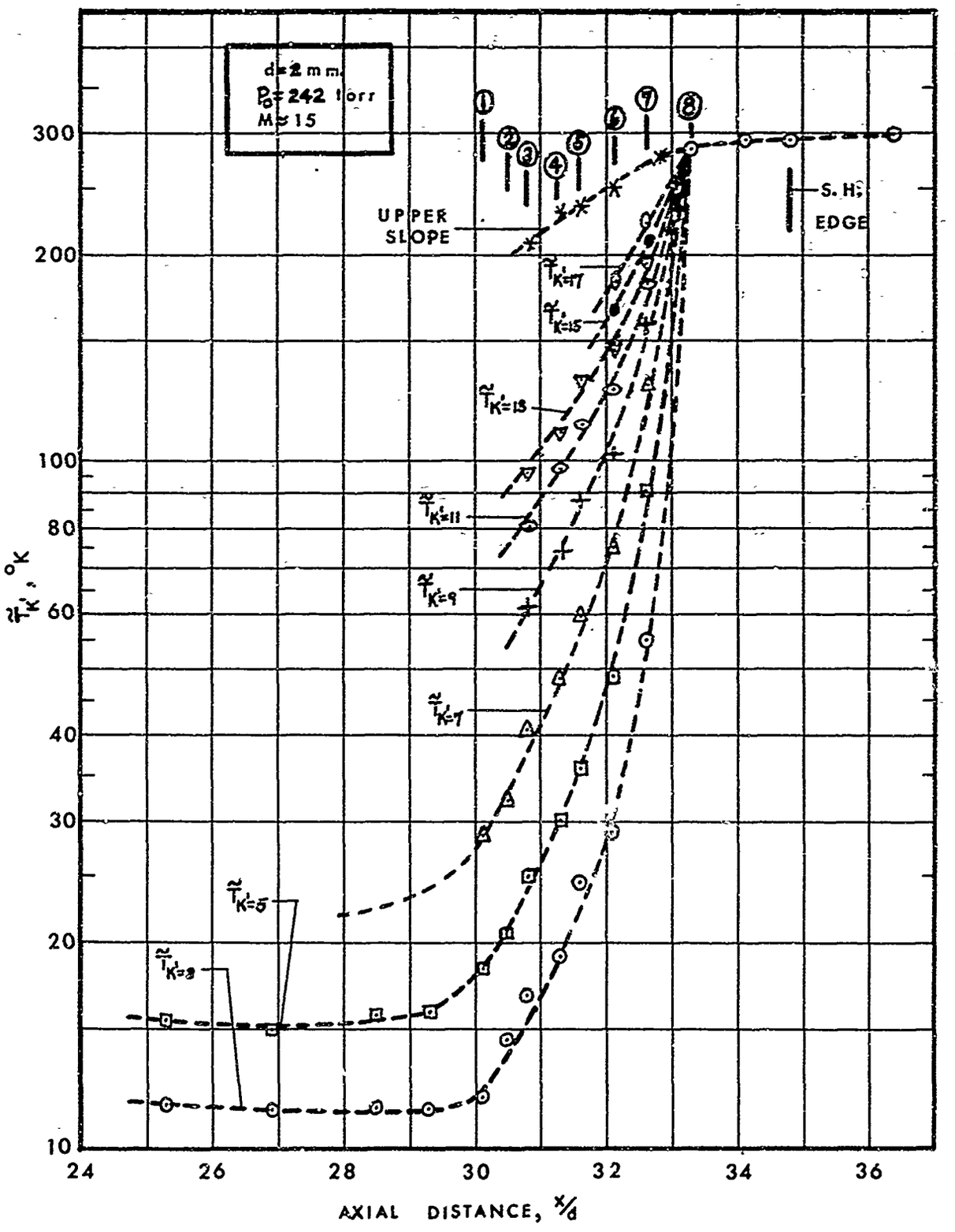

FIG. 27(d) SHOCK WAVE TEMPERATURE PROFILE, M ≈ 15

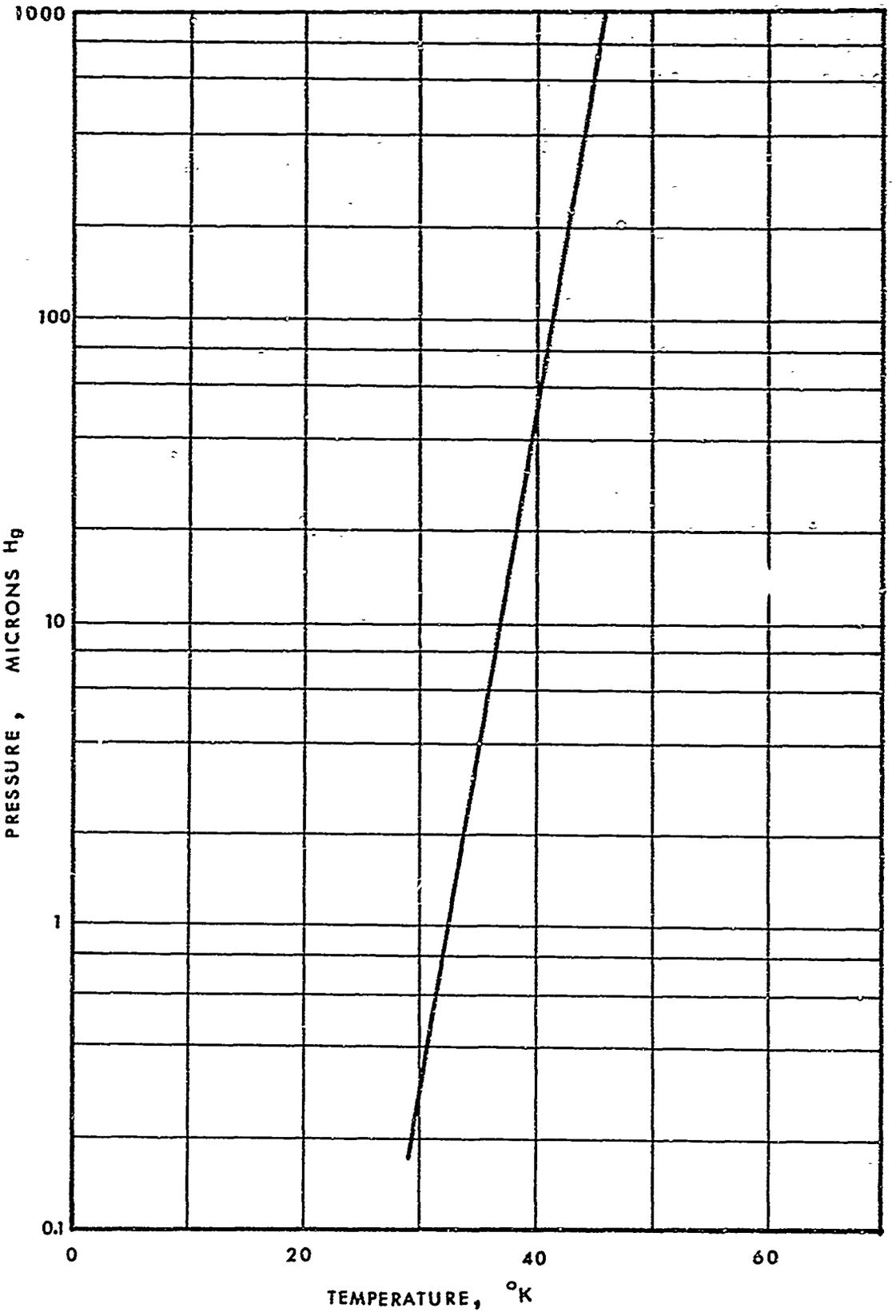

FIG. 28 VAPOR PRESSURE OF NITROGEN

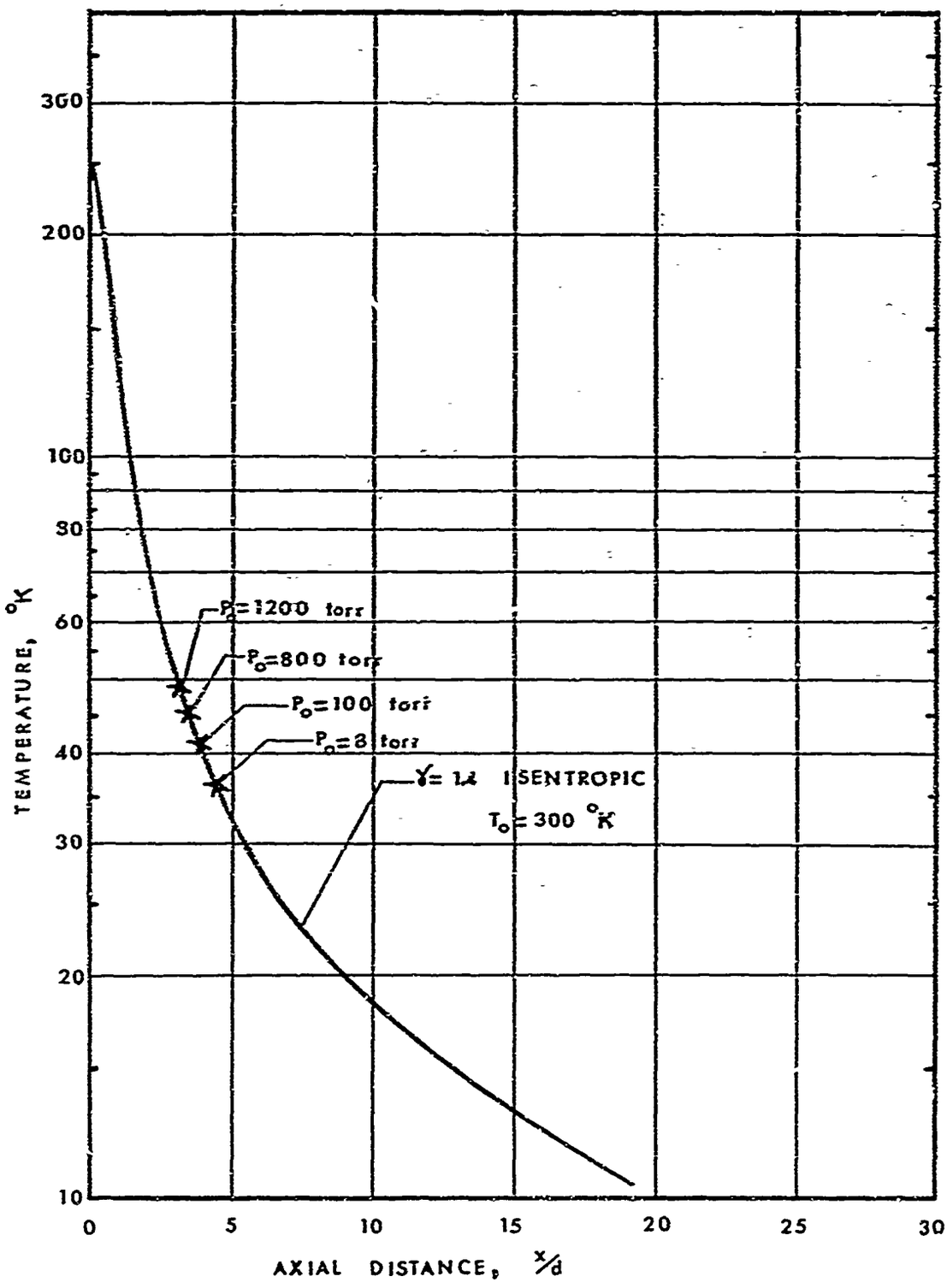

FIG. 29 APPROXIMATE NITROGEN CONDENSATION CALCULATION FOR A FREE JET

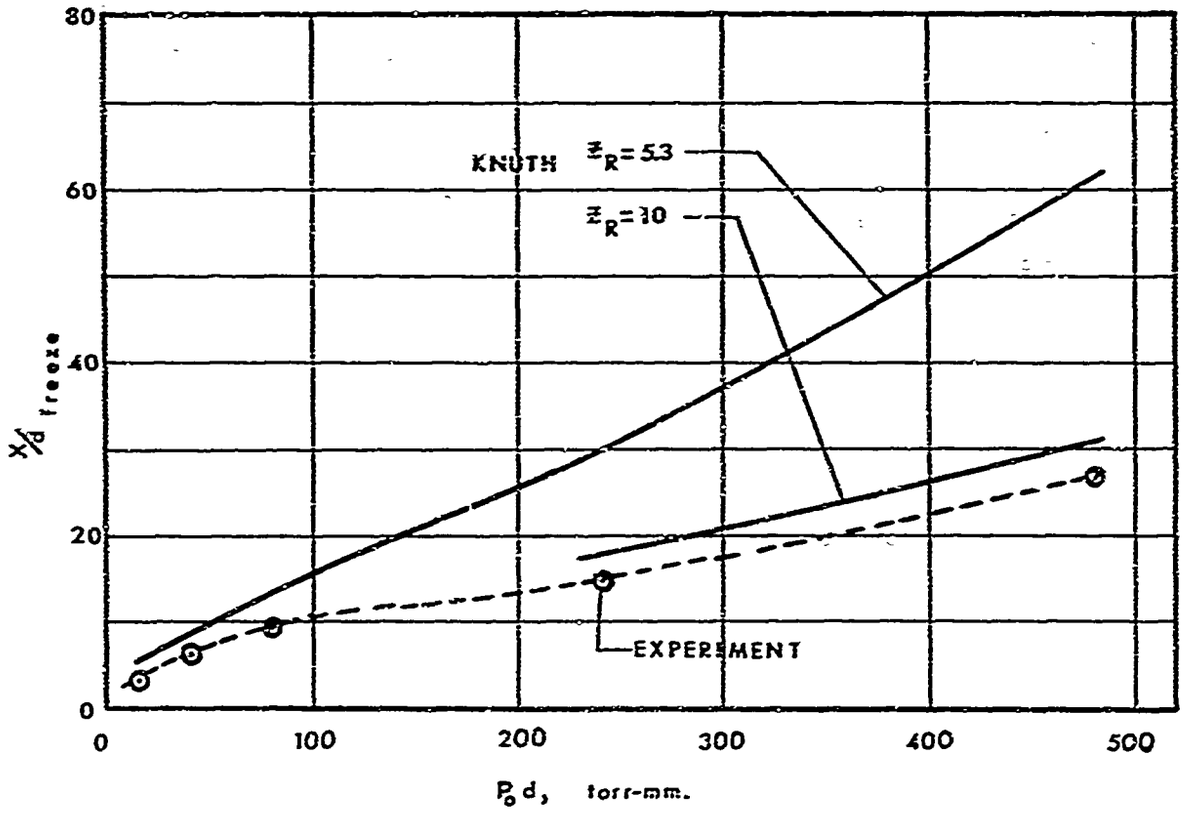

FIG. 30(a) ROTATIONAL FREEZING IN NITROGEN JETS

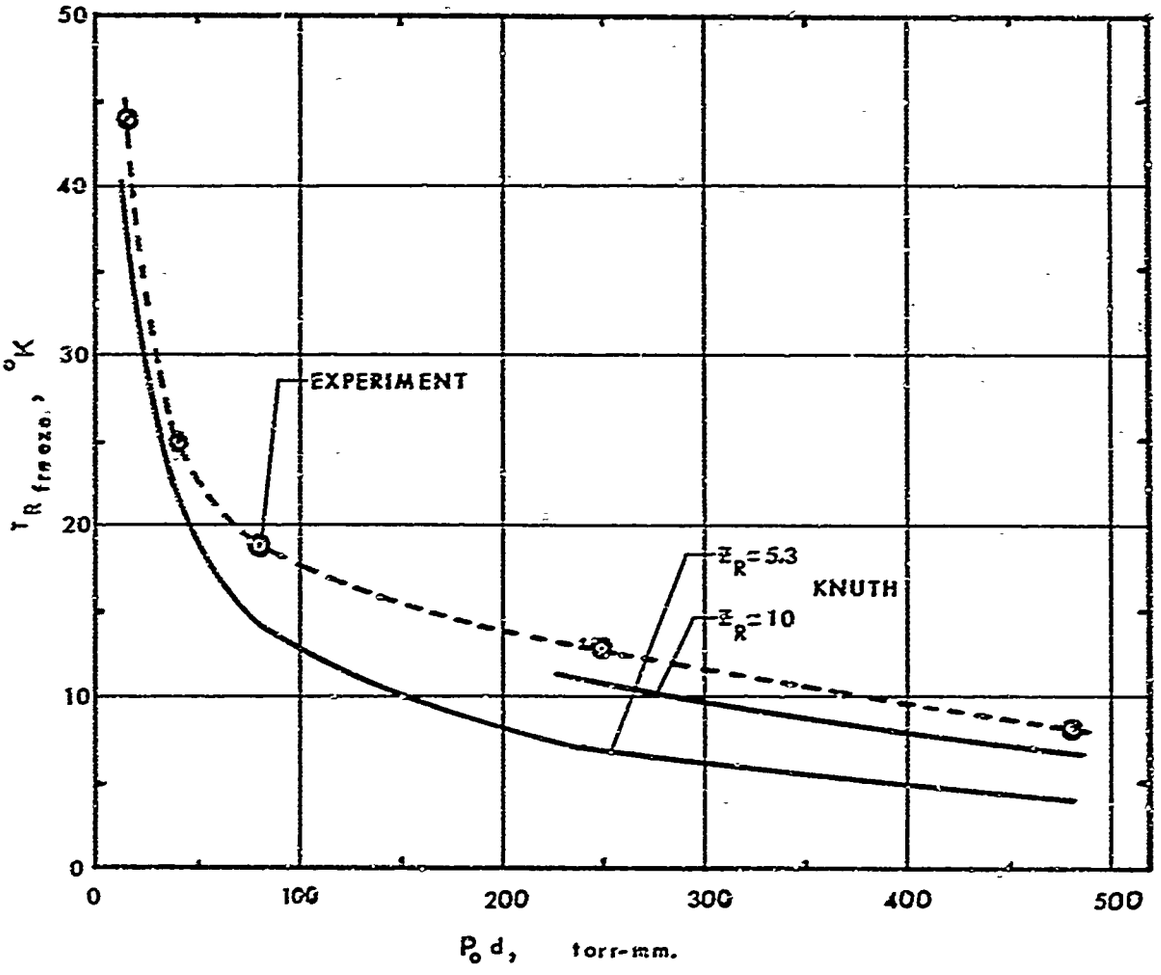

FIG. 30(b) ROTATIONAL FREEZING IN NITROGEN JETS

UTIAS REPORT NO. 113

Institute for Aerospace Studies, University of Toronto

Rotational Temperature and Density Measurements in Underexpanded Jet and Shock Waves Using an Electron Beam Probe.

P.V. Marrone   January 1966   35 pages   48 figures

1. Electron Beams
2. Free Jets
3. Shock Structure
4. Rotational Temperature
I. Marrone, P.V.
II. UTIAS Report No. 113

An electron beam probe was used to obtain measurements of rotational temperature and gas density in supersonic nitrogen jets expanding from room temperature. The parameter P_od (where P_o is the stagnation pressure in torr, and d is the orifice exit diameter in mm) was varied from 15 to 480 torr-mm. This corresponds to a sonic Reynolds number range of 290 to 9,320. Density measurements were made using a photomultiplier with an interference filter centered at 3900 A° and having a half-width of 100 A°. The experimental density data follow the axial isentropic density distribution in regions of rotational nonequilibrium. Rotational temperature measurements were obtained from rotational spectra of the N_2^+ first negative 0-0 band at 3914 A° using a high dispersion spectrograph. The experimentally determined rotational temperature values follow the axial isentropic temperature distribution in a free jet down to approximately 85 °K for P_od = 15 torr-mm, and 50°K for P_od = 480 torr-mm, with a scatter of about ± 3%. Below these temperatures, the T_R data depart from the isentropic curve and freeze at a constant temperature, which is dependent on the value of P_od. A shock holder was inserted in the jet and a number of shock waves in the range M = 4 to M = 15 were investigated. Density profiles through the shock waves were obtained. Rotational spectra indicate a large departure from a Boltzmann distribution in the rotational levels in the center of a shock front. This effect is small at M = 4, but very pronounced at M = 15. An apparent non-Boltzmann rotational distribution in the jet expansion flow was also observed.

Available copies of this report are limited. Return this card to UTIAS, if you require a copy.

UTIAS REPORT NO. 113

Institute for Aerospace Studies, University of Toronto

Rotational Temperature and Density Measurements in Underexpanded Jet and Shock Waves Using an Electron Beam Probe.

P.V. Marrone   January 1966   35 pages   48 figures

1. Electron Beams
2. Free Jets
3. Shock Structure
4. Rotational Temperature
I. Marrone, P.V.
II. UTIAS Report No. 113

An electron beam probe was used to obtain measurements of rotational temperature and gas density in supersonic nitrogen jets expanding from room temperature. The parameter P_od (where P_o is the stagnation pressure in torr, and d is the orifice exit diameter in mm) was varied from 15 to 480 torr-mm. This corresponds to a sonic Reynolds number range of 290 to 9,320. Density measurements were made using a photomultiplier with an interference filter centered at 3900 A° and having a half-width of 100 A°. The experimental density data follow the axial isentropic density distribution in regions of rotational nonequilibrium. Rotational temperature measurements were obtained from rotational spectra of the N_2^+ first negative 0-0 band at 3914 A° using a high dispersion spectrograph. The experimentally determined rotational temperature values follow the axial isentropic temperature distribution in a free jet down to approximately 85 °K for P_od = 15 torr-mm, and 50°K for P_od = 480 torr-mm, with a scatter of about ± 3%. Below these temperatures, the T_R data depart from the isentropic curve and freeze at a constant temperature, which is dependent on the value of P_od. A shock holder was inserted in the jet and a number of shock waves in the range M = 4 to M = 15 were investigated. Density profiles through the shock waves were obtained. Rotational spectra indicate a large departure from a Boltzmann distribution in the rotational levels in the center of a shock front. This effect is small at M = 4, but very pronounced at M = 15. An apparent non-Boltzmann rotational distribution in the jet expansion flow was also observed.

Available copies of this report are limited. Return this card to UTIAS, if you require a copy.

UTIAS REPORT NO. 113

Institute for Aerospace Studies, University of Toronto

Rotational Temperature and Density Measurements in Underexpanded Jet and Shock Waves Using an Electron Beam Probe.

P.V. Marrone   January 1966   35 pages   48 figures

1. Electron Beams
2. Free Jets
3. Shock Structure
4. Rotational Temperature
I. Marrone, P.V.
II. UTIAS Report No. 113

An electron beam probe was used to obtain measurements of rotational temperature and gas density in supersonic nitrogen jets expanding from room temperature. The parameter P_od (where P_o is the stagnation pressure in torr, and d is the orifice exit diameter in mm) was varied from 15 to 480 torr-mm. This corresponds to a sonic Reynolds number range of 290 to 9,320. Density measurements were made using a photomultiplier with an interference filter centered at 3900 A° and having a half-width of 100 A°. The experimental density data follow the axial isentropic density distribution in regions of rotational nonequilibrium. Rotational temperature measurements were obtained from rotational spectra of the N_2^+ first negative 0-0 band at 3914 A° using a high dispersion spectrograph. The experimentally determined rotational temperature values follow the axial isentropic temperature distribution in a free jet down to approximately 85 °K for P_od = 15 torr-mm, and 50°K for P_od = 480 torr-mm, with a scatter of about ± 3%. Below these temperatures, the T_R data depart from the isentropic curve and freeze at a constant temperature, which is dependent on the value of P_od. A shock holder was inserted in the jet and a number of shock waves in the range M = 4 to M = 15 were investigated. Density profiles through the shock waves were obtained. Rotational spectra indicate a large departure from a Boltzmann distribution in the rotational levels in the center of a shock front. This effect is small at M = 4, but very pronounced at M = 15. An apparent non-Boltzmann rotational distribution in the jet expansion flow was also observed.

Available copies of this report are limited. Return this card to UTIAS, if you require a copy.

UTIAS REPORT NO. 113

Institute for Aerospace Studies, University of Toronto

Rotational Temperature and Density Measurements in Underexpanded Jet and Shock Waves Using an Electron Beam Probe.

P.V. Marrone   January 1966   35 pages   48 figures

1. Electron Beams
2. Free Jets
3. Shock Structure
4. Rotational Temperature
I. Marrone, P.V.
II. UTIAS Report No. 113

An electron beam probe was used to obtain measurements of rotational temperature and gas density in supersonic nitrogen jets expanding from room temperature. The parameter P_od (where P_o is the stagnation pressure in torr, and d is the orifice exit diameter in mm) was varied from 15 to 480 torr-mm. This corresponds to a sonic Reynolds number range of 290 to 9,320. Density measurements were made using a photomultiplier with an interference filter centered at 3900 A° and having a half-width of 100 A°. The experimental density data follow the axial isentropic density distribution in regions of rotational nonequilibrium. Rotational temperature measurements were obtained from rotational spectra of the N_2^+ first negative 0-0 band at 3914 A° using a high dispersion spectrograph. The experimentally determined rotational temperature values follow the axial isentropic temperature distribution in a free jet down to approximately 85 °K for P_od = 15 torr-mm, and 50°K for P_od = 480 torr-mm, with a scatter of about ± 3%. Below these temperatures, the T_R data depart from the isentropic curve and freeze at a constant temperature, which is dependent on the value of P_od. A shock holder was inserted in the jet and a number of shock waves in the range M = 4 to M = 15 were investigated. Density profiles through the shock waves were obtained. Rotational spectra indicate a large departure from a Boltzmann distribution in the rotational levels in the center of a shock front. This effect is small at M = 4, but very pronounced at M = 15. An apparent non-Boltzmann rotational distribution in the jet expansion flow was also observed.

Available copies of this report are limited. Return this card to UTIAS, if you require a copy.

UTIAS REPORT NO. 113

Institute for Aerospace Studies, University of Toronto

Rotational Temperature and Density Measurements in Underexpanded Jet and Shock Waves Using an Electron Beam Probe.

P.V. Marrone | January 1966 | 35 pages | 48 figures

1. Electron Beams
2. Free Jets
3. Shock Structure
4. Rotational Temperature

I. Marrone, P.V.
II. UTIAS Report No. 113

An electron beam probe was used to obtain measurements of rotational temperature and gas density in supersonic nitrogen jets expanding from room temperature. The parameter P_od (where P_o is the stagnation pressure in torr, and d is the orifice exit diameter in mm) was varied from 15 to 480 torr-mm. This corresponds to a sonic Reynolds number range of 290 to 9,320. Density measurements were made using a photomultiplier with an interference filter centered at 3900 A° and having a half-width of 100 A°. The experimental density data follow the axial isentropic density distribution in regions of rotational nonequilibrium. Rotational temperature measurements were obtained from rotational spectra of the N_2^+ first negative 0-0 band at 3914 A° using ahigh dispersion spectrograph. The experimentally determined rotational temperature values follow the axial isentropic temperature distribution in a free jet down to approximately 85 °K for P_od = 15 torr-mm, and 50°K for P_od = 480 torr-mm, with a scatter of about ± 3%. Below these temperatures, the T_R data depart from the isentropic curve and freeze at a constant temperature, which is dependent on the value of P_od. A shock holder was inserted in the jet and a number of shock waves in the range M = 4 to M = 15 were investigated. Density profiles through the shock waves were obtained. Rotational spectra indicate a large departure from a Boltzmann distribution in the rotational levels in the center of a shock front. This effect is small at M = 4, but very pronounced at M = 15. An apparent non-Boltzmann rotational distribution in the jet expansion flow was also observed.

Available copies of this report are limited. Return this card to UTIAS, if you require a copy.

UTIAS REPORT NO. 113

Institute for Aerospace Studies, University of Toronto

Rotational Temperature and Density Measurements in Underexpanded Jet and Shock Waves Using an Electron Beam Probe.

P.V. Marrone | January 1966 | 35 pages | 48 figures

1. Electron Beams
2. Free Jets
3. Shock Structure
4. Rotational Temperature

I. Marrone, P.V.
II. UTIAS Report No. 113

An electron beam probe was used to obtain measurements of rotational temperature and gas density in supersonic nitrogen jets expanding from room temperature. The parameter P_od (where P_o is the stagnation pressure in torr, and d is the orifice exit diameter in mm) was varied from 15 to 480 torr-mm. This corresponds to a sonic Reynolds number range of 290 to 9,320. Density measurements were made using a photomultiplier with an interference filter centered at 3900 A° and having a half-width of 100 A°. The experimental density data follow the axial isentropic density distribution in regions of rotational nonequilibrium. Rotational temperature measurements were obtained from rotational spectra of the N_2^+ first negative 0-0 band at 3914 A° using ahigh dispersion spectrograph. The experimentally determined rotational temperature values follow the axial isentropic temperature distribution in a free jet down to approximately 85 °K for P_od = 15 torr-mm, and 50°K for P_od = 480 torr-mm, with a scatter of about ± 3%. Below these temperatures, the T_R data depart from the isentropic curve and freeze at a constant temperature, which is dependent on the value of P_od. A shock holder was inserted in the jet and a number of shock waves in the range M = 4 to M = 15 were investigated. Density profiles through the shock waves were obtained. Rotational spectra indicate a large departure from a Boltzmann distribution in the rotational levels in the center of a shock front. This effect is small at M = 4, but very pronounced at M = 15. An apparent non-Boltzmann rotational distribution in the jet expansion flow was also observed.

Available copies of this report are limited. Return this card to UTIAS, if you require a copy.

UTIAS REPORT NO. 113

Institute for Aerospace Studies, University of Toronto

Rotational Temperature and Density Measurements in Underexpanded Jet and Shock Waves Using an Electron Beam Probe.

P.V. Marrone | January 1966 | 35 pages | 48 figures

1. Electron Beams
2. Free Jets
3. Shock Structure
4. Rotational Temperature

I. Marrone, P.V.
II. UTIAS Report No. 113

An electron beam probe was used to obtain measurements of rotational temperature and gas density in supersonic nitrogen jets expanding from room temperature. The parameter P_od (where P_o is the stagnation pressure in torr, and d is the orifice exit diameter in mm) was varied from 15 to 480 torr-mm. This corresponds to a sonic Reynolds number range of 290 to 9,320. Density measurements were made using a photomultiplier with an interference filter centered at 3900 A° and having a half-width of 100 A°. The experimental density data follow the axial isentropic density distribution in regions of rotational nonequilibrium. Rotational temperature measurements were obtained from rotational spectra of the N_2^+ first negative 0-0 band at 3914 A° using ahigh dispersion spectrograph. The experimentally determined rotational temperature values follow the axial isentropic temperature distribution in a free jet down to approximately 85 °K for P_od = 15 torr-mm, and 50°K for P_od = 480 torr-mm, with a scatter of about ± 3%. Below these temperatures, the T_R data depart from the isentropic curve and freeze at a constant temperature, which is dependent on the value of P_od. A shock holder was inserted in the jet and a number of shock waves in the range M = 4 to M = 15 were investigated. Density profiles through the shock waves were obtained. Rotational spectra indicate a large departure from a Boltzmann distribution in the rotational levels in the center of a shock front. This effect is small at M = 4, but very pronounced at M = 15. An apparent non-Boltzmann rotational distribution in the jet expansion flow was also observed.

Available copies of this report are limited. Return this card to UTIAS, if you require a copy.

UTIAS REPORT NO. 113

Institute for Aerospace Studies, University of Toronto

Rotational Temperature and Density Measurements in Underexpanded Jet and Shock Waves Using an Electron Beam Probe.

P.V. Marrone | January 1966 | 35 pages | 48 figures

1. Electron Beams
2. Free Jets
3. Shock Structure
4. Rotational Temperature

I. Marrone, P.V.
II. UTIAS Report No. 113

An electron beam probe was used to obtain measurements of rotational temperature and gas density in supersonic nitrogen jets expanding from room temperature. The parameter P_od (where P_o is the stagnation pressure in torr, and d is the orifice exit diameter in mm) was varied from 15 to 480 torr-mm. This corresponds to a sonic Reynolds number range of 290 to 9,320. Density measurements were made using a photomultiplier with an interference filter centered at 3900 A° and having a half-width of 100 A°. The experimental density data follow the axial isentropic density distribution in regions of rotational nonequilibrium. Rotational temperature measurements were obtained from rotational spectra of the N_2^+ first negative 0-0 band at 3914 A° using ahigh dispersion spectrograph. The experimentally determined rotational temperature values follow the axial isentropic temperature distribution in a free jet down to approximately 85 °K for P_od = 15 torr-mm, and 50°K for P_od = 480 torr-mm, with a scatter of about ± 3%. Below these temperatures, the T_R data depart from the isentropic curve and freeze at a constant temperature, which is dependent on the value of P_od. A shock holder was inserted in the jet and a number of shock waves in the range M = 4 to M = 15 were investigated. Density profiles through the shock waves were obtained. Rotational spectra indicate a large departure from a Boltzmann distribution in the rotational levels in the center of a shock front. This effect is small at M = 4, but very pronounced at M = 15. An apparent non-Boltzmann rotational distribution in the jet expansion flow was also observed.

Available copies of this report are limited. Return this card to UTIAS, if you require a copy.